ON RADIATIVE FORCING AND LAND USE CHANGE: CAUSES, CONSEQUENCES AND SOLUTIONS

By

Grant Falvo

A DISSERTATION

Submitted to
Michigan State University
in partial fulfillment of the requirements
for the degree of

Crop and Soil Sciences —Doctor of Philosophy

2024

ABSTRACT

Over the past millennium, more than half of the globe's natural vegetation has been transformed by humans for agriculture, forestry, and other land uses. This reconfiguration of the Earth's surface has changed the composition of the atmosphere, the planetary energy balance, and as a result, the climate. The associated changes in temperature and precipitation patterns will continue to have cascading impacts on terrestrial ecosystems through a myriad of interrelated mechanisms. Opportunities exist for preparing more climate-resilient ecosystems and employing land in climate mitigation efforts. In this dissertation I quantify the causes, consequences and solutions associated with radiative forcing and land use change. In Chapter 1 I provide a comprehensive regional assessment in southwest Michigan, USA, of the radiative forcing, or climate impacts, of both historical land use change and the adoption of nature based climate solutions ranging from conservation agriculture to managed forestry and natural forest regeneration. I found that the globally significant radiative forcing caused by historical deforestation of the region (1851 \pm 71 μ W m⁻²) can be partially mitigated by the adoption of conservation agriculture (0 to $-62 \pm 50 \,\mu\text{W m}^{-2}$), managed forestry (-322 to $-674 \pm 71 \,\mu\text{W m}^{-2}$), and natural forest regeneration (-1359 \pm 71 μ W m⁻²). In Chapter 2 I quantify the response of soil greenhouse gas fluxes to projected climate changes by experimentally increasing precipitation variability or inducing a growing season drought across conventionally tilled row-crops, no-till row-crops and an early successional plant community. I found that the resulting changes to soil water content were largely able to predict the responses of soil N₂O and CH₄ fluxes, but that CO₂ fluxes exhibited higher than expected emissions following pulse rewetting events. The overall finding is that increased precipitation variability and drought caused equal or reduced radiative forcing, respectively. In Chapter 3, I present a mechanistic understanding of the response of

atmospheric nitrogen fixation in legumes to increased precipitation variability and drought. Using stable isotope techniques, leaf level gas exchange measurements, remote sensing and soil microbial assays, I found that plant and microbial nitrogen cycling were resistant to increased precipitation variability, but not to drought. Chapter 4 focuses on a climate change solution called bioenergy with carbon capture and storage. I compared three common methods of quantifying the net ecosystem carbon balance of the fields where bioenergy crops were established, namely 1) eddy covariance flux measurements, 2) plant and soil carbon inventories, and 3) a process-based ecosystem model. I took these different estimates and put them in the context of the other radiative forcing budget components, namely, soil N2O and CH4 fluxes, land surface albedo, farming-related fossil fuel emissions, and geologically stored carbon from the bioenergy processing facilities. I found that each method agreed that bioenergy with carbon capture and storage can provide significant negative radiative forcing, or cooling effects, but that methods sometimes did not agree on the magnitude of this effect. While this work highlights the complex and nuanced relationships between land and climate, it also shows how resilient ecosystems can be to some climate extremes as well as how nature can play a significant role in cooling the Earth.

ACKNOWLEDGMENTS

I would like to thank the many people who made this dissertation possible. First, I would like to thank Dr. G. Philp Robertson for his years of enduring support and for the wisdom he imparted on me during my time at Michigan State University. His depth of knowledge on the scientific topics discussed here is only surpassed by his ability to lead the all-too-human endeavor of maintaining lasting scientific collaborations from the lab to the university, national networks and beyond. I would also like to thank my committee members Dr. Sarah Evans, Dr. Stephen Hamilton, and Dr. Alexandra Kravchenko for their guidance over the years and for their willingness to help shape this formative experience at the foundation of my scientific career. Their enthusiastic and generous engagement with the details of my research was an essential part of making this dissertation come to fruition.

I would also like to thank all of the people that contributed to this dissertation for their help with each aspect of the research process. In addition to the former staff and research technicians that made contributions, I would like to thank Dr. Michael Abraha, Dr. Tyler Bassett, Dr. Nameer Baker, Dr. Bruno Basso, Dr. Sven Bohm, Dr. Jiquan Chen, Dr. Carolina Cordova, Dr. Francesca Cotrufo, Dr. Nicholas Haddad, Mark Hammond, Dr. Hsun-Yi Hsieh, Kevin Kahmark, Dr. Jennifer Lau, Dr. Cheyenne Lei, Catherine McMinn, Dr. Samantha Mosier, Sophie Perry, Dr. Sarah Roley, Jane Schuette, Dr. Ashley Shade, Joseph Simmons, Katie Steeves, Dr. Yahn-Jauh Su, Dr. Maurico Tejera, Ruben Ulbrich, Dr. Taylor Ulbrich, Stacey Vanderwulp, Dr. Carmella Vizza, David Weed, Dr. Brook Wilke, Kaija Windeler, Dr. Phoebe Zarnetsky, and Dr. Yao Zhang.

Finally, I would like to thank all of my friends and family that supported me throughout my higher education, through the challenging trials of life, and the wonderful adventures that mark our time here together on Earth.

TABLE OF CONTENTS

CHAPTER 1: Introduction	1
CHAPTER 2: Nature-based climate solutions can help repay the climate debt of deforestation. REFERENCES	
APPENDIX A: CHAPTER 2 TABLES AND FIGURES	27
CHAPTER 3: Land use mediates the response of soil CH ₄ , N ₂ O and CO ₂ fluxes to changing precipitation regimes	32
REFERENCES	
APPENDIX B: CHAPTER 3 TABLES AND FIGURES	
CHAPTER 4: Symbiotic nitrogen fixation is resistant to increased precipitation variability but	t
not to drought	63
REFERENCES	83
APPENDIX C: CHAPTER 4 TABLES AND FIGURES	89
CHAPTER 5: Combining field measurements, eddy covariance towers and an ecosystem mod	
improves confidence in the climate impacts of bioenergy with carbon capture and storage	96
REFERENCES	123
APPENDIX D: CHAPTER 5 TABLES AND FIGURES	129

CHAPTER 1: Introduction

Over the past millennium more than half of the natural vegetation on Earth has been transformed by humans for agriculture, forestry, and other land uses. The reconfiguration of the Earth's surface has changed the composition of the atmosphere, the planetary energy balance and as a result, the climate. The associated shifts in temperature and precipitation patterns across the globe will continue to perturb terrestrial ecosystems in a myriad of ways, each with their own cascading consequences for nature and society. The job of scientists then is to fill in the gaps in our knowledge of how this chain of events unfolds and inform the public of the foremost causes, consequences, and solutions.

In this dissertation I leverage an intensively measured, long term research site designed to elucidate the causes, consequences and solutions of radiative forcing, or climate impacts, associated with land use change. Long term, in situ measurements of replicated experiments are invaluable to the scientific community and society at large because they provide the gold-standard ground truth data that more synthetic or coarse scaled scientific approaches require for calibration and validation. These long term, replicated measurements are often needed to detect the globally significant but difficult to quantify ecosystem responses to land use and climate change. The responses I investigate in this dissertation include those that cause climate change, such as CO₂, N₂O and CH₄ gas fluxes and land surface albedo, as well as those that respond to climate change such as soil water content and plant nitrogen acquisition. Responses to land use change, climate change and their interactions and feedbacks are investigated, as are the different methodologies used for quantifying these responses. Several findings emerge that have relevance to stakeholders involved in each aspect of land use and climate change decision making, from field scale management decisions to regional regulation and incentive policies.

In Chapter 1 I quantified the climate impacts of both historical land use change in the U.S. upper Midwest and the adoption of eight nature based climate solutions. To estimate the radiative forcing impacts of the deforestation that occurred in the region during the late 19th century, I coupled the original witness tree data from the U.S. Public Land Survey that occurred in the region from 1828 to 1839 with contemporary in situ measurements of plant and soil carbon stocks, soil N₂O and CH₄ fluxes and satellite-based land surface albedo measurements in both old growth forests and agricultural fields. To investigate the radiative forcing impacts of adopting nature based climate solutions on already existing agricultural land, ranging from conservation agriculture to managed forestry and natural forest regeneration, I combined U.S. Forest Inventory and Analysis tree data with contemporary in situ measurements of plant and soil carbon stocks, soil N₂O and CH₄ fluxes and satellite-based land surface albedo measurements in eight replicated land use treatments. With the in situ measurements that span up to 40 years, this chapter provides the most comprehensive data driven, bottom up assessment of the climate impacts of land use change in the region of southwest Michigan.

In Chapter 2 I examine the impacts of a changing climate on soil greenhouse gas emissions themselves. Specifically, I examined how soil CH₄, N₂O and CO₂ fluxes would respond to changing precipitation regimes in conventionally tilled row-crops, no-till row-crops and an early successional plant community. I measured these fluxes over three years in the field in response to increased precipitation variability and a growing season drought. These manipulations were achieved by putting out large precipitation exclusion shelters equipped with irrigation systems underneath them. I specifically investigated whether or not those fluxes were strictly dependent on changes to soil water content or if there were other factors driving higher than expected responses to extremes like pulse rewetting events. The value of this study comes

from its design where the precipitation manipulations tested are plausible realizations of regional climate projections that were performed at a sufficiently large scale to capture fully integrated ecosystem responses, thus providing estimates of credible greenhouse gas fluxes for future climate scenarios in the region.

In Chapter 3 I leverage the precipitation manipulation experiment to investigate the response of symbiotic nitrogen fixation to increased precipitation variability and a growing season drought. I utilized stable isotope techniques to quantify the amount of atmospheric nitrogen fixed by microbial symbionts in both the soybeans of the tilled and no-till row-crop land uses and the red clover in the early successional plant community. I quantified important drivers of plant drought and nitrogen acquisition responses to altered precipitation both in the soil and in the plants. Utilizing stable isotopes of carbon, leaf level gas exchange measurements and remote sensing techniques I identified the likely water stress response mechanisms of the plants. In the soil, I measured how each land use mediated the redistribution of water following the precipitation manipulations as well as how the microbial community maintained organic matter decomposition and nitrogen supply to the plants. Results provide a holistic view of the nitrogen fixation response in legumes to two plausible future climate change scenarios.

In Chapter 4 I turn to an investigation of a proposed climate change solution, bioenergy with carbon capture and storage. Leveraging a 13-year land use change experiment where bioenergy plants were established, I asked to what degree different methodologies for quantifying how the net ecosystem carbon balance might change the radiative forcing impacts of bioenergy with carbon capture and storage. Specifically, I used 1) eddy covariance flux towers that measured carbon dioxide exchange in each field continuously throughout the study period, 2) repeated plant and soil carbon inventories taken at the beginning, middle and end of the study

period and 3) a process-based ecosystem model calibrated to each of those datasets. To the best of my knowledge, this is the first study to perform such a comparison in a bioenergy context. With the methodological differences in net ecosystem carbon balance in hand, I was able to construct the full radiative forcing budget for the bioenergy with carbon capture and storage scenarios. I added in situ measurements of soil N₂O and CH₄ fluxes, satellite-based land surface albedo, farming-derived fossil fuel emissions and the presumed mass of geologically stored carbon from the bioenergy processing facility to summarize the net climate impact of each land use and each methodology. Results provide information on both the strengths of each method for quantifying the net ecosystem carbon balance and the comprehensive climate impacts of bioenergy with carbon capture and storage.

Overall, in this dissertation I provide a unique data driven look at the causes, consequences and solutions that are associated with radiative forcing and land use change. The results provide credible climate impact assessments of land uses that can warm or cool the planet, realistic feedbacks of soil greenhouse gas fluxes to changing precipitation regimes, mechanistic insight into the response of plant nitrogen acquisition to changing precipitation regimes, and a comprehensive evaluation of the radiative forcing impacts of a major land-based climate mitigation technology.

CHAPTER 2: Nature-based climate solutions can help repay the climate debt of deforestation **Abstract**

Widespread expansion of agriculture, forestry and other land uses has remade the surface of the Earth, changing the composition of the atmosphere and as a result, the climate. Here we quantified the radiative forcing impacts of historical deforestation in the U.S. upper Midwest and the subsequent adoption of eight nature-based climate solutions (NBCS) using 40 years of data collected from a replicated land use change experiment. Deforestation of the region in the late 19^{th} century caused net global warming ($1851 \pm 71 \mu W m^{-2}$), mainly from the 76 % reduction of ecosystem carbon stocks, but also from the 84 % reduction of the soil methane (CH₄) sink and the 115 % increase in soil nitrous oxide (N2O) emissions, with the change in albedo offsetting 18 % of the greenhouse gas induced warming. For the nature-based climate solutions, we found tradeoffs for society, nature, and climate, with conservation agriculture providing 0 to -62 ± 50 μ W m⁻² of climate mitigation, short/medium length forestry rotations providing -322 to -674 \pm 71 μ W m⁻² of climate mitigation, and natural forest regeneration providing -1359 \pm 71 μ W m⁻² of climate mitigation. As the impacts of climate change on nature and society intensify, consideration should be given to the climate mitigation and ecosystem services that nature-based climate solutions can provide.

Introduction

Over the past millennium, 75 x 10⁶ km², or 59 % of primary natural vegetation, was altered by humans to support agriculture, forestry and other land uses (AFOLU) globally (Hurtt et al., 2020). These historical activities continue to significantly alter the Earth's energy balance through changes in terrestrial greenhouse gas fluxes and land surface albedo. AFOLU directly contributed 12.0 Pg CO₂-eq y⁻¹ of emissions, representing 23 % of all anthropogenic greenhouse gas induced radiative forcing during the period from 2007 to 2016 (Jia et al., 2019). Furthermore, changes in global land surface albedo from AFOLU during the period from 1700 to 2005 amounted to a radiative forcing impact of -0.15 W m⁻² (Ghimire et al., 2014). With land use exerting this degree of control on the global climate, many have proposed the adoption of sustainable land use practices as so-called nature-based climate solutions (NBCS; Fargione et al., 2018; Griscom et al., 2017; Robertson et al., 2022; Roe et al., 2019). However, our understanding of the overall climate impacts of NBCS is hampered by the lack of long-term, replicated land use change experiments that measure each of the major radiative forcing budget components.

Here we compile long term radiative forcing budgets for ten different land uses in the U.S. upper Midwest to quantify the climate impact of NBCS ranging from natural forest regeneration to conservation agriculture. Our continuous measurements of ecosystem C stock components, soil N₂O and CH₄ fluxes, as well as land surface albedo span 40 years from 1984 to 2023. For soil and root carbon stocks we took 510 large diameter hydraulic cores to a depth of 100 cm. For soil N₂O and CH₄ fluxes we used 14,568 manual static chamber fluxes. For land surface albedo we acquired 47,075 high resolution satellite observations. Using the replicated long-term experiment at the Kellogg Biological Station Long Term Ecological Research site we

estimate the climate impact of both historical land use change in the region, as well as the future adoption of proposed NBCS (Robertson & Hamilton, 2015). We scale our results to an ecologically representative study region, the U.S. E.P.A. Level III Ecoregion 56, which covers 51.7 x 10³ km⁻² in southwestern Michigan (Omernik & Griffith, 2014). For the historical land use change scenario, we supplement the data collected at our site with 113,643 original witness trees identified, measured, and mapped by the United States Public Land Survey that occurred from 1828 to 1839 in the study area that provide the aboveground biomass data for our ecosystem carbon stock budget (Paciorek et al., 2021). Similarly, for the reforestation scenarios we supplement the data collected at our site with aboveground biomass data from the United States Forest Inventory and Analysis program from a total of 439 plots in the study area that met our inclusion criteria (Stanke et al., 2020).

The ten different land uses studied here include three modifications of the predominant land use in the region, a conventional (CON) corn-soybean-winter wheat rotation (*Zea mays*, *Glycine max*, *Triticum aestivum*), which serves as the reference baseline for the NBCS scenarios. The three modified row crop agriculture systems are a no-till (NT) system managed with conventional fertilizer and pesticide inputs, a reduced input (RI) system which receives one-third the fertilizer and pesticide inputs, and an organic (ORG) system which receives no external inputs. The RI and ORG systems also include a winter cover crop. Three perennial agriculture systems of different rotation lengths were investigated, including alfalfa (ALF; *Medicago sativa*), rotated every 6 years, a poplar plantation (POP; *Populus nigra x Populus deltoids* and *Populus nigra x Populus maximowiczii*), harvested every 10 years, and an eastern white pine plantation (PIN; *Pinus strobus*) harvested every 50 years. Lastly, we studied three phases of ecosystem restoration denoted here as early (ES) mid- (MS) and late succession (LS). The ES system is

managed with annual prescribed fire while the MS system has been unmanaged and aggrading into second growth forest for more than 50 years. The LS system represents some of the last remaining intact temperate deciduous broadleaf forest in the U.S. upper Midwest.

Results

Widespread conversion of native vegetation in the region occurred in a brief boom-bust fashion from the mid 19th to early 20th century, resulting in lasting, net positive radiative forcing (1851 \pm 71 μ W m⁻²; Figure 2.1 and Table 2.1). The loss of the region's woody biomass (617 Tg C) as well as the 31 % reduction in soil carbon to a 100 cm depth contributed most to the CO₂ induced radiative forcing of 2165 \pm 72 μ W m⁻² (Figure 2.1, Tables 2.1 and 2.2). Furthermore, the 85 % reduction in soil methane oxidation rates and the 115 % increase in soil nitrous oxide emissions contributed to warming of 35 \pm 2 and 63 \pm 7 μ W m⁻², respectively. On the other hand, a cooling effect of land surface albedo change (-412 \pm 6 μ W m⁻²) occurred due to the more reflective vegetation and the lack of tree cover that formerly obscured some of the highly reflective underlying snow during winter months.

The NBCS similarly owed much of their radiative forcing differences to ecosystem carbon stock changes (Figure 2.2). For the NT, RI and ORG conservation agriculture scenarios, soil carbon sequestration rates of 4.5, 3.6 and 7.1 ± 2.3 Mg C ha⁻¹, respectively, were predominantly responsible for the radiative forcing changes (Table 2.2). For the ALF, POP and PIN perennial crop scenarios, both soil carbon sequestration (9.3, 10.6 and 8.1 ± 3.1 Mg C ha⁻¹, respectively) and woody biomass carbon accumulation (0.0, 10.3, and 38.9 ± 0.5 Mg C ha⁻¹, respectively) made important contributions to negative radiative forcing. The ES and MS scenarios similarly relied on soil and woody biomass carbon gains for negative radiative forcing. The ES scenarios sequestered the most soil carbon (13.5 \pm 2.8 Mg C ha⁻¹) of the scenarios with

herbaceous vegetation despite the annual prescribed fire removing its aboveground biomass. In the absence of prescribed fire, the MS natural forest regeneration scenario was able to store 61.8 \pm 0.5 Mg C ha⁻¹ in woody biomass. This jump in magnitude highlights the ability of woody biomass to sequester carbon well after soil carbon stocks saturate.

The next largest component of the NBCS radiative forcing budgets was land surface albedo (Figure 2.2; Tables 2.1 and 2.3). Outgoing shortwave radiation at the top of the atmosphere (SW_{out}^{toa}) responded most to the inherent reflectivity of the different vegetation types during the growing season, as well as the canopy's ability to obstruct solar radiation from reflecting off underlying snow cover during winter months. The conventional and conservation agriculture scenarios as well as the ALF scenario had the highest SW_{out}^{toa} , with a range of 15.1-15.4 \pm 0.1 W m⁻². The short and medium length forest rotations, POP and PIN, each had lower SW_{out}^{toa} of 13.9 and 9.3 \pm 0.1 W m⁻², respectively, owing to their darker vegetation and taller stature. Similarly, the ES and MS scenarios had lower SW_{out}^{toa} (13.9 and 12.1 \pm 0.1 W m⁻², respectively), caused by their less reflective vegetation and protruding stems during periods of snow cover.

Following carbon stock and albedo changes, the next largest component of the radiative forcing budget was soil nitrous oxide emissions (with the exception of CH₄ emissions from biomass burning in ES, described below; Figure 2.2 and Table 2.3). Surprisingly, the conservation agriculture scenarios had equal or higher soil nitrous oxide emissions despite reduced or eliminated synthetic nitrogen fertilizer inputs. The NT, RI and ORG scenarios produced 1.5, 1.4 and 1.7 ± 0.1 kg N₂O ha⁻¹ y⁻¹, compared to the CON scenario of 1.3 ± 0.1 kg N₂O ha⁻¹ y⁻¹. The highest nitrous oxide emissions came from the ALF scenario (2.0 ± 0.1 kg N₂O ha⁻¹ y⁻¹), which is a perennial nitrogen fixing crop. The PIN forest scenario had intermediate

nitrous oxide emissions $(1.3 \pm 0.1 \text{ kg N}_2\text{O ha}^{-1} \text{ y}^{-1})$ when compared to the lowest emitting scenarios, POP, ES and MS, whose emissions were 0.7, 0.5 and $0.8 \pm 0.1 \text{ kg N}_2\text{O ha}^{-1} \text{ y}^{-1}$, respectively. Notably, the direct nitrous oxide emissions from the prescribed fire in the ES system more than doubled the system's soil emissions from $0.5 \pm 0.1 \text{ kg N}_2\text{O ha}^{-1} \text{ y}^{-1}$ to $1.1 \pm 0.1 \text{ kg N}_2\text{O ha}^{-1} \text{ y}^{-1}$.

Finally, the soil methane oxidation sink had the smallest impact on the total radiative forcing budgets (Figure 2.2 and Table 2.3). The strong methane sink in the intact LS forest of - $3.7 \text{ kg} \pm 0.1 \text{ CH}_4 \text{ ha}^{-1} \text{ y}^{-1}$ was greatly diminished upon conversion to agricultural land uses. The other scenarios with herbaceous vegetation were largely unable to recover that original sink strength (-0.5 to -0.8 kg \pm 0.1 CH₄ ha⁻¹ y⁻¹). Only the PIN and MS forest scenarios partially recovered the soil methane sink with rates of -3.0 and -2.9 \pm 0.4 kg CH₄ ha⁻¹ y⁻¹, respectively. Methane fluxes from the prescribed fire in the ES system took the ecosystem from a net sink of - 0.7 kg CH₄ ha⁻¹ y⁻¹, to a net source of 9.4 kg CH₄ ha⁻¹ y⁻¹ when combining both the soil methane oxidation sink and fire.

Summing each component of the radiative forcing budgets, we found that the net climate impact of the different NCBS strategies presented clear tradeoffs for climate, nature and society. Conservation agriculture provided the smallest amount of climate mitigation with the NT, RI and ORG scenarios contributing net radiative forcings of -62, -23 and -48 \pm 50 μ W m⁻², respectively (Table 2.1). The perennial crops ALF, POP and PIN each provided more climate mitigation (-179, -322 and -693 \pm 71 μ W m⁻², respectively). In the ES scenario, the albedo induced forcing of 154 \pm 4 μ W m⁻² as well as the soil and fire CH₄ emission forcing of 95 \pm 2 μ W m⁻² completely offset the carbon sequestration benefit, making the net impact of this scenario climate neutral (-

 $18 \pm 50~\mu W~m^{-2}$). Finally, the largest amount of climate mitigation was provided by the MS natural forest regeneration scenario at -1359 \pm 71 $\mu W~m^{-2}$.

Discussion

Our pairing of a large volume of in situ data from a long term replicated land use change experiment with the best available historical and contemporary forest inventory data provides the most comprehensive bottom-up assessment of net radiative forcing caused by land use change in the region to date. Our work expands on previous bottom-up studies in the area that focused on select aspects of the radiative forcing budget and/or select land uses (Gelfand et al., 2016; Levine et al., 2011; Robertson et al., 2000; Robertson & Tiedje, 1984; Syswerda et al., 2011). The length of our study period allowed us to definitively demarcate the end of the transient response of variables to land use transitions that can be slow to change such as soil carbon stocks, land surface albedo and soil CH4 fluxes (He et al., 2014; Kravchenko & Robertson, 2011; McNamara et al., 2015; Necpalova et al., 2014).

Land touches a wide range of natural and human domains other than climate that are important to consider when evaluating the broader impacts of the changes to radiative forcing quantified by our research. Land is property, habitat, territory; it is part of livelihoods, food security, and many other aspects of natural and human life. Contentious battles for how to use land, who gets to use it, and for what ends will continue for many lifetimes to come. It's therefore worthwhile to consider that the conservation agriculture scenarios studied here (NT, RI, and ORG) provide little habitat for native plants and animals (Bahlai et al., 2013; Helms et al., 2021; Kemmerling et al., 2023; Robertson et al., 2011, 2012; Smith et al., 2008). However, they do provide food and economic returns that are readily scalable, making conservation agriculture's relatively small climate mitigation per unit of land potentially impactful if applied

extensively (Kravchenko et al., 2017). The perennial agriculture land uses in this study (ALF, POP, and PIN) provide food or fiber returns and some limited habitat for plants and animals (Bahlai et al., 2013; Freckman & Ettema, 1993; Smith et al., 2008). The ES scenario supports a diverse community of herbaceous plants that attract insects and other wildlife (Bahlai et al., 2013; Colunga-Garcia et al., 1997; Smith et al., 2008; Wickings & Grandy, 2013), but it does not provide food or fiber.

The natural forest regeneration scenario (MS) slowly but steadily recruits trees that attract insects and other wildlife (Bahlai et al., 2013; Colunga-Garcia et al., 1997; Smith et al., 2008; Tatina, 2016). Persisting well after these changes for perhaps 150 years after the last disturbance, the trees at the stand level continue to sequester carbon, including in downed woody materials and roots (Tatina, 2021). The United States Forest Inventory and Analysis data in our study region that the MS scenario relies on has very few plots with a stand age greater than 100 years, but studies from the small number of well documented old-growth forests in the region suggest whole ecosystem carbon sequestration potential upwards of 243 - 359 Mg C ha⁻¹, as compared with the 100 year old MS scenario's 199 Mg C ha⁻¹ from this study (Morris et al., 2007; Stanke et al., 2020; Tatina, 2021). On the other hand, our preindustrial witness tree data (sampled from 1828 to 1839) showed a wide range of total ecosystem carbon stocks with the 5th and 95th percentiles having 188 and 345 Mg C ha⁻¹. This suggests that disturbances like wind, snow/ice damage, insect and fungal diseases, fire and human exploitation created a mosaic of stand ages from young to old (Paciorek et al., 2021). As the study region's second growth forests continue to mature, stakeholders can take the climate mitigation potentials our study provides into account when deciding how to manage these disturbances.

Stakeholders can also factor in the climate mitigation potentials we provide for the agricultural and forestry NBCS when evaluating the tradeoffs involved in placing them on the landscape. Expanding these NBCS with food, fiber, and economic returns onto the maturing second growth forests would sacrifice the substantial climate mitigation they are already providing and come at significant costs to plant and animal habitat. In contrast, integrating these NBCS into existing agricultural landscapes would make significant, if modest, steps towards repaying the climate debt of past deforestation in the region. Reconfiguring land for climate benefits is not a simple task, but the pressures of a changing climate, a growing human population and an increasingly precarious natural world motivate the effort to chart a sustainable trajectory for the Earth system with resolve and determination.

Methods

Study site

Analyses here are based on data from the W.K. Kellogg Biological Station Long Term Ecological Research site established by Michigan State University in 1989 (42.4 N, 85.4 W, 288 m elevation; Robertson & Hamilton, 2015). Prior to the initiation of the experiment, the site was managed to produce annual row crops from circa 1850 to 1988. Before 1850 the site existed in a matrix of mid- to late succession temperate deciduous broadleaf forest. The site has a mean annual surface air temperature of 9.3 °C and a mean annual precipitation of 1067 mm (Thornton et al., 2022). The soils are well drained fine-loamy, mixed, active, mesic Typic Hapludalfs and consist of loamy glacial outwash overlying sand (Luehmann et al., 2016).

The main experimental site follows a randomized complete block design with 6 replicates of each land use and a plot size of 1 ha. However, three of the forested land uses studied here, PIN, MS and LS, are located adjacent to this main site (< 1 km distant) on the same soil series

with only 3 replicates. The year that the three PIN replicates were planted to eastern white pine is unknown, but periodic aerial photographs that began in 1938 suggest dates of 1959, 1962, and 1972. Similarly, the precise year of cropland abandonment for the three MS replicates is not known, but was approximated through observations of initial tree colonization in 1970, 1979 and 1981. The ALF system was transitioned to a different land use in 2019 so, for that land use, all data (apart from the soil carbon stocks) used in this study came before that change. Similarly, the RI and ORG land uses had a strip of prairie planted in them in 2019, which we avoided when taking measurements for this study.

Soil N2O and CH4

Soil N₂O and CH₄ flux measurements began at the main site in 1991 and 1992, respectively, while measurements in the adjacent forested sites started in 1993. Measurements occurred bi-weekly to monthly through to 2023, although some land uses were not sampled in certain years totaling 1 year (CON, NT, ORG, and ES), 2 years (RI, POP, ALF, and LS) or 12 years (PIN and MS). Measurements were conducted following the static chamber method (Gelfand et al., 2016). Briefly, 28 cm diameter chambers were inserted into the soil and fitted with a lid for 1.5 h, during which time 4 headspace gas samples were taken and stored in vials (Labco Limited, Lampeter, UK). Samples were then analyzed for N₂O and CH₄ on a gas chromatograph (Hewlett-Packard 5890 series, CA, USA, until 2008 and 7890A Agilent Technologies Inc., CA, USA, thereafter) equipped with a ⁶³Ni electron capture detector (350 °C), a Poropak Q column (1.8 m, 80/100 mesh) at 80 °C, and a carrier gas of argon/methane (90/10). Areal fluxes were calculated from changes in the headspace gas concentration over time with the ideal gas law and assumed to represent the daily mean flux. Positive fluxes indicate emission to

the atmosphere whereas negative fluxes indicate uptake. Between 681 and 1,779 fluxes were available for each land use, for a total of 14,568 fluxes measured from 1991 to 2023.

Biomass burning N₂O and CH₄ were estimated separately for the ES scenario that is burned each Spring. Biomass was clipped at 5 stations within each plot in the dormant season post-senescence and pre-burn from a 1 m⁻² quadrat, dried in an oven at 60 °C, and weighed. When this post-senescence data was missing, pre-senescence data collected in the same manner was used and adjusted by the observed post-senescence biomass loss rate, which was 39 % at our site. Emission factors for g N₂O and CH₄ per kg of biomass burned were then applied to these weights by considering the plant functional type as 'Savanna and Grassland' (Andreae, 2019). A total of 879 observations were available from 1991 to 2022.

Ecosystem carbon stocks

Soil and fine root carbon and nitrogen stocks were measured after the growing season and before the first soil freeze event in Fall 2022 with a hydraulic probe (Geoprobe 540MT, Salinas, KS USA). After clearing the surface litter, two intact cores 7.6 cm in diameter were taken to a depth of 1.2 m at each of 5 stations in each experimental unit for a total of 510 cores. Each core was then split into 4 sections by depth at 0-10 cm, 10-25 cm, 25-50 cm, and 50-end cm, where the end depth was between 90 and 115 cm. Each section was sieved to 4 mm to remove gravel, which was weighed and recorded as the coarse fraction. Roots were taken from the top of the 4 mm sieve as well as from the soil passed through the sieve. Roots were then washed with water over a 0.25 mm sieve, dried at 60 °C, and weighed. Similarly, soil passed through the sieve was dried at 60 °C and weighed. The coarse fraction free dry weight of the soil and the section's volume were used to determine the bulk density of the sample. A total of 510 cores split into 4

depths gave 2,040 paired observations of gravel content, bulk density, root biomass, carbon concentrations and nitrogen concentrations.

Surface litter carbon and nitrogen stocks were sampled in the three forested sites at the same 5 stations within a 75 by 115 cm quadrat by collecting leaves, stems, and branches smaller than 5 cm diameter. Woody material was separated by hand, dried at 60 °C, weighed, and recorded as fine woody debris. Non-woody material was similarly treated and recorded as non-woody surface litter. Coarse woody debris, defined as non-living woody material having a diameter of > 5 cm, was sampled with the transect method used by the U.S. Forest Inventory Analysis program (Woodall & Williams, 2005). Five 50 m transects were conducted in each experimental unit where intersected pieces meeting our definition were recorded for diameter, species, cardinal direction and decay class. Areal standing carbon stocks were then calculated according to Eq. 3.2 in Woodall & Williams, (2005).

Soil, fine root, non-woody surface litter, and fine woody surface litter samples were pulverized to less than 0.25 mm in a shatterbox in preparation for carbon and nitrogen concentration measurements (SPEX SamplePrep Shatterbox 8530, Metuchen, New Jersey USA). Elemental analysis by dry combustion was conducted with three analytical replicates (Costech ECS 4010 CHNSO Analyzer, Valencia, California, USA). Soil samples with inorganic carbonates present were identified by their excessive carbon to nitrogen ratio and checked for effervescence with HCl. These samples (14 of 2,200) were found in the > 50 cm depth increment and removed from the analysis.

Land surface albedo

Land surface albedo was measured for each experimental unit from 1984 to 2023 with the Landsat 5, 7, 8, and 9 satellites as well as the Sentinel 2A and 2B satellites following Wang et al.

(2017). Data were acquired from Google Earth Engine. For Sentinel 2, Level 1C top of atmosphere reflectances were processed to surface reflectance with the Sensor Invariant Atmospheric Correction method (Yin et al., 2022). Sentinel 2 clouds were detected with the s2cloudless method (Skakun et al., 2022). For Landsat, Level 2 surface reflectances were taken from Collection 2 Tier 1 which the United States Geologic Survey (USGS) certifies to meet inter-sensor calibration standards and < 12 m georegistration accuracy. These are the highest quality data available and lower quality data were not used. The mean georegistation accuracy at our site was 5.1 m. Accordingly, plot boundaries were shrunk in order for the USGS to certify that all pixels used in this analysis were wholly within the plot boundaries. For each overpass, the shrunk boundaries of each experimental unit were used to extract the mean surface reflectance of each band, as well as the associated quality control and metadata information. Observations with clouds, shadows, excessive aerosols and radiometric saturation were filtered out and the bands were combined into total shortwave reflectance using narrow to broadband coefficients (Bonafoni & Sekertekin, 2020; Liang, 2001).

Shortwave broadband albedo was calculated using the albedo:reflectance ratio technique (Shuai et al., 2011, 2014; Wang et al., 2017). Landsat and Sentinel surface reflectance data are provided without surface anisotropy corrections, which are necessary to estimate land surface albedo. The bidirectional reflectance distribution function (BRDF) was used for this correction. To obtain the parameters for the BRDF, adjacent representative pixels were taken from the MODIS albedo product during overpasses concurrent with the Landsat and Sentinel overpasses. The MCD43A1 V6.1 Bidirectional Reflectance Distribution Function and Albedo Model Parameters data product was acquired from the National Aeronautics and Space Administration's Application for Extracting and Exploring Analysis Ready Samples application programing

interface. Pre-MODIS era Landsat observations used the climatologically averaged BRDF parameters from the study site. The Landsat and/or Sentinel sun-sensor geometry, MODIS-derived BRDF parameters, and the diffuse radiation fraction are used to calculate the shortwave surface albedo and shortwave reflectance. The diffuse radiation fraction at the land surface level for the study site was obtained for the hour of each satellite over pass from the ERA5 data product produced by the European Centre for Medium-Range Weather Forecasts as distributed by the Copernicus Climate Change Service Climate Data Store (Hersbach et al., 2023). The resulting albedo:reflectance ratio is applied to the Landsat and Sentinel surface reflectance to calculate the land surface albedo at 30 and 20 m resolution, respectively. Between 2,817 and 5,546 albedo observations that passed all quality screening criteria were available for each land use, resulting in a total of 47,075 albedo observations measured from 1984 to 2023.

Woody biomass carbon stocks

Aboveground live woody biomass data for the NBCS and historical scenarios were extracted for the U.S. E.P.A. Level III Ecoregion 56 (Omernik & Griffith, 2014). The PIN and MS leveraged aboveground live woody biomass data from the U.S. Forest Inventory and Analysis program (Stanke et al., 2020). For the MS natural forest regeneration scenario, protected areas with no documented disturbance or artificial planting were stratified by stand age from 0-100 years to obtain the natural regeneration growth curve for the study region. A total of 439 plots and 717 plot years in the study region met these criteria and were used here. Similarly, for PIN, areas classified as northern pine plantations were stratified by stand age from 0-50 years. A total of 29 plots and 51 plot years in the study region met these criteria and were used here. Belowground live woody biomass and coarse woody debris estimates from these plots were extracted in parallel.

For the historical scenario, the original witness tree data from the U.S. Public Land Survey was collected for the region from 1828 to 1839 (Paciorek et al., 2021). In the study region, 10,229 survey points had 2 trees identified to species and measured for diameter at breast height, and 23,155 survey points had 4 trees identified and measured for a total of 113,643 trees used in this study. With the survey points typically spaced 0.8 km apart, we used the aggregated 8 km resolution Level 1 data that estimates total aboveground biomass on an areal basis as provided on the Data Observation Network for Earth application programing interface. This raw data was used for all analyses, however, for visualization purposes, we created a 1.6 km resolution map of the study region (Figure 2.1A). This was accomplished by regressing the aboveground biomass data with each variable in the SoilGrids250 database for the study region (Hengl et al., 2017). Belowground live woody biomass was calculated using the average aboveground:belowground ratio from the contemporary data described above (24 %) and a carbon concentration of 48 % was assumed.

Radiative forcing calculations and statistics

Radiative forcing calculations for each scenario used the annual SW_{out}^{toa} , CO₂, N₂O and CH₄ fluxes from the measurements described above as well as gas-specific atmospheric lifetimes and radiative efficiencies (Neubauer & Megonigal, 2015, 2019). The atmospheric lifetime of N₂O and CH₄ was modeled according to Eq. (1)

$$C_{i+1} = F_i + C_i * e^{(-\frac{1}{L})}$$
 Eq. (1)

Where C_i is the atmospheric concentration in the i^{th} year, F_i is the annual flux in the i^{th} year, and L is the atmospheric lifetime of the gas. The atmospheric lifetime of CO_2 was modeled according to Eq. (2).

$$C_{i+1} = \sum_{p=1}^{4} (f_p * F_i) + C_{i,p} * e^{(-\frac{1}{L_p})}$$
 Eq. (2)

Where C_i is the atmospheric concentration in the ith year, f_p is the fraction of emissions associated with each pool, F_i is the annual flux in the ith year, C_{i,p} is the atmospheric concentration of the pth pool in the ith year and L_p is the atmospheric lifetime of CO₂ in the pth pool. Radiative forcings for each gas were calculated as the product of the atmospheric concentration and the radiative efficiency. Constants for atmospheric lifetimes and pool fractions for Eqs. 1 and 2 can be found in Neubauer & Megonigal, 2015, 2019), as can the constants for the radiative efficiencies of each gas.

Annual fluxes were estimated with a separate statistical model for each component (e.g., land surface albedo, soil N₂O fluxes, etc.). For soil N₂O and CH₄ fluxes as well as land surface albedo, a generalized additive mixed effect model was fit with land use as a fixed effect, land use nested within block as a random intercept, and a continuous smooth function of month and year. Repeated measures were accounted for by fitting an autocorrelation structure of order 1, with a continuous time covariate for each land use nested within block. Assumptions of normal residuals and homogeneous variance were checked, and transformations of the response variables were performed as needed. These models were used to estimate the annual average fluxes for each experimental unit.

Annual CO₂ fluxes for each experimental unit were calculated as the sum of annual changes in each ecosystem carbon stock component, including soil, live biomass, and surface litter pools. A time series of carbon stocks was constructed for each scenario using our measured data and assumptions about the transition timeline. For the historical scenario, initial values for soil carbon stocks, as well as surface litter pools, were taken from the LS forest data at our site. Above and belowground live woody biomass carbon were taken from the original witness tree data described above. These components were assumed to transition to the conventional land use

in the region, for which we used the CON land use's measured carbon stocks. Soil and vegetation carbon stock changes were assumed to take place over 25 years. The vegetation transitions also impacted land surface albedo trajectories. For the NBCS scenarios, initial values for carbon stocks were assumed to be those measured in the CON land use. Each NBCS scenario's measured soil carbon stocks were assumed to be realized after a period of 25 years and unchanging after that. Herbaceous vegetation changes were assumed to happen over 2 years while the POP, PIN and MS vegetation changes were assumed to take place over 10, 50 and 100 years, respectively. The vegetation transitions also impacted land surface albedo trajectories. Transitions between carbon stocks and land surface albedo were assumed to be linear and were interpolated annually accordingly.

Once each carbon stock time series was constructed for each scenario, the total change in ecosystem carbon stocks each year was taken as the annual CO₂ flux to be used in the radiative forcing calculations. Both the historical and NBCS scenarios were assumed to take place on the vegetated area of U.S. E.P.A. Level III Ecoregion 56, which was 51.7 x 10⁹ m⁻². Final radiative forcing budget components as well as their net climate impacts were extracted for each experimental unit as the mean value during the 100 year time period. These final values were used as the response variable in a linear regression model with land use and budget component as fixed effects, including their interaction. Heterogeneous variance was specified for each budget component.

REFERENCES

- Andreae, M. O. (2019). Emission of trace gases and aerosols from biomass burning an updated assessment. *Atmospheric Chemistry and Physics*, *19*(13), 8523–8546. https://doi.org/10.5194/acp-19-8523-2019
- Bahlai, C. A., Colunga-Garcia, M., Gage, S. H., & Landis, D. A. (2013). Long-term functional dynamics of an aphidophagous coccinellid community remain unchanged despite repeated invasions. *PLoS ONE*, *8*(12), e83407. https://doi.org/10.1371/journal.pone.0083407
- Bonafoni, S., & Sekertekin, A. (2020). Albedo retrieval from Sentinel-2 by new narrow-to-broadband conversion coefficients. *IEEE Geoscience and Remote Sensing Letters*, 17(9), 1618–1622. https://doi.org/10.1109/LGRS.2020.2967085
- Colunga-Garcia, M., Gage, S. H., & Landis, D. A. (1997). Response of an assemblage of coccinellidae (coleoptera) to a diverse agricultural landscape. *Environmental Entomology*, 26(4), 797–804. https://doi.org/10.1093/ee/26.4.797
- Fargione, J. E., Bassett, S., Boucher, T., Bridgham, S. D., Conant, R. T., Cook-Patton, S. C.,
 Ellis, P. W., Falcucci, A., Fourqurean, J. W., Gopalakrishna, T., Gu, H., Henderson, B.,
 Hurteau, M. D., Kroeger, K. D., Kroeger, T., Lark, T. J., Leavitt, S. M., Lomax, G.,
 McDonald, R. I., ... Griscom, B. W. (2018). Natural climate solutions for the United
 States. Science Advances, 4(11), eaat1869. https://doi.org/10.1126/sciadv.aat1869
- Freckman, D. W., & Ettema, C. H. (1993). Assessing nematode communities in agroecosystems of varying human intervention. *Agriculture, Ecosystems & Environment*, 45(3–4), 239–261. https://doi.org/10.1016/0167-8809(93)90074-Y
- Gelfand, I., Shcherbak, I., Millar, N., Kravchenko, A. N., & Robertson, G. P. (2016). Long-term nitrous oxide fluxes in annual and perennial agricultural and unmanaged ecosystems in the upper Midwest USA. *Global Change Biology*, *22*(11), 3594–3607. https://doi.org/10.1111/gcb.13426
- Ghimire, B., Williams, C. A., Masek, J., Gao, F., Wang, Z., Schaaf, C., & He, T. (2014). Global albedo change and radiative cooling from anthropogenic land cover change, 1700 to 2005 based on MODIS, land use harmonization, radiative kernels, and reanalysis. *Geophysical Research Letters*, 41(24), 9087–9096. https://doi.org/10.1002/2014GL061671
- Griscom, B. W., Adams, J., Ellis, P. W., Houghton, R. A., Lomax, G., Miteva, D. A., Schlesinger, W. H., Shoch, D., Siikamäki, J. V., Smith, P., Woodbury, P., Zganjar, C., Blackman, A., Campari, J., Conant, R. T., Delgado, C., Elias, P., Gopalakrishna, T., Hamsik, M. R., ... Fargione, J. (2017). Natural climate solutions. *Proceedings of the National Academy of Sciences*, 114(44), 11645–11650. https://doi.org/10.1073/pnas.1710465114
- He, T., Liang, S., & Song, D. (2014). Analysis of global land surface albedo climatology and spatial-temporal variation during 1981–2010 from multiple satellite products. *Journal of Geophysical Research: Atmospheres*, 119(17). https://doi.org/10.1002/2014JD021667

- Helms, J. A., Smith, J., Clark, S., Knupp, K., & Haddad, N. M. (2021). Ant communities and ecosystem services in organic versus conventional agriculture in the U.S. Corn Belt. *Environmental Entomology*, 50(6), 1276–1285. https://doi.org/10.1093/ee/nvab105
- Hengl, T., Mendes De Jesus, J., Heuvelink, G. B. M., Ruiperez Gonzalez, M., Kilibarda, M., Blagotić, A., Shangguan, W., Wright, M. N., Geng, X., Bauer-Marschallinger, B., Guevara, M. A., Vargas, R., MacMillan, R. A., Batjes, N. H., Leenaars, J. G. B., Ribeiro, E., Wheeler, I., Mantel, S., & Kempen, B. (2017). SoilGrids250m: Global gridded soil information based on machine learning. *PLOS ONE*, 12(2), e0169748. https://doi.org/10.1371/journal.pone.0169748
- Hersbach, H., Bell, B., & Berrisford, P., Biavati, G., Horányi, A., Muñoz Sabater, J., Nicolas, J., Peubey, C., Radu, R., Rozum, I., Schepers, D., Simmons, A., Soci, C., Dee, D., Thépaut, J-N. (2023). *ERA5 hourly data on single levels from 1940 to present*. Copernicus Climate Change Service Climate Data Store. https://doi.org/10.24381/CDS.ADBB2D47
- Hurtt, G. C., Chini, L., Sahajpal, R., Frolking, S., Bodirsky, B. L., Calvin, K., Doelman, J. C., Fisk, J., Fujimori, S., Klein Goldewijk, K., Hasegawa, T., Havlik, P., Heinimann, A., Humpenöder, F., Jungclaus, J., Kaplan, J. O., Kennedy, J., Krisztin, T., Lawrence, D., ... Zhang, X. (2020). Harmonization of global land use change and management for the period 850–2100 (LUH2) for CMIP6. *Geoscientific Model Development*, *13*(11), 5425–5464. https://doi.org/10.5194/gmd-13-5425-2020
- Jia, G., Shevliakova, E., Artaxo, N., De Noblet-Ducoudré, R., & Houghton, J. (2019). Land-climate interactions. In: Climate Change and Land: An IPCC special report on climate change, desertification, land degradation, sustainable land management, food security, and greenhouse gas fluxes in terrestrial ecosystems. Cambridge University Press. https://doi.org/10.1017/9781009157988
- Kemmerling, L. R., McCarthy, A. C., Brown, C. S., & Haddad, N. M. (2023). Butterfly biodiversity increases with prairie strips and conservation management in row crop agriculture. *Insect Conservation and Diversity*, *16*(6), 828–837. https://doi.org/10.1111/icad.12675
- Kravchenko, A. N., & Robertson, G. P. (2011). Whole-profile soil carbon stocks: The danger of assuming too much from analyses of too little. *Soil Science Society of America Journal*, 75(1), 235–240. https://doi.org/10.2136/sssaj2010.0076
- Kravchenko, A. N., Snapp, S. S., & Robertson, G. P. (2017). Field-scale experiments reveal persistent yield gaps in low-input and organic cropping systems. *Proceedings of the National Academy of Sciences*, *114*(5), 926–931. https://doi.org/10.1073/pnas.1612311114
- Levine, U. Y., Teal, T. K., Robertson, G. P., & Schmidt, T. M. (2011). Agriculture's impact on microbial diversity and associated fluxes of carbon dioxide and methane. *The ISME Journal*, *5*(10), 1683–1691. https://doi.org/10.1038/ismej.2011.40

- Liang, S. (2001). Narrowband to broadband conversions of land surface albedo I. *Remote Sensing of Environment*, 76(2), 213–238. https://doi.org/10.1016/S0034-4257(00)00205-4
- Luehmann, M. D., Peter, B. G., Connallon, C. B., Schaetzl, R. J., Smidt, S. J., Liu, W., Kincare, K. A., Walkowiak, T. A., Thorlund, E., & Holler, M. S. (2016). Loamy, two-storied soils on the outwash plains of southwestern lower Michigan: pedoturbation of loess with the underlying sand. *Annals of the American Association of Geographers*, 106(3), 551–572. https://doi.org/10.1080/00045608.2015.1115388
- McNamara, N. P., Gregg, R., Oakley, S., Stott, A., Rahman, Md. T., Murrell, J. C., Wardle, D. A., Bardgett, R. D., & Ostle, N. J. (2015). Soil methane sink capacity response to a long-term wildfire chronosequence in northern Sweden. *PLOS ONE*, *10*(9), e0129892. https://doi.org/10.1371/journal.pone.0129892
- Morris, S. J., Bohm, S., Haile-Mariam, S., & Paul, E. A. (2007). Evaluation of carbon accrual in afforested agricultural soils. *Global Change Biology*, *13*(6), 1145–1156. https://doi.org/10.1111/j.1365-2486.2007.01359.x
- Necpalova, M., Anex, R. P., Kravchenko, A. N., Abendroth, L. J., Del Grosso, S. J., Dick, W. A., Helmers, M. J., Herzmann, D., Lauer, J. G., Nafziger, E. D., Sawyer, J. E., Scharf, P. C., Strock, J. S., & Villamil, M. B. (2014). What does it take to detect a change in soil carbon stock? A regional comparison of minimum detectable difference and experiment duration in the north central United States. *Journal of Soil and Water Conservation*, 69(6), 517–531. https://doi.org/10.2489/jswc.69.6.517
- Neubauer, S. C., & Megonigal, J. P. (2015). Moving beyond global warming potentials to quantify the climatic role of ecosystems. *Ecosystems*, 18(6), 1000–1013. https://doi.org/10.1007/s10021-015-9879-4
- Neubauer, S. C., & Megonigal, J. P. (2019). Correction to: Moving beyond global warming potentials to quantify the climatic role of ecosystems. *Ecosystems*, 22(8), 1931–1932. https://doi.org/10.1007/s10021-019-00422-5
- Omernik, J. M., & Griffith, G. E. (2014). Ecoregions of the conterminous United States: Evolution of a hierarchical spatial framework. *Environmental Management*, *54*(6), 1249–1266. https://doi.org/10.1007/s00267-014-0364-1
- Paciorek, C. J., Cogbill, C. V., Peters, J. A., Williams, J. W., Mladenoff, D. J., Dawson, A., & McLachlan, J. S. (2021). The forests of the midwestern United States at Euro-American settlement: Spatial and physical structure based on contemporaneous survey data. *PLOS ONE*, 16(2), e0246473. https://doi.org/10.1371/journal.pone.0246473
- Robertson, B. A., Doran, P. J., Loomis, L. R., Robertson, J. R., & Schemske, D. W. (2011). Perennial biomass feedstocks enhance avian diversity: Biomass feedstocks and avian diversity. *GCB Bioenergy*, *3*(3), 235–246. https://doi.org/10.1111/j.1757-1707.2010.01080.x

- Robertson, B. A., Porter, C., Landis, D. A., & Schemske, D. W. (2012). Agroenergy crops influence the diversity, biomass, and guild structure of terrestrial arthropod communities. *BioEnergy Research*, *5*(1), 179–188. https://doi.org/10.1007/s12155-011-9161-3
- Robertson, G. P., & Hamilton, S. K. (2015). Conceptual and experimental approaches to understanding agricultural ecosystems. In: Hamilton SK, Doll JE, Robertson GP (eds) The ecology of agricultural landscapes: Long-term research on the path to sustainability. Oxford University Press, New York.
- Robertson, G. P., Hamilton, S. K., Paustian, K., & Smith, P. (2022). Land-based climate solutions for the United States. *Global Change Biology*, *28*(16), 4912–4919. https://doi.org/10.1111/gcb.16267
- Robertson, G. P., Paul, E. A., & Harwood, R. R. (2000). Greenhouse gases in intensive agriculture: contributions of individual gases to the radiative forcing of the atmosphere. *Science*, 289(5486), 1922–1925. https://doi.org/10.1126/science.289.5486.1922
- Robertson, G. P., & Tiedje, J. M. (1984). Denitrification and nitrous oxide production in successional and old-growth Michigan forests. *Soil Science Society of America Journal*, 48(2), 383–389. https://doi.org/10.2136/sssaj1984.03615995004800020032x
- Roe, S., Streck, C., Obersteiner, M., Frank, S., Griscom, B., Drouet, L., Fricko, O., Gusti, M., Harris, N., Hasegawa, T., Hausfather, Z., Havlík, P., House, J., Nabuurs, G.-J., Popp, A., Sánchez, M. J. S., Sanderman, J., Smith, P., Stehfest, E., & Lawrence, D. (2019). Contribution of the land sector to a 1.5 °C world. *Nature Climate Change*, *9*(11), 817–828. https://doi.org/10.1038/s41558-019-0591-9
- Shuai, Y., Masek, J. G., Gao, F., & Schaaf, C. B. (2011). An algorithm for the retrieval of 30-m snow-free albedo from Landsat surface reflectance and MODIS BRDF. *Remote Sensing of Environment*, 115(9), 2204–2216. https://doi.org/10.1016/j.rse.2011.04.019
- Shuai, Y., Masek, J. G., Gao, F., Schaaf, C. B., & He, T. (2014). An approach for the long-term 30-m land surface snow-free albedo retrieval from historic Landsat surface reflectance and MODIS-based a priori anisotropy knowledge. *Remote Sensing of Environment*, 152, 467–479. https://doi.org/10.1016/j.rse.2014.07.009
- Skakun, S., Wevers, J., Brockmann, C., Doxani, G., Aleksandrov, M., Batič, M., Frantz, D., Gascon, F., Gómez-Chova, L., Hagolle, O., López-Puigdollers, D., Louis, J., Lubej, M., Mateo-García, G., Osman, J., Peressutti, D., Pflug, B., Puc, J., Richter, R., ... Žust, L. (2022). Cloud Mask Intercomparison eXercise (CMIX): An evaluation of cloud masking algorithms for Landsat 8 and Sentinel-2. *Remote Sensing of Environment*, 274, 112990. https://doi.org/10.1016/j.rse.2022.112990
- Smith, R., Mcswiney, C., Grandy, A., Suwanwaree, P., Snider, R., & Robertson, G. (2008). Diversity and abundance of earthworms across an agricultural land-use intensity gradient. *Soil and Tillage Research*, 100(1–2), 83–88. https://doi.org/10.1016/j.still.2008.04.009

- Stanke, H., Finley, A. O., Weed, A. S., Walters, B. F., & Domke, G. M. (2020). rFIA: An R package for estimation of forest attributes with the US Forest Inventory and Analysis database. *Environmental Modelling & Software*, *127*, 104664. https://doi.org/10.1016/j.envsoft.2020.104664
- Syswerda, S. P., Corbin, A. T., Mokma, D. L., Kravchenko, A. N., & Robertson, G. P. (2011). Agricultural management and soil carbon storage in surface vs. Deep layers. *Soil Science Society of America Journal*, 75(1), 92–101. https://doi.org/10.2136/sssaj2009.0414
- Tatina, R. (2016). Forty years of change in the composition of the forest at Robinson Woods Preserve, Berrien County, Michigan. *The Michigan Botanist*, 55, 2–17.
- Tatina, R. (2021). Succession from pasture to forest in a mesic southern forest in Michigan, USA. *Natural Areas Journal*, 41(1). https://doi.org/10.3375/043.041.0104
- Thornton, M. M., Shrestha, R., Wei, Y., Thornton, P. E., Kao, S.-C., & Wilson, B. E. (2022). Daymet: Daily surface weather data on a 1-km grid for North America, Version 4 R1. ORNL DAAC, Oak Ridge, Tennessee, USA. https://doi.org/10.3334/ORNLDAAC/2129
- Wang, Z., Schaaf, C. B., Sun, Q., Kim, J., Erb, A. M., Gao, F., Román, M. O., Yang, Y., Petroy, S., Taylor, J. R., Masek, J. G., Morisette, J. T., Zhang, X., & Papuga, S. A. (2017). Monitoring land surface albedo and vegetation dynamics using high spatial and temporal resolution synthetic time series from Landsat and the MODIS BRDF/NBAR/albedo product. *International Journal of Applied Earth Observation and Geoinformation*, *59*, 104–117. https://doi.org/10.1016/j.jag.2017.03.008
- Wickings, K., & Grandy, A. S. (2013). Management intensity interacts with litter chemistry and climate to drive temporal patterns in arthropod communities during decomposition. *Pedobiologia*, *56*(2), 105–112. https://doi.org/10.1016/j.pedobi.2013.01.001
- Woodall, C., & Williams, M. S. (2005). Sampling protocol, estimation, and analysis procedures for the down woody materials indicator of the FIA program. USDA Forest Service, North Central Research Station.
- Yin, F., Lewis, P. E., & Gómez-Dans, J. L. (2022). Bayesian atmospheric correction over land: Sentinel-2/MSI and Landsat 8/OLI. *Geoscientific Model Development*, 15(21), 7933–7976. https://doi.org/10.5194/gmd-15-7933-2022

APPENDIX A: CHAPTER 2 TABLES AND FIGURES

Table 2.1. Radiative forcing components for each scenario (mean \pm s.e.). Letters denote statistical differences between scenarios within a component. Positive values indicate a warming effect and negative values indicate a cooling effect.

Scenario	CO_2	Albedo	N_2O	CH ₄	Net
	$\mu W m^{-2}$				
Conventional	$0 \pm 51 e$	$0 \pm 4 bc$	0 ± 5 bc	$0 \pm 2 b$	$0 \pm 50 e$
No tillage	$-66 \pm 51 \text{ e}$	$-8 \pm 4 b$	12 ± 5 c	$0 \pm 2 b$	$-62 \pm 50 \text{ de}$
Reduced input	$-49 \pm 51 \text{ e}$	11 ± 4 c	8 ± 5 c	7 ± 2 c	$-23 \pm 50 \text{ e}$
Organic	$-109 \pm 51 \text{ de}$	$26\pm4\ d$	$28 \pm 5 \ d$	7 ± 2 c	$-48 \pm 50 \text{ de}$
Alfalfa	$-224 \pm 51 \text{ cd}$	$2 \pm 4 bc$	$46 \pm 5 e$	$-2 \pm 2 b$	$-179 \pm 50 \text{ d}$
Poplar plantation	$-353 \pm 51 \text{ c}$	$74\pm4\ e$	$-42 \pm 5 a$	$0 \pm 2 b$	$-322 \pm 50 \text{ c}$
Pine plantation	$-980 \pm 72 \text{ b}$	$310 \pm 6 \; h$	$0 \pm 7 \ bc$	$-23 \pm 2 \text{ a}$	$-693 \pm 71 \text{ b}$
Early succession	$-255 \pm 51 \text{ c}$	$154 \pm 4 \ f$	$-13 \pm 5 b$	$95 \pm 2 e$	$-18 \pm 50 \text{ e}$
Mid succession	$-1508 \pm 72 \text{ a}$	$226 \pm 6 \text{ g}$	-47 ± 7 a	$-29 \pm 2 \text{ a}$	$-1359 \pm 71 \text{ a}$
Historical	$2165 \pm 72 \text{ f}$	-412 ± 6 a	$63 \pm 7 \text{ f}$	$35 \pm 2 d$	$1851 \pm 71 \text{ f}$

Table 2.2. Ecosystem carbon stock components for each scenario (mean \pm s.e.). The values for the NBCS represent the mean over the 100-year duration of each scenario. The live woody component contains both aboveground and belowground live coarse woody biomass. The surface litter component contains coarse and fine woody debris, as well as non-woody surface litter. Letters denote statistical differences between scenarios within components.

Scenario	Live woody	Soil	Surface litter	Fine root	Total
			Mg C ha ⁻¹		
Conventional		$43.1 \pm 2.2 \text{ a}$	$2.1 \pm 0.5 \text{ a}$	0.1 ± 0.1 a	$47.8 \pm 1.6 \text{ a}$
No tillage		$47.6 \pm 2.3 \text{ bc}$	$2.1 \pm 0.5 \text{ a}$	$0.1 \pm 0.1 \; a$	$52.3 \pm 1.8 \text{ ab}$
Reduced input		$46.7 \pm 2.3 \text{ ab}$	$2.1 \pm 0.5 \text{ a}$	0.1 ± 0.1 a	$51.3 \pm 1.7 \text{ ab}$
Organic		$50.3 \pm 2.5 \text{ bcd}$	$2.1 \pm 0.5 \text{ a}$	$0.3 \pm 0.1 \text{ a}$	$55.3 \pm 1.9 \text{ b}$
Alfalfa		52.4 ± 2.6 cde	$1.6 \pm 0.5 \text{ a}$		62.4 ± 2.1 c
Poplar plantation	$10.3 \pm 0.2 \text{ a}$	$53.7 \pm 2.6 \text{ de}$	$1.6 \pm 0.5 \text{ a}$	2.2 ± 0.3 b	$70.9 \pm 2.4 d$
Pine plantation	$38.9 \pm 0.4 \text{ b}$	51.2 ± 3.1 bcde	$16.7 \pm 2.1 \text{ b}$	$3.9 \pm 0.5 \; c$	$113.7 \pm 5.4 \text{ e}$
Early succession		$56.6 \pm 2.8 \text{ ef}$	$1.6 \pm 0.5 \text{ a}$	$3.7 \pm 0.3 \text{ c}$	$64.7 \pm 2.2 \text{ cd}$
Mid succession	$61.8 \pm 0.5 \text{ c}$	$50.0 \pm 3.0 \text{ bcde}$	$22 \pm 2.4 \text{ b}$	$3.6 \pm 0.5 \text{ c}$	$139.9 \pm 6.6 \text{ f}$

 $62.9 \pm 4.0 \text{ f}$

 $29.9 \pm 2.8 \text{ c}$

 8.1 ± 0.7 e

 $196.1 \pm 9.3 \text{ g}$

Historical

 $90.2 \pm 0.9 d$

Table 2.3. Soil CH₄ and N₂O fluxes as well as top of atmosphere outgoing shortwave radiation (SW_{out}^{toa}) for each scenario (mean \pm s.e.). Positive values indicate emissions to the atmosphere and negative values indicate removals from the atmosphere. Letters denote statistical differences between scenarios for each column.

Scenario	CH ₄	N_2O	Albedo
	kg CH4 ha ⁻¹ y ⁻¹	kg N2O ha ⁻¹ y ⁻¹	SW _{out} to a W m ⁻²
Conventional	$-0.6 \pm 0.1 \text{ de}$	$1.3 \pm 0.1 \text{ c}$	$15.4 \pm 0.1 \text{ fg}$
No tillage	$-0.6 \pm 0.1 \text{ de}$	$1.5 \pm 0.1 \text{ cd}$	$15.5 \pm 0.1 \text{ g}$
Reduced input	$-0.5 \pm 0.1 \text{ de}$	$1.4 \pm 0.1 \text{ cd}$	$15.3 \pm 0.1 \text{ ef}$
Organic	$-0.5 \pm 0.1 \text{ e}$	$1.7 \pm 0.1 \text{ de}$	15.1 ± 0.1 e
Alfalfa	$-0.8 \pm 0.1 \text{ c}$	$2.0 \pm 0.1 e$	$15.4 \pm 0.1 \text{ fg}$
Poplar plantation	$-0.6 \pm 0.1 \text{ de}$	$0.7 \pm 0.1 \ b$	$13.9 \pm 0.1 d$
Pine plantation	$-3.0 \pm 0.7 \text{ ab}$	$1.3 \pm 0.1 \text{ c}$	$9.3 \pm 0.1 \text{ a}$
Early succession	$-0.7 \pm 0.1 \text{ cd*}$	$0.5 \pm 0.1 \ a^*$	$13.9 \pm 0.1 d$
Mid succession	$-2.9 \pm 0.1 \text{ b}$	$0.8 \pm 0.1 \text{ b}$	12.1 ± 0.1 c
Historical	-3.7 ± 0.1 a	$0.6 \pm 0.1 \text{ ab}$	$10.9 \pm 0.1 \text{ b}$

^{*}Biomass burning emissions of 10.1 kg CH₄ ha⁻¹ y⁻¹ and 0.6 kg N₂O ha⁻¹ y⁻¹ are not included in the table values.

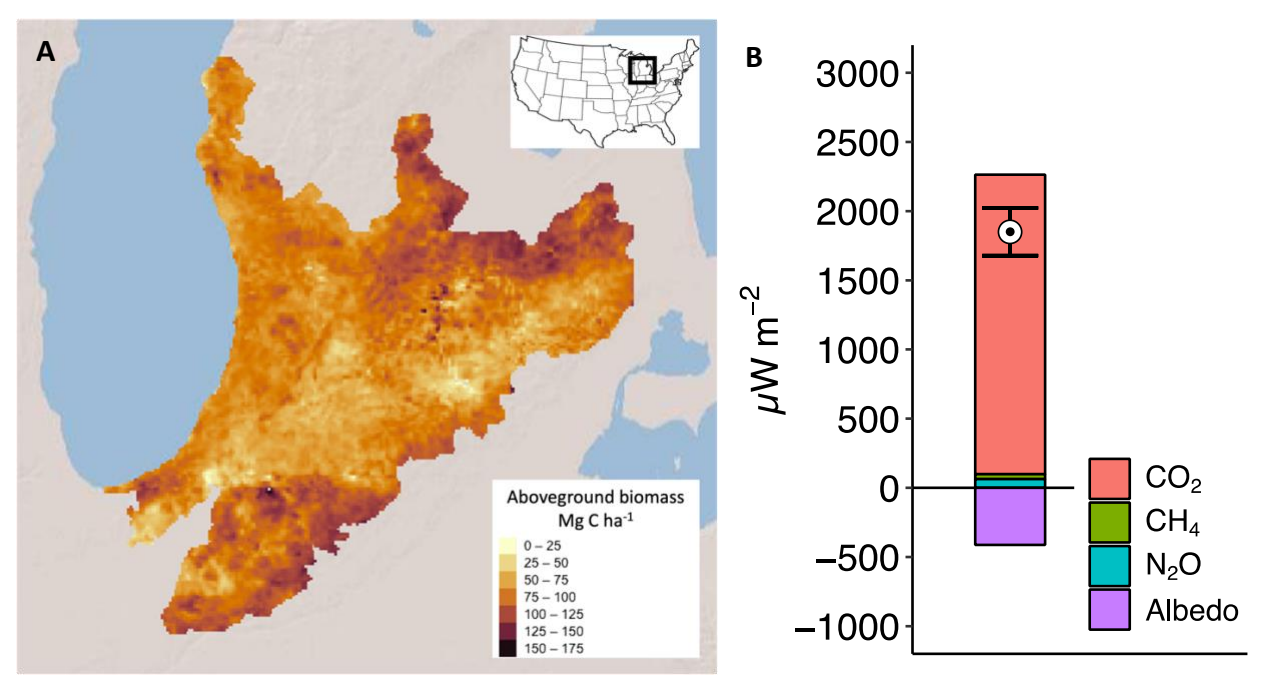


Figure 2.1. A) Original witness tree aboveground biomass data from the U.S. Public Land Survey for the study region, U.S. EPA Level III Ecoregion 56, that occurred from 1828 to 1839. B) Each component of the radiative forcing budget from the historical land use change scenario. The encircled point represents the net effect of all components (mean \pm s.e). Positive values indicate a warming effect and negative values indicate a cooling effect.

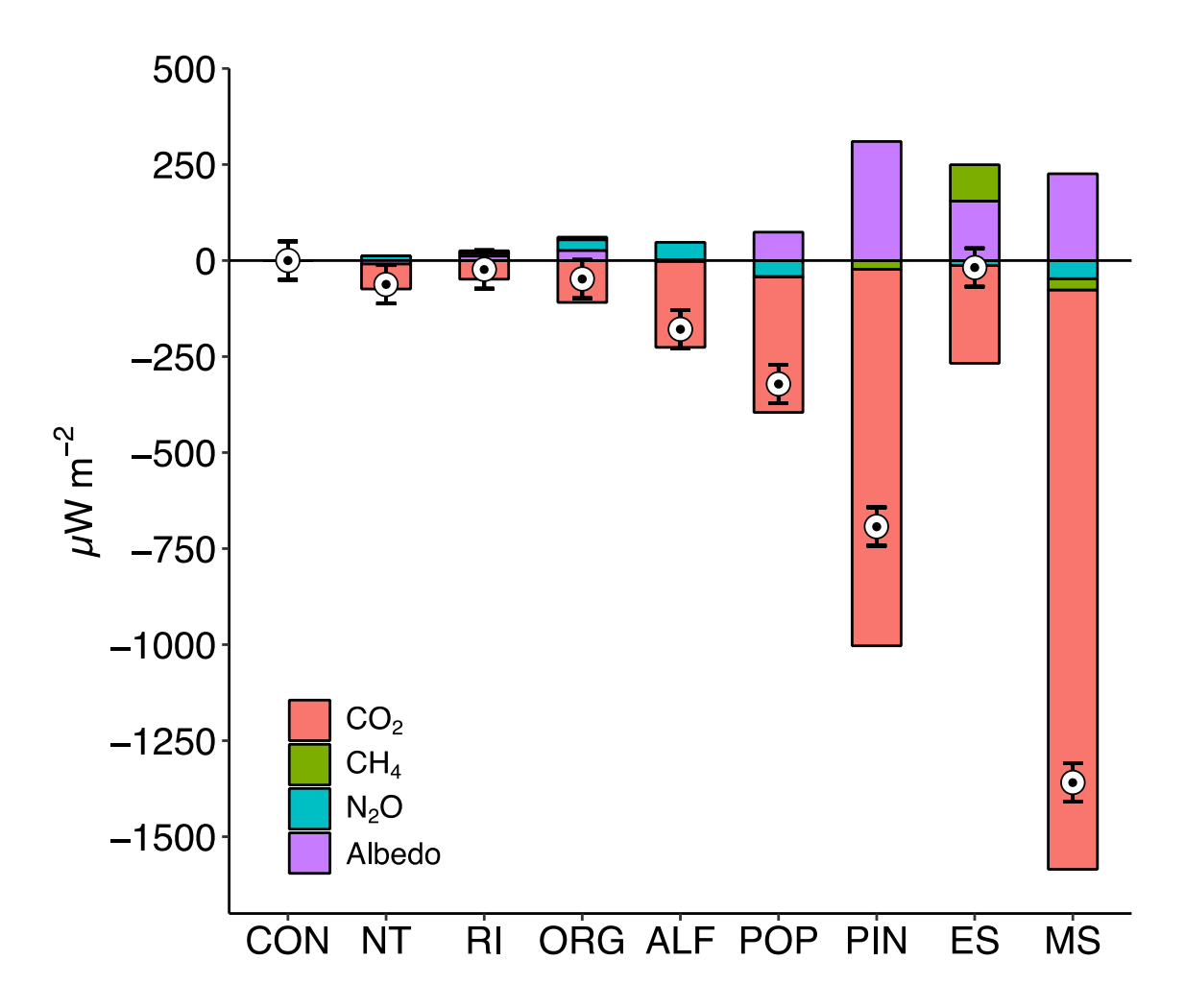


Figure 2.2. Annual average radiative forcing for each land use and component over the 100-year time period for the NBCS scenarios. Encircled points show the net radiative forcing of each land use (mean \pm s.e.). Positive values indicate a warming effect and negative values indicate a cooling effect.

CHAPTER 3: Land use mediates the response of soil CH₄, N₂O and CO₂ fluxes to changing precipitation regimes

Abstract

As climate change alters precipitation regimes, resulting changes to soil water content may alter patterns of soil greenhouse gas fluxes and these responses may be different across diverse land uses. Here we show how 3 years of experimentally induced drought or increased precipitation variability differentially affect soil CH₄, N₂O, and CO₂ fluxes in conventionally tilled row crops (CON), no-till row crops (NT) and an early successional plant community (ES). Soil CH₄ oxidation rates were strengthened during periods of drought relative to irrigated control plots, especially in the ES (-7.33 vs -6.90 g CH₄ ha⁻¹ d⁻¹, respectively, p <0.01) and NT (-3.33 vs -2.67 g CH₄ ha⁻¹ d⁻¹, respectively, p < 0.01) systems. In contrast, soil N₂O fluxes were diminished during drought, with emissions significantly reduced (p < 0.04) in the CON, NT, and ES land uses by 49%, 57% and 31%, respectively. Heterotrophic CO₂ fluxes from soil, as measured in situ following winter wheat harvest when plants were absent, were resilient to drought where depressed rates during the drought were fully compensated by higher rates following rewetting. This episodic response of soil heterotrophic respiration to precipitation events could be important to represent in Earth system models as strict dependence of soil heterotrophic respiration on soil water content would underpredict respiration immediately following drought.

Introduction

Soil greenhouse gas fluxes are a globally significant regulator of the Earth's climate. Heterotrophic respiration rates and net primary production (55.9 ± 1.1 Pg C y⁻¹) roughly balanced each other during the Holocene, helping to maintain a relatively stable atmospheric CO₂ concentration and climate (Beyer et al., 2020; Friedlingstein et al., 2023; Osman et al., 2021; Richardson et al., 2023). Natural sources of N₂O and CH₄ also kept pace with their abiotic oxidation rates in the atmosphere, contributing to relatively low variability in atmospheric concentrations during the Holocene when compared with recent anthropogenic increases (Flückiger et al., 2002; Saunois et al., 2020; Schilt et al., 2010; Tian et al., 2020; Yang et al., 2017).

Soil water content is a key driver of CH₄, N₂O, and CO₂ fluxes (Falloon et al., 2011; Oertel et al., 2016; Smith et al., 2003). As the climate changes, precipitation patterns are shifting and causing cascading effects on soil moisture (Berg et al., 2017; Marvel et al., 2021). In the midwestern United States, Earth system model projections for soil moisture under Shared Socioeconomic Pathway 3-7.0 suggest that a one-in-ten year summer drought may become as frequent as one in three years (Cook et al., 2020).

Furthermore, changes to the quantity and distribution of precipitation events as well as changes in evaporative conditions may result in non-linear responses of soil water content (Li et al., 2021; Rastogi et al., 2024; Zhao et al., 2023). The partitioning of precipitation into interception, overland flow, infiltration, evaporation, transpiration, and deep percolation is a multifaceted and interrelated set of processes. Each step can respond to changing precipitation regimes in non-linear ways. For example, overland flow does not become significant until a

threshold in infiltration capacity is passed. Similarly, transpiration can stop if plants die during a drought, so transpiration may not recover even when precipitation returns.

The microorganisms responsible for soil CH₄, N₂O and CO₂ fluxes can also respond to a wide array of biotic and abiotic factors that change along with soil water content (Groffman & Tiedje, 1988; Schimel, 2018; Sokol et al., 2022). Crucially, when thresholds in cell water potential are passed, loss of turgor pressure and osmotic stress can cause cell death, halting the metabolic transformations necessary for greenhouse gas fluxes. When soils are wet, gas transport can slow to the point of oxygen deprivation, constraining aerobic metabolism and promoting anaerobic metabolism. Soil N2O production generally increases with soil water content, but complete denitrification of N₂O to N₂ proceeds more readily in saturated conditions (Robertson and Groffman, 2024). Nitrogen-climate interactions can be non-intuitive, and therefore a systems-level understanding is necessary, and better quantitative models require better data informed by experiments like this one (Robertson et al., 2013). For CH₄ oxidation, rates slow as gas diffusion becomes limiting during saturating conditions and methanogens can begin to dominate, potentially shifting upland soils from a sink to a source (Nazaries et al., 2013). During drying conditions, CH₄ oxidation rates can decline when soils are too dry to support methanotrophs (Blankinship et al., 2010; Tate, 2015; Van Den Pol-van Dasselaar et al., 1998; Voigt et al., 2023).

Studies that investigate the effect of soil water content on greenhouse gas fluxes are often carried out in microcosms. While these studies can provide mechanistic detail, they may not fully capture ecosystem scale dynamics not easily represented in microcosms. Field studies that experimentally manipulate precipitation are needed capture the complex feedbacks caused by the differential distribution of precipitation through soils and to measure their interactions with soil

greenhouse gas fluxes. Land use can mediate how precipitation is partitioned in soil and also affect the other biogeochemical factors involved in soil greenhouse gas fluxes, such as organic matter availability, physical soil disturbance and vegetation water use.

Here we present results from a 3-year precipitation manipulation experiment where we simulated both a six-week growing season drought and an increase in precipitation variability and measured subsequent effects on soil CH₄, N₂O and CO₂ fluxes. We conducted this experiment in a tilled row crop, no-till row crop, and early successional plant community. For CO₂ we hypothesize that heterotrophic respiration will exhibit a strict dependence on soil water content until large precipitation events cause higher than expected fluxes. We hypothesize that N₂O emissions will also follow this pattern. For CH₄ we hypothesize that drought will cause an overall increase in oxidation rates, presumably due to the increased diffusion of CH₄ through air-filled pore space; however, we expect that very dry soils will lose this sink strength as methanotrophs succumb to water stress.

Methods

Study site

This experiment was conducted at the W.K. Kellogg Biological Station Long Term Ecological Research site in southwestern Michigan, USA (42.4 N, 85.4 W). The mean annual precipitation is 1067 mm and the mean annual surface air temperature is 9.3 °C (Thornton et al., 2022). During the growing season, from April through October, the mean weekly precipitation is 24.1 mm (Thornton et al., 2022). Soils are well drained fine-loamy, mixed, active, mesic Typic Hapludalfs and consists of loamy glacial outwash overlying sand (Luehmann et al., 2016). The Main Cropping System Experiment (MCSE) at the site is a replicated land use change experiment established in 1989 (Robertson & Hamilton, 2015).

In this study we used three of the land use treatments in the MCSE. The Conventional (CON) and No-till (NT) row crop land uses are managed as a soybean, winter wheat, and corn rotation that includes the use of synthetic N fertilizer and herbicides. We also used the Early Successional (ES) treatment, which is managed only with annual prescribed fire each Spring. Each land use treatment is replicated six times in 1 ha sized plots in a randomized complete block design. We used four of these replicates for the CON and NT land use treatments. For the ES land use we used all six replicates as ES has considerably higher spatial variation in plant community composition.

The study took place from 2021 to 2023. In each plot, three 4 by 5 m rain exclusion shelters (Kahmark et al., 2024) were deployed each year during the growing season. Each shelter had plastic roofing to allow light but not precipitation to penetrate. Overhead irrigation sprinklers were controlled by electric pumps connected to closed tanks filled weekly with local groundwater. The shelters were managed to provide three precipitation treatments: a 1-Week irrigation schedule to reflect historical rainfall patterns (one 31 mm event per week), a 3-Week irrigation schedule to represent increased precipitation variability (one 92 mm event every 3rd week), and a 6-week drought. The three weeks preceding the 6-week drought were irrigated as in the 1-Week precipitation treatment. Over the 9-week period when the shelters were in place, the 6-week drought received a rainfall deficit of 66% relative to the other treatments (82 mm in the drought vs 240 mm in the 1-Week precipitation treatments). Partway through the 2021 and 2022 but not 2023 rainfall exclusion periods there was an unexpectedly large rainfall event that caused significant overland flow into some of the plots. Observations made in these plots after these two events were removed from the analysis.

Soil gas fluxes

Soil gas fluxes were measured weekly during the growing season with static chambers 28 cm in diameter that were inserted 2 cm into the soil of each plot (Gelfand et al., 2016; Kahmark et al., 2020). During measurements, chambers were fitted with a lid that had ports for incoming and outgoing gas streams in order to circulate headspace with a diaphragm pump at 500 mL per minute (KNF N920, Metuchen NJ, USA) to a laser absorption-based gas analyzer (Los Gatos Research GLA351-N2OM1, Quebec City, Quebec, CA) that measured N2O and CH4. The same stream was passed through an infrared gas analyzer to measure CO₂ (LI-830, LICOR, Lincoln, Nebraska, USA). After a two-minute period for equilibration, the change in concentration of each gas was recorded at 1Hz for seven minutes, followed by a one-minute flushing procedure between plots. Areal fluxes were calculated with the ideal gas law and assumed to represent the daily flux. In situ soil CO₂ fluxes were only used in the CON and NT land uses and only in 2022 after winter wheat was harvested. There were no plants present in these plots at this time, allowing for the isolation of soil heterotrophic respiration. One large rainfall event in 2021 and 2022 occurred when the shelters were in place and caused significant overland flow into some of the plots. Observations made after these events in the affected plots were removed from this analysis. A total of 994 fluxes were used in this study.

Soil water content and C and N mineralization

Soil volumetric water content was measured every hour with 30 cm long Campbell Scientific CS650 probes that were angled to measure the top 25 cm of the soil (Logan, UT, USA). One probe installed in the center of each plot. Separately, soil samples (0-25 cm) were collected with a 2.5 cm diameter probe from each plot the week prior to the end of the drought. The samples were immediately sieved to 2 mm and a 20 g subsample was placed in a 60 °C oven

to measure its gravimetric water content. A separate 40 g subsample was placed in a glass jar fitted loosely with a lid to allow gas exchange and to minimize moisture loss. The jars were placed in an incubator at 25 °C and 80 % relative humidity overnight. The following day lids with rubber septa were secured to initiate the accumulation of CO₂ in the headspace. Over the course of 1.5 h four 1 mL headspace samples were removed and injected into an infrared gas analyzer (LI-830, LICOR, Nebraska, USA) via a stream of N₂ carrier gas. The change in concentration over time was used with the ideal gas law and the soil moisture content to express the potential soil respiration rate as μg CO₂ g dry soil⁻¹ d⁻¹.

From the same sieved soil sample two 10 g samples were extracted with 100 mL of 1M KCl for NH₄⁺ and NO₃⁻ determinations. The mixture was shaken for 60 s, allowed to sit overnight, shaken again for 60 s, allowed to sit for 1 h, and then passed through a 1 μm glass fiber filter (Whatman, Boston, MA, USA) to remove soil particles. To measure net nitrogen (N) mineralization the jars described above were incubated for 14 days, after which two 10 g subsamples were similarly extracted in KCl. Extracts were frozen until analysis on a Lachat QuickChem 8500 Series 2 Flow Injection Analysis System (Hach, Loveland CO, USA) for NH₄⁺ and NO₃⁻. The difference in NH₄⁺-N plus NO₃⁻-N concentrations between samples before and after the 14 day incubation were used as a measure of net N mineralization, expressed as ng N g dry soil⁻¹ d⁻¹.

Statistical analysis

This experiment follows a split plot design with the three land use treatments as the whole plot factor and the precipitation treatment as the subplot factor. The whole plots are arranged in a randomized block design. Soil gas flux measurements were analyzed with generalized additive mixed effect models (Wood, 2017). Land use was included as a fixed effect

in the model and whole plot was included as a random effect. To account for the repeated measurements at each plot an autocorrelation structure of order 1 was fitted with a continuous time covariate for each plot. To test our hypotheses about the dependence of soil gas fluxes on soil water content we supplied the measured 0-25 cm volumetric water contents as a continuous covariate. This term was included as a smooth function with a minimized number of thin plate regression spline basis functions to ensure a monotonic response and was allowed to vary in shape for each land use treatment. To test our hypothesis about the strict dependence of fluxes on soil volumetric water content, an identical model was fit with an added continuous variable that counts the days since the last precipitation event of at least 5 mm d⁻¹ in size (up to 7 days). This term was fit with a smooth function with a minimized number of thin plate regression spline basis functions to ensure a monotonic response and was allowed to vary in shape for each land use treatment. If the addition of this days since precipitation term significantly improved the model as measured by Akaike's Information Criterion we rejected the hypothesis that the fluxes exhibit a strict dependence on soil water content.

As is common in other N₂O flux studies, our N₂O data were skewed, with many low emission observations and few high emission observations. A Tweedie distribution was used for the N₂O model to achieve satisfactory compliance with model assumptions (Tweedie, 1984). Normality of the residuals and homogeneity of variance across treatment groups were checked. Furthermore, the addition of synthetic N fertilizer in the winter wheat and corn phases of the row crop rotations significantly impacted N₂O emissions. It was therefore important to include an additional model term for fertilization rate and timing. Rate was applied as a continuous variable (50 kg N ha⁻¹ for winter wheat and 150 kg N ha⁻¹ for corn) as was timing (days since

application). These terms were combined in a two-dimensional smooth term with a low dimension basis function.

Average daily flux rates for the study period were estimated with the output of the generalized additive models described above in a two-step process. First, daily fluxes were gap filled with the predictions of the model using the daily observations of soil volumetric water content measured in each plot. Then the average daily fluxes were used as the response variable in a final linear mixed effect model with land use and precipitation treatments as fixed effects and whole plot as a random effect. Average daily fluxes of each land use and precipitation treatment combination were extracted from this final model as the estimated marginal means and pairwise comparisons were made with an alpha of 0.05.

Separately, but using the same final model structure, the daily average soil volumetric water content of each land use and precipitation treatment was also estimated in this fashion. For visualization purposes, Figure 3.1 was produced by aligning the precipitation schedules of all three years and showing their mean daily values. Also for visualization purposes, Figures 2A and 3A were produced by binning the soil volumetric water contents at 0.02 cm³ water cm⁻³ soil intervals and plotting the mean flux values of each land use treatment.

Soil C and N mineralization measurements from the sieved soil samples as well as their gravimetric soil water contents were analyzed with a linear mixed effect model. Land use and precipitation treatments, including their interaction, were used as fixed effects and whole plot was used as a random effect. Estimated marginal means were extracted and compared for pairwise differences with an alpha of 0.05. For visualization purposes, Figures 5A and 6A were binned at 0.02 g water g⁻¹ soil and plotted with the mean flux values of each land use treatment.

Results

Soil water content

Both precipitation treatment and land use impacted soil water content (Figure 3.1). As designed, the 3-Week precipitation treatment increased the range of soil water content variability relative to the 1-Week precipitation treatment while the drought substantially decreased soil water content. Land use mediated these responses, with the highest average soil water contents in observed NT, followed by CON and then ES. Relative to the 1-Week precipitation treatment in the NT land use, drought caused 26%, 41%, and 52% decreases in the daily mean soil volumetric water content in the CON, NT, and ES land use treatments, respectively (Table 3.1). While the shelters were in place, the CON, NT, and ES treatments under imposed drought had mean soil volumetric water contents of 0.12, 0.15, and 0.10 cm³ water cm⁻³ soil, respectively (s.e. < 0.02 cm³ water cm⁻³ soil; Table 3.1). During the same period, the 1-Week and 3-Week precipitation treatments had similar mean soil volumetric water contents within land use treatments. Within precipitation treatments, the CON, NT, and ES land uses had soil volumetric water contents of 0.17-0.19, 0.21, and 0.14-0.15 cm³ water cm⁻³ soil, respectively (s.e. < 0.02 cm³ water cm⁻³ soil; Table 3.1).

Soil CH4 fluxes

Soil CH₄ fluxes were influenced by both soil water content and land use (Figure 3.2). The soil CH₄ sink strengthened as soils dried, but at different rates depending on land use. For the CON and NT land uses, a change in soil volumetric water content from 0.10 to 0.30 cm³ water cm⁻³ soil was associated with a change in soil CH₄ oxidation rates of approximately -4 to -2 g CH₄ ha⁻¹ d⁻¹, respectively, whereas the same soil water content change in the ES land use was associated with a change of -8 to -3 g CH₄ ha⁻¹ d⁻¹ (Figure 3.2). The statistical model with the

days after precipitation term was not significantly better than the statistical model with the continuous soil volumetric water content term (p = 0.74). Using the model with soil volumetric water content, then, we found that overall soil CH₄ oxidation rates were increased by drought, but only in the NT and ES land uses (Figure 3.2; Table 3.1). Relative to the 1-Week precipitation treatment, drought increased soil CH₄ oxidation rates from -2.7 to -3.3 and -6.9 to -7.3 g CH₄ ha⁻¹ d⁻¹ in the NT and ES land uses, respectively (s.e. < 0.6 g CH₄ ha⁻¹ d⁻¹). Methane oxidation rates were stronger in the NT than in the CON land use at low soil water content levels (e.g., 0.10 cm³ water cm⁻³ soil; p = 0.01). However, the NT land use tended to be wetter than the CON land use, resulting in no overall difference between the two land uses within a precipitation treatment (Figure 3.2). Soil CH₄ oxidation rates were similar in the 1-Week and 3-Week precipitation treatments within a land use, where CON, NT and ES had rates of -1.7 to -1.8, -2.7, and -6.7 to -6.9 g CH₄ ha⁻¹ d⁻¹, respectively (s.e. < 0.6 g CH₄ ha⁻¹ d⁻¹).

Soil water content and land use also affected soil N₂O emissions, with synthetic N fertilizer adding a further element to the dynamics (Figure 3.3). Higher emissions were associated with higher soil water content in each land use. An increase in soil water content from 0.10 to 0.30 cm³ water cm⁻³ soil was associated with an increase in N₂O emissions in the CON, NT, and ES land uses of approximately 3 to 30, 2 to 20 and 0.5 to 1.5 g N₂O ha⁻¹ d⁻¹, respectively. The statistical model with the days after precipitation term was significantly better than the statistical model with the continuous soil volumetric water content term (p = <0.01). However, the improvement was marginal with an R² value of 0.513 vs 0.524. Nevertheless, using the model that includes the days after precipitation term, the overall emissions within each land use were statistically similar in the 1-Week and 3-Week precipitation treatments. For these

precipitation treatments the CON, NT, and ES land uses had N₂O emission rates of 17.3-18.8, 16.2-17.7, and 1.3-1.5 g N₂O ha⁻¹ d⁻¹ (s.e. < 3.1 for CON and NT, and < 0.5 for ES; Table 3.2 and Figure 3.3). The drought significantly reduced N₂O emissions in each land use. Relative to their 1-Week precipitation treatments, drought caused 49%, 57%, and 31% decreases in the CON, NT, and ES land uses, respectively.

Soil CO₂ flux

Soil heterotrophic respiration in the CON and NT land uses declined as soils were exposed to drought following wheat harvest in 2022 (Figure 3.4). Upon re-wetting, CO_2 emissions were significantly higher than would be predicted from the statistical relationship to soil water content alone. The statistical model that included days after precipitation was significantly improved (p < 0.01) and increased the model R^2 from 0.282 to 0.491.

Lab-based respiration potentials (Figure 3.5) showed that soil water content strongly affected CO₂ emissions in each land use. An increase in soil gravimetric water content from 0.05 to 0.20 g water g soil⁻¹ was associated with an increase in potential respiration from approximately 10 to 20 μg CO₂ g soil⁻¹ d⁻¹ in the CON and NT land uses, whereas in the ES land use potential respiration increased from 25 to 50 μg CO₂ g soil⁻¹ d⁻¹. Drought significantly reduced soil potential respiration, but only in the ES land use (40.1 vs 28.7, s.e. < 4.5 μg CO₂ g soil⁻¹ d⁻¹, Figure 3.5 and Table 3.2). CO₂ fluxes in the CON and NT land uses were statistically similar across all precipitation treatments with a range of 13.5 to 17.3 μg CO₂ g soil⁻¹ d⁻¹ (s.e. < 2.9 μg CO₂ g soil⁻¹ d⁻¹).

Soil N mineralization

Potential soil N mineralization rates were also significantly associated with soil water content (Figure 3.6). An increase of 0.05 to 0.20 g water g soil⁻¹ was associated with a 100-200

ng N g soil⁻¹ d⁻¹ increase in soil N mineralization rates. However, soil N mineralization rates were variable; there were no significant effects of precipitation regime within any land use treatment. That said, rates tended to be lower in ES when compared with CON and NT (131-299 vs 33-85 ng N g soil⁻¹ d⁻¹, respectively, s.e. < 75 ng N g soil⁻¹ d⁻¹).

Discussion

Soil water content

The phenology of each vegetation type was a key determinant of differences in soil water content dynamics among the land use treatments. The earlier green up of ES vegetation and winter wheat resulted in greater rates of precipitation interception and transpiration, causing rapid declines in soil water content relative to the corn and soybean phases of the CON and NT land uses. Furthermore, after winter wheat senesced and was harvested, the 1-Week and 3-Week precipitation treatments in the absence of transpiration caused soil water contents to increase rather than decrease. In the ES land use, early green up and high rates of interception and transpiration caused ES soils to be drier than in the CON and NT land uses (Figure 3.1). Nevertheless, within the annual crops soil water content in the NT land use tended to be higher than the CON land use, potentially due to differences in energy and water partitioning. Surface residue and intact surface soil structure in the NT land use appeared to reduce overland flow and thus increased infiltration relative to the CON land use (Zhai et al., 1990). It is also likely that surface residue in the NT land use was able to reflect and/or re-radiate incoming solar radiation more effectively than the bare soil in the CON land use, decreasing the energy available for evaporation from mineral soil (Schwartz et al., 2010).

Soil CH4 fluxes

The overall pattern in soil methane fluxes was that of increasing oxidation rates as soils dried. A key limiting factor for the methanotrophs appears to be atmospheric CH₄ availability, confirming our hypothesis about soil water effects on gas diffusion. Wet soils appeared to limit gas diffusion to the point of limiting methane oxidation, while dry soils allowed for higher oxidation rates. In the ES land use, we observed a plateaued methane oxidation rate in the driest soils (Figure 3.2). We expected that oxidation rates would then decrease to nil as soils dried further and cell water potentials become too extreme to support cellular functioning (Blankinship et al., 2010; Tate, 2015; Van Den Pol-van Dasselaar et al., 1998; Voigt et al., 2023). This was not observed, however, perhaps because wetter soils below our 25 cm observation depth were allowing methane oxidation to continue. Furthermore, the strong dependence of ES methane oxidation rates on soil water content despite only small effects of precipitation treatments may be because 1-Week and 3-Week precipitation treatments were sufficiently dry to be in the same plateau phase of the moisture dependence curve as the drought plots.

Soil N₂O flux

We hypothesized that drying soils would lower soil N₂O emissions, as found in earlier studies (e.g. Gelfand et al., 2015), but that rewetting events would cause higher than expected emission spikes (Muhr et al., 2008). While we did find support for higher than expected emissions following precipitation events, the effect appeared to be small relative to the other drivers of N₂O emissions, namely excess dissolved N species and soil water content. Our findings are in line with a recent meta-analysis of drying-rewetting studies (Sang et al., 2022), which showed that some studies found pulses of N₂O emissions after rewetting events but that

the overall effect was not significant across studies. However, this meta-analysis included both included laboratory and field manipulation experiments.

The highest spikes in N₂O emissions came in the days following synthetic N fertilizer applications in the winter wheat and corn phases of the CON and NT land uses. However, these events occurred before the rain exclusion shelters were deployed and thus before the precipitation manipulations were imposed. We suspect that, had the two coincided, we might have seen effects of the 1-Week small event size precipitation treatment vs the 3-Week large event size precipitation treatment (Barrat et al., 2021). Nevertheless, we observed decreases in N₂O emissions with drought across all three land uses. This decrease can be explained by the reduction in soil water content and the resulting reduction in soil N mineralization rates. However, while we documented a dependence of soil N mineralization rates on soil water content (Figure 3.6A), we did not detect significant effects of drought on soil N mineralization rates in any land use (Figure 3.6B). This suggests that reductions in N₂O emissions were due to physiological stress of the denitrifiers and perhaps the nitrifiers as well (Song et al., 2010; Stres et al., 2008).

Soil CO₂ flux

We hypothesized that soil heterotrophic CO₂ fluxes would decrease predictably as soils dry, but respond to rewetting events with higher emissions than predicted from soil water content alone. We found support for this hypothesis (Figure 3.4) where a simple dependence of CO₂ fluxes on soil water content was insufficient to capture the post-rewetting pulse events. This confirms previous findings of pulse rewetting studies (Sang et al., 2022). For the sieved soil samples measured for CO₂ production in the lab, we documented the predictable dependence of heterotrophic respiration on soil water content before rewetting events (Figure 3.5). The decline

of in situ CO₂ fluxes during the drought seemed to be fully compensated for by the 'extra' emissions following rewetting such that the cumulative flux during the shelter period was equivalent between all three precipitation treatments. This suggests that capturing these non-linear pulse responses would be important to getting to total heterotrophic respiration amount correct.

Conclusions

Overall, our study found that each greenhouse gas can respond uniquely to changing precipitation regimes and that land use mediates these responses. We found that both N₂O and especially CO₂ fluxes did not follow strict dependence relationships to soil water content. For CO₂ we found results that agree with previous studies where pulses of heterotrophic respiration can fully compensate for lower rates observed during drought (Jarvis et al., 2007; Sang et al., 2022; Unger et al., 2010). The novelty of our study is that we documented this effect in situ as a response to plausible precipitation regime changes under future climate scenarios. Soil heterotrophic respiration is almost never measured in situ without experimental interventions such as root-trenching or plant removals (Kuzyakov & Larionova, 2005). The implications of our finding is that droughts caused by climate change will change soil heterotrophic respiration dynamics, but not the cumulative amount of CO₂ produced over the drought and subsequent rewetting period.

For CH₄, increases in oxidation rates as soils dried plateaued in the very dry soils of the ES land use treatment. We suspect that the plateau observed for areal fluxes is a mixture of low fluxes in the very dry topsoil and stronger fluxes in the wetter subsoil. The implications of this finding is that models aiming to predict soil CH₄ oxidation rates should fully resolve this relationship with a deeper, multiprobe profile of soil water content measurements (Zhang et al.,

2024). Careful laboratory studies that control both soil gas diffusion rates (with water content) and microbial osmotic stress (with salt concentration) find both to be important drivers of methanotroph activity rates (Schnell & King, 1996). This relationship needs to be resolved in situ for soils of different textures as the same soil volumetric water contents will have different gas diffusion rates and matric potentials causing differences in CH₄ supply rates and cell water stress, respectively (Abdelbaki, 2021; Jin & Jury, 1996).

For N₂O, our results largely support the strict dependence of fluxes on soil water content, but we also found support for higher emissions following rewetting events. Mixed results are common in this field with some studies documenting higher than expected rewetting pulse events and others not (Guo et al., 2014; Harris et al., 2021). A recent meta-analysis of drying-rewetting studies aggregates the studies that do and no not support pulse emissions following rewetting (Sang et al., 2022). The range of variability in those results was relatively wide, suggesting that further study of the drivers behind the occurrence of rewetting pulse emission events could yield greater insight into this phenomenon. There are many interacting processes that underpin N₂O emissions from soils ranging from physical, to chemical and biological mechanisms, all of which contribute to that wide range of variability in experiments investigating responses to soil water content (Beare et al., 2009; Chen et al., 2014; Liu et al., 2018). Taken together, we found that increased precipitation variability may not result in significant changes to cumulative fluxes of soil CH₄, N₂O or CO₂ and that drought will lead to greater CH₄ oxidation, lower N₂O emissions and similar CO₂ emissions. Therefore, a scenario with more frequent droughts would cause less radiative forcing overall.

REFERENCES

- Abdelbaki, A. M. (2021). Assessing the best performing pedotransfer functions for predicting the soil-water characteristic curve according to soil texture classes and matric potentials. *European Journal of Soil Science*, 72(1), 154–173. https://doi.org/10.1111/ejss.12959
- Barrat, H. A., Evans, J., Chadwick, D. R., Clark, I. M., Le Cocq, K., & M. Cardenas, L. (2021). The impact of drought and rewetting on N₂O emissions from soil in temperate and Mediterranean climates. *European Journal of Soil Science*, 72(6), 2504–2516. https://doi.org/10.1111/ejss.13015
- Beare, M. H., Gregorich, E. G., & St-Georges, P. (2009). Compaction effects on CO₂ and N₂O production during drying and rewetting of soil. *Soil Biology and Biochemistry*, 41(3), 611–621. https://doi.org/10.1016/j.soilbio.2008.12.024
- Berg, A., Sheffield, J., & Milly, P. C. D. (2017). Divergent surface and total soil moisture projections under global warming. *Geophysical Research Letters*, 44(1), 236–244. https://doi.org/10.1002/2016GL071921
- Beyer, R. M., Krapp, M., & Manica, A. (2020). High-resolution terrestrial climate, bioclimate and vegetation for the last 120,000 years. *Scientific Data*, 7(1), 236. https://doi.org/10.1038/s41597-020-0552-1
- Blankinship, J. C., Brown, J. R., Dijkstra, P., Allwright, M. C., & Hungate, B. A. (2010). Response of terrestrial CH₄ uptake to interactive changes in precipitation and temperature along a climatic gradient. *Ecosystems*, *13*(8), 1157–1170. https://doi.org/10.1007/s10021-010-9391-9
- Chen, C., Whalen, J. K., & Guo, X. (2014). Earthworms reduce soil nitrous oxide emissions during drying and rewetting cycles. *Soil Biology and Biochemistry*, 68, 117–124. https://doi.org/10.1016/j.soilbio.2013.09.020
- Cook, B. I., Mankin, J. S., Marvel, K., Williams, A. P., Smerdon, J. E., & Anchukaitis, K. J. (2020). Twenty-first century drought projections in the CMIP6 forcing scenarios. *Earth's Future*, 8(6), e2019EF001461. https://doi.org/10.1029/2019EF001461
- Falloon, P., Jones, C. D., Ades, M., & Paul, K. (2011). Direct soil moisture controls of future global soil carbon changes: An important source of uncertainty: Soil moisture and soil carbon. *Global Biogeochemical Cycles*, 25(3). https://doi.org/10.1029/2010GB003938
- Flückiger, J., Monnin, E., Stauffer, B., Schwander, J., Stocker, T. F., Chappellaz, J., Raynaud, D., & Barnola, J. (2002). High-resolution Holocene N₂O ice core record and its relationship with CH₄ and CO₂. *Global Biogeochemical Cycles*, 16(1). https://doi.org/10.1029/2001GB001417
- Friedlingstein, P., O'Sullivan, M., Jones, M. W., Andrew, R. M., Bakker, D. C. E., Hauck, J., Landschützer, P., Le Quéré, C., Luijkx, I. T., Peters, G. P., Peters, W., Pongratz, J., Schwingshackl, C., Sitch, S., Canadell, J. G., Ciais, P., Jackson, R. B., Alin, S. R.,

- Anthoni, P., ... Zheng, B. (2023). Global Carbon Budget 2023. *Earth System Science Data*, 15(12), 5301–5369. https://doi.org/10.5194/essd-15-5301-2023
- Gelfand, I., Cui, M., Tang, J., & Robertson, G. P. (2015). Short-term drought response of N₂O and CO₂ emissions from mesic agricultural soils in the US Midwest. *Agriculture, Ecosystems & Environment*, 212, 127–133. https://doi.org/10.1016/j.agee.2015.07.005
- Gelfand, I., Shcherbak, I., Millar, N., Kravchenko, A. N., & Robertson, G. P. (2016). Long-term nitrous oxide fluxes in annual and perennial agricultural and unmanaged ecosystems in the upper Midwest USA. *Global Change Biology*, *22*(11), 3594–3607. https://doi.org/10.1111/gcb.13426
- Groffman, P. M., & Tiedje, J. M. (1988). Denitrification hysteresis during wetting and drying cycles in soil. *Soil Science Society of America Journal*, *52*(6), 1626–1629. https://doi.org/10.2136/sssaj1988.03615995005200060022x
- Guo, X., Drury, C. F., Yang, X., Daniel Reynolds, W., & Fan, R. (2014). The extent of soil drying and rewetting affects nitrous oxide emissions, denitrification, and nitrogen mineralization. *Soil Science Society of America Journal*, 78(1), 194–204. https://doi.org/10.2136/sssaj2013.06.0219
- Harris, E., Diaz-Pines, E., Stoll, E., Schloter, M., Schulz, S., Duffner, C., Li, K., Moore, K. L., Ingrisch, J., Reinthaler, D., Zechmeister-Boltenstern, S., Glatzel, S., Brüggemann, N., & Bahn, M. (2021). Denitrifying pathways dominate nitrous oxide emissions from managed grassland during drought and rewetting. *Science Advances*, 7(6), eabb7118. https://doi.org/10.1126/sciadv.abb7118
- Jarvis, P., Rey, A., Petsikos, C., Wingate, L., Rayment, M., Pereira, J., Banza, J., David, J., Miglietta, F., Borghetti, M., Manca, G., & Valentini, R. (2007). Drying and wetting of Mediterranean soils stimulates decomposition and carbon dioxide emission: The "Birch effect." *Tree Physiology*, 27(7), 929–940. https://doi.org/10.1093/treephys/27.7.929
- Jin, Y., & Jury, W. A. (1996). Characterizing the Dependence of Gas Diffusion Coefficient on Soil Properties. *Soil Science Society of America Journal*, 60(1), 66–71. https://doi.org/10.2136/sssaj1996.03615995006000010012x
- Kahmark, K., Millar, N., & Robertson, G. P. (2020). Static Chamber Method for Measuring Soil Greenhouse Gas Fluxes. https://doi.org/10.5281/zenodo.4630396
- Kahmark, K., Jones, M., Bohm, S., Baker, N., & Robertson, G. P. (2024). Rainfall Manipulation Shelters for Agricultural Research. https://doi.org/10.5281/zenodo.10607631
- Kuzyakov, Y., & Larionova, A. A. (2005). Root and rhizomicrobial respiration: A review of approaches to estimate respiration by autotrophic and heterotrophic organisms in soil. *Journal of Plant Nutrition and Soil Science*, 168(4), 503–520. https://doi.org/10.1002/jpln.200421703

- Li, C., Zwiers, F., Zhang, X., Li, G., Sun, Y., & Wehner, M. (2021). Changes in annual extremes of daily temperature and precipitation in CMIP6 models. *Journal of Climate*, *34*(9), 3441–3460. https://doi.org/10.1175/JCLI-D-19-1013.1
- Liu, S., Schloter, M., & Brüggemann, N. (2018). Accumulation of NO₂ during periods of drying stimulates soil N₂O emissions during subsequent rewetting. *European Journal of Soil Science*, 69(5), 936–946. https://doi.org/10.1111/ejss.12683
- Luehmann, M. D., Peter, B. G., Connallon, C. B., Schaetzl, R. J., Smidt, S. J., Liu, W., Kincare, K. A., Walkowiak, T. A., Thorlund, E., & Holler, M. S. (2016). Loamy, Two-Storied Soils on the Outwash Plains of Southwestern Lower Michigan: Pedoturbation of Loess with the Underlying Sand. *Annals of the American Association of Geographers*, 106(3), 551–572. https://doi.org/10.1080/00045608.2015.1115388
- Marvel, K., Cook, B. I., Bonfils, C., Smerdon, J. E., Williams, A. P., & Liu, H. (2021). Projected changes to hydroclimate seasonality in the continental United States. *Earth's Future*, *9*(9), e2021EF002019. https://doi.org/10.1029/2021EF002019
- Muhr, J., Goldberg, S. D., Borken, W., & Gebauer, G. (2008). Repeated drying–rewetting cycles and their effects on the emission of CO₂, N₂O, NO, and CH₄ in a forest soil. *Journal of Plant Nutrition and Soil Science*, 171(5), 719–728. https://doi.org/10.1002/jpln.200700302
- Nazaries, L., Murrell, J. C., Millard, P., Baggs, L., & Singh, B. K. (2013). Methane, microbes and models: Fundamental understanding of the soil methane cycle for future predictions. *Environmental Microbiology*, *15*(9), 2395–2417. https://doi.org/10.1111/1462-2920.12149
- Oertel, C., Matschullat, J., Zurba, K., Zimmermann, F., & Erasmi, S. (2016). Greenhouse gas emissions from soils—A review. *Geochemistry*, 76(3), 327–352. https://doi.org/10.1016/j.chemer.2016.04.002
- Osman, M. B., Tierney, J. E., Zhu, J., Tardif, R., Hakim, G. J., King, J., & Poulsen, C. J. (2021). Globally resolved surface temperatures since the Last Glacial Maximum. *Nature*, 599(7884), 239–244. https://doi.org/10.1038/s41586-021-03984-4
- Rastogi, D., Trok, J., Depsky, N., Monier, E., & Jones, A. (2024). Historical evaluation and future projections of compound heatwave and drought extremes over the conterminous United States in CMIP6. *Environmental Research Letters*, *19*(1), 014039. https://doi.org/10.1088/1748-9326/ad0efe
- Richardson, K., Steffen, W., Lucht, W., Bendtsen, J., Cornell, S. E., Donges, J. F., Drüke, M., Fetzer, I., Bala, G., Von Bloh, W., Feulner, G., Fiedler, S., Gerten, D., Gleeson, T., Hofmann, M., Huiskamp, W., Kummu, M., Mohan, C., Nogués-Bravo, D., ... Rockström, J. (2023). Earth beyond six of nine planetary boundaries. *Science Advances*, *9*(37), eadh2458. https://doi.org/10.1126/sciadv.adh2458

- Robertson, G. P., Bruulsema, T. W., Gehl, R. J., Kanter, D., Mauzerall, D. L., Rotz, C. A., & Williams, C. O. (2013). Nitrogen–climate interactions in US agriculture. *Biogeochemistry*, 114(1–3), 41–70. https://doi.org/10.1007/s10533-012-9802-4
- Robertson, G. P., & Hamilton, S. K. (2015). Conceptual and experimental approaches to understanding agricultural ecosystems. In: Hamilton SK, Doll JE, Robertson GP (eds) The ecology of agricultural landscapes: long-term research on the path to sustainability. Oxford University Press, New York.
- Sang, J., Lakshani, M. M. T., Chamindu Deepagoda, T. K. K., Shen, Y., & Li, Y. (2022). Drying and rewetting cycles increased soil carbon dioxide rather than nitrous oxide emissions: A meta-analysis. *Journal of Environmental Management*, 324, 116391. https://doi.org/10.1016/j.jenvman.2022.116391
- Saunois, M., Stavert, A. R., Poulter, B., Bousquet, P., Canadell, J. G., Jackson, R. B., Raymond, P. A., Dlugokencky, E. J., Houweling, S., Patra, P. K., Ciais, P., Arora, V. K., Bastviken, D., Bergamaschi, P., Blake, D. R., Brailsford, G., Bruhwiler, L., Carlson, K. M., Carrol, M., ... Zhuang, Q. (2020). The Global Methane Budget 2000–2017. *Earth System Science Data*, 12(3), 1561–1623. https://doi.org/10.5194/essd-12-1561-2020
- Schilt, A., Baumgartner, M., Blunier, T., Schwander, J., Spahni, R., Fischer, H., & Stocker, T. F. (2010). Glacial–interglacial and millennial-scale variations in the atmospheric nitrous oxide concentration during the last 800,000 years. *Quaternary Science Reviews*, 29(1–2), 182–192. https://doi.org/10.1016/j.quascirev.2009.03.011
- Schimel, J. P. (2018). Life in dry soils: Effects of drought on soil microbial communities and processes. *Annual Review of Ecology, Evolution, and Systematics*, 49(1), 409–432. https://doi.org/10.1146/annurev-ecolsys-110617-062614
- Schnell, S., & King, G. M. (1996). Responses of methanotrophic activity in soils and cultures to water stress. *Applied and Environmental Microbiology*, 62(9), 3203–3209. https://doi.org/10.1128/aem.62.9.3203-3209.1996
- Schwartz, R. C., Baumhardt, R. L., & Evett, S. R. (2010). Tillage effects on soil water redistribution and bare soil evaporation throughout a season. *Soil and Tillage Research*, 110(2), 221–229. https://doi.org/10.1016/j.still.2010.07.015
- Smith, K. A., Ball, T., Conen, F., Dobbie, K. E., Massheder, J., & Rey, A. (2003). Exchange of greenhouse gases between soil and atmosphere: Interactions of soil physical factors and biological processes. *European Journal of Soil Science*, *54*(4), 779–791. https://doi.org/10.1046/j.1351-0754.2003.0567.x
- Sokol, N. W., Slessarev, E., Marschmann, G. L., Nicolas, A., Blazewicz, S. J., Brodie, E. L., Firestone, M. K., Foley, M. M., Hestrin, R., Hungate, B. A., Koch, B. J., Stone, B. W., Sullivan, M. B., Zablocki, O., LLNL Soil Microbiome Consortium, Trubl, G., McFarlane, K., Stuart, R., Nuccio, E., ... Pett-Ridge, J. (2022). Life and death in the soil microbiome: How ecological processes influence biogeochemistry. *Nature Reviews Microbiology*, 20(7), 415–430. https://doi.org/10.1038/s41579-022-00695-z

- Song, K., Lee, S.-H., Mitsch, W. J., & Kang, H. (2010). Different responses of denitrification rates and denitrifying bacterial communities to hydrologic pulsing in created wetlands. *Soil Biology and Biochemistry*, *42*(10), 1721–1727. https://doi.org/10.1016/j.soilbio.2010.06.007
- Stres, B., Danevčič,, T., Pal, L., Fuka, M. M., Resman, L., Leskovec, S., Hacin, J., Stopar, D., Mahne, I., & Mandic-Mulec, I. (2008). Influence of temperature and soil water content on bacterial, archaeal and denitrifying microbial communities in drained fen grassland soil microcosms. *FEMS Microbiology Ecology*, 66(1), 110–122. https://doi.org/10.1111/j.1574-6941.2008.00555.x
- Tate, K. R. (2015). Soil methane oxidation and land-use change from process to mitigation. Soil Biology and Biochemistry, 80, 260–272. https://doi.org/10.1016/j.soilbio.2014.10.010
- Thornton, M. M., Shrestha, R., Wei, Y., Thornton, P. E., Kao, S.-C., & Wilson, B. E. (2022). Daymet: Daily surface weather data on a 1-km grid for North America, Version 4 R1. ORNL DAAC, Oak Ridge, Tennessee, USA. https://doi.org/10.3334/ORNLDAAC/2129
- Tian, H., Xu, R., Canadell, J. G., Thompson, R. L., Winiwarter, W., Suntharalingam, P., Davidson, E. A., Ciais, P., Jackson, R. B., Janssens-Maenhout, G., Prather, M. J., Regnier, P., Pan, N., Pan, S., Peters, G. P., Shi, H., Tubiello, F. N., Zaehle, S., Zhou, F., ... Yao, Y. (2020). A comprehensive quantification of global nitrous oxide sources and sinks. *Nature*, 586(7828), 248–256. https://doi.org/10.1038/s41586-020-2780-0
- Tweedie, M. (1984). An index which distinguishes between some important exponential families. *Statistics: Applications and New Directions*, *579*.
- Unger, S., Máguas, C., Pereira, J. S., David, T. S., & Werner, C. (2010). The influence of precipitation pulses on soil respiration Assessing the "Birch effect" by stable carbon isotopes. *Soil Biology and Biochemistry*, *42*(10), 1800–1810. https://doi.org/10.1016/j.soilbio.2010.06.019
- Van Den Pol-van Dasselaar, A., Van Beusichem, M. L., & Oenema, O. (1998). Effects of soil moisture content and temperature on methane uptake by grasslands on sandy soils. *Plant and Soil*, 204(2), 213–222. https://doi.org/10.1023/A:1004371309361
- Voigt, C., Virkkala, A.-M., Hould Gosselin, G., Bennett, K. A., Black, T. A., Detto, M., Chevrier-Dion, C., Guggenberger, G., Hashmi, W., Kohl, L., Kou, D., Marquis, C., Marsh, P., Marushchak, M. E., Nesic, Z., Nykänen, H., Saarela, T., Sauheitl, L., Walker, B., ... Sonnentag, O. (2023). Arctic soil methane sink increases with drier conditions and higher ecosystem respiration. *Nature Climate Change*, *13*(10), 1095–1104. https://doi.org/10.1038/s41558-023-01785-3
- Wood, S. N. (2017). *Generalized additive models: An introduction with R* (2nd ed.). Chapman and Hall/CRC. https://doi.org/10.1201/9781315370279

- Yang, J.-W., Ahn, J., Brook, E. J., & Ryu, Y. (2017). Atmospheric methane control mechanisms during the early Holocene. *Climate of the Past*, 13(9), 1227–1242. https://doi.org/10.5194/cp-13-1227-2017
- Zhai, R., Kachanoski, R. G., & Voroney, R. P. (1990). Tillage effects on the spatial and temporal variations of soil water. *Soil Science Society of America Journal*, *54*(1), 186–192. https://doi.org/10.2136/sssaj1990.03615995005400010029x
- Zhang, L., Lin, W., Sardans, J., Li, X., Hui, D., Yang, Z., Wang, H., Lin, H., Wang, Y., Guo, J., Peñuelas, J., & Yang, Y. (2024). Soil warming-induced reduction in water content enhanced methane uptake at different soil depths in a subtropical forest. *Science of The Total Environment*, 927, 171994. https://doi.org/10.1016/j.scitotenv.2024.171994
- Zhao, J., Gan, T. Y., Zhang, G., & Zhang, S. (2023). Projected changes of precipitation extremes in North America using CMIP6 multi-climate model ensembles. *Journal of Hydrology*, 621, 129598. https://doi.org/10.1016/j.jhydrol.2023.129598

APPENDIX B: CHAPTER 3 TABLES AND FIGURES

Table 3.1. Daily mean (\pm s.e.) soil volumetric water content across the 0-25 cm depth interval and soil gas fluxes for each land use and precipitation treatment. Years 2021-2023 are combined as described in Methods. Letters denote statistical differences among all groups, within a column.

Land use	Precipitation	Soil volumetric	Soil CH ₄ flux	Soil N2O flux
		water content		
		cm³ water cm⁻³ soil	$g CH_4 ha^{-1} d^{-1}$	$g N_2 O ha^{-1} d^{-1}$
Tilled	1-Week	$0.19 \pm 0.02 \text{ de}$	$-1.72 \pm 0.51 d$	$18.8 \pm 3.0 d$
	3-Week	0.17 ± 0.01 cde	-1.77 ± 0.50 cd	$17.3 \pm 2.7 d$
	Drought	$0.12 \pm 0.02 \text{ ab}$	-1.92 ± 0.51 cd	$9.5 \pm 1.6 \text{ c}$
No-till	1-Week	0.21 ± 0.01 e	$-2.67 \pm 0.50 \text{ d}$	$17.7 \pm 2.8 d$
	3-Week	0.21 ± 0.01 e	$-2.66 \pm 0.50 \text{ d}$	$16.2 \pm 2.6 d$
	Drought	$0.15 \pm 0.02 \text{ bcd}$	-3.33 ± 0.51 c	$7.6 \pm 1.5 \text{ c}$
Early	1-Week	$0.14 \pm 0.01 \text{ bc}$	-6.90 ± 0.41 b	$1.3 \pm 0.3 \text{ b}$
Successional	3-Week	0.15 ± 0.01 bc	-6.72 ± 0.41 b	$1.5 \pm 0.4 \text{ b}$
	Drought	0.10 ± 0.01 a	-7.33 ± 0.41 a	$0.9 \pm 0.3 \text{ a}$

Table 3.2. Soil gravimetric water content, CO_2 flux and N mineralization rates for each land use and precipitation treatment (mean \pm s.e.). Data are from 2021-2023 sieved soil samples taken the week before the end of the drought. Letters denote statistical differences among all groups, within a column.

Land use	Precipitation	Soil gravimetric	Soil CO ₂ flux	Soil N mineralization
		water content		
		g water g ⁻¹ soil	$\mu g CO_2 g soil^{-1} d^{-1}$	$ng N g soil^{-1} d^{-1}$
Tilled	1-Week	$0.14 \pm 0.01 \text{ cd}$	$17.3 \pm 2.4 \text{ a}$	$299 \pm 69 c$
	3-Week	$0.12 \pm 0.01 \; bcd$	$13.7 \pm 1.9 \text{ a}$	$221 \pm 58 \text{ bc}$
	Drought	$0.06 \pm 0.02 \; a$	$16.0 \pm 2.8 \ a$	154 ± 74 abc
No-till	1-Week	$0.14 \pm 0.01 d$	$16.0 \pm 2.2 \text{ a}$	200 ± 55 bc
	3-Week	$0.12 \pm 0.01 \text{ cd}$	$17.1 \pm 2.3 \text{ a}$	$253 \pm 63 \text{ c}$
	Drought	0.10 ± 0.02 abc	$13.5 \pm 1.9 \text{ a}$	$131 \pm 50 \text{ abc}$
Early	1-Week	$0.13 \pm 0.01 \text{ cd}$	$40.1 \pm 4.5 \text{ c}$	$58 \pm 29 \text{ a}$
Successional	3-Week	$0.11 \pm 0.01 \text{ cd}$	$40.3 \pm 4.5 \text{ c}$	$33 \pm 26 \text{ a}$
	Drought	$0.07 \pm 0.01 \text{ ab}$	$28.7 \pm 3.4 \text{ b}$	85 ± 36 ab

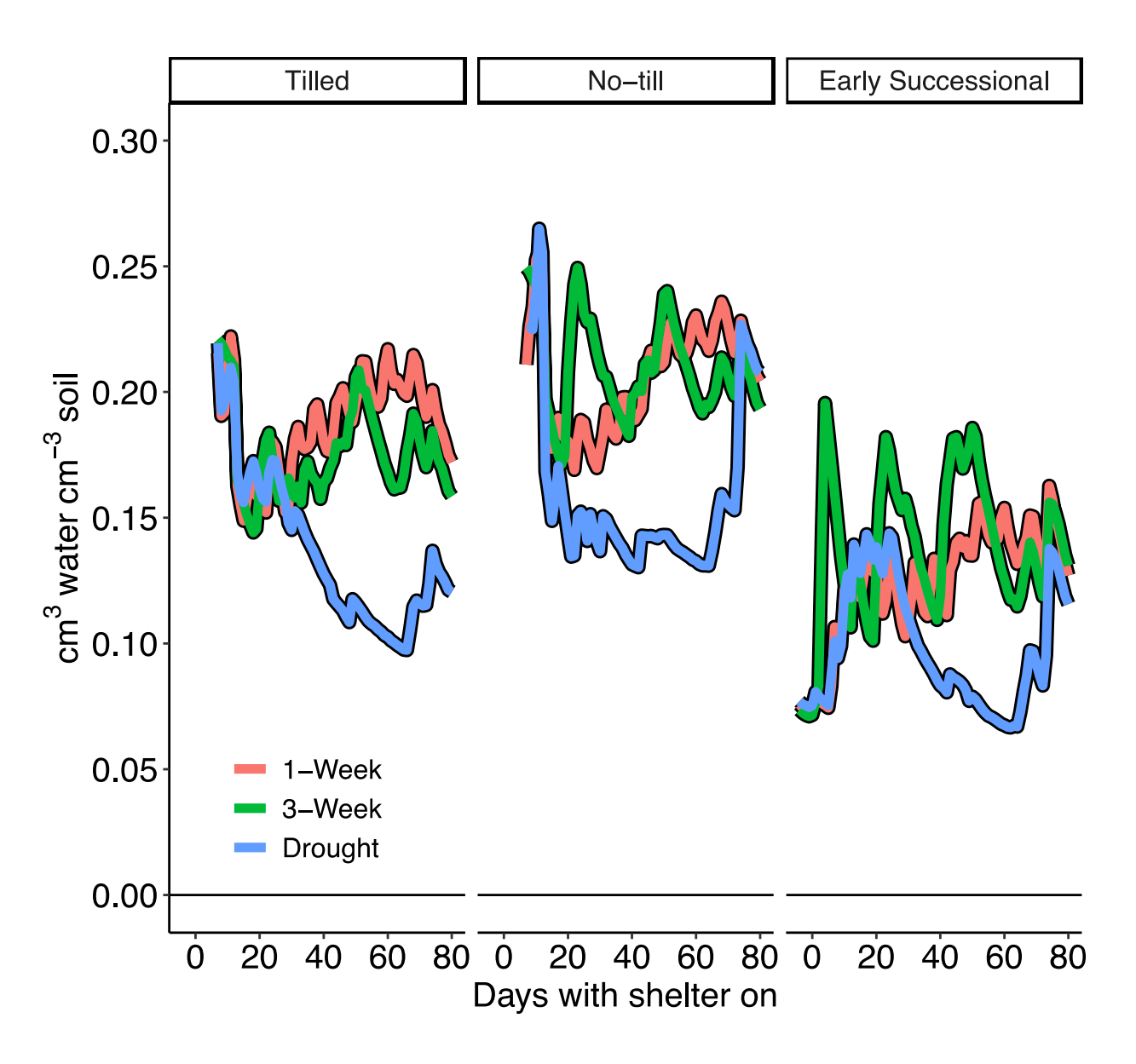


Figure 3.1. Daily mean soil volumetric water content across the 0-25 cm depth interval for each land use and precipitation treatment. Years 2021-2023 are combined here for visual clarity by aligning their precipitation schedules.

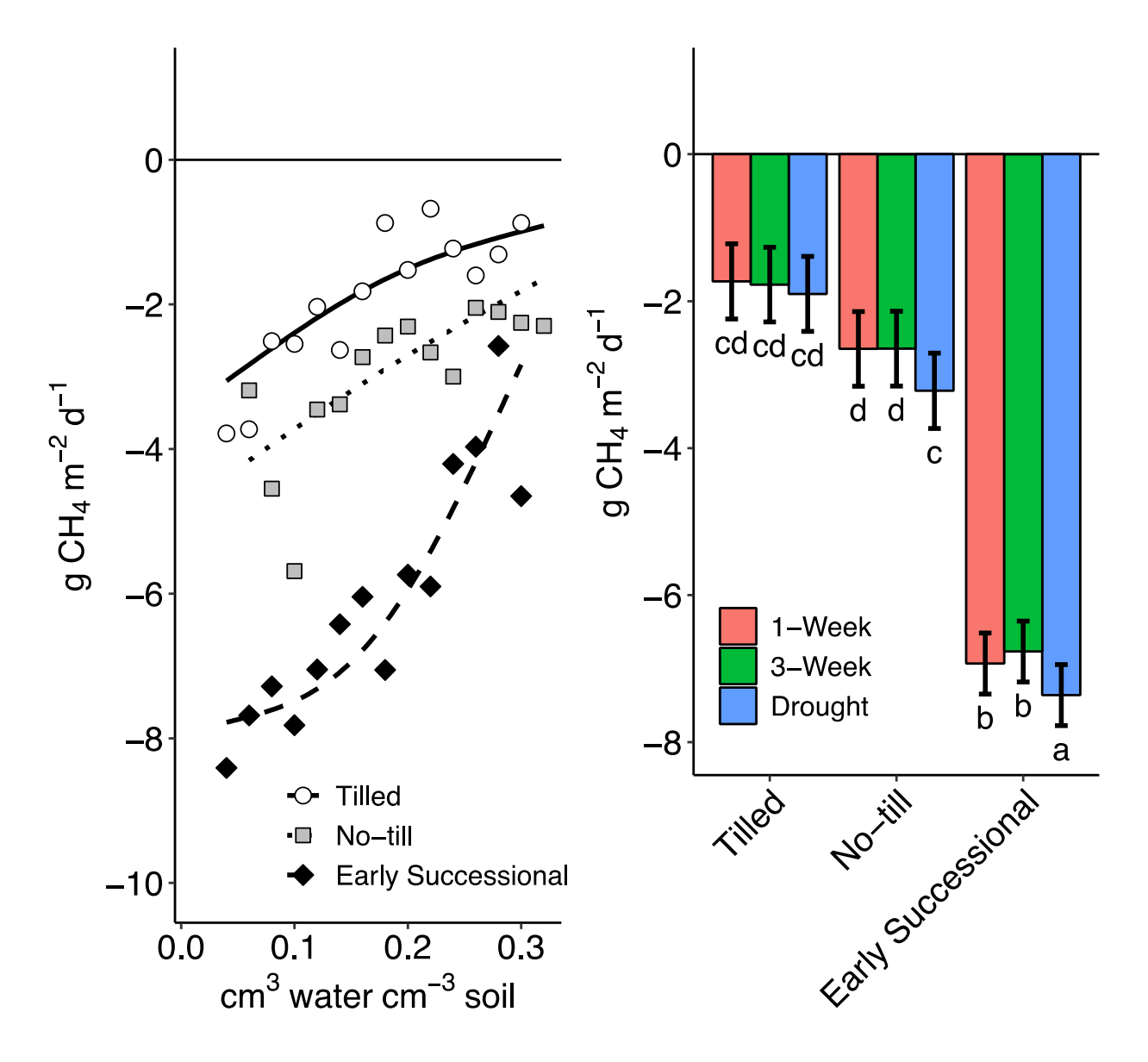


Figure 3.2. A) Relationship between daily soil CH₄ flux and soil volumetric water content for each land use (left). Points represent the mean methane flux for the binned soil volumetric water content, for each land use while the lines represent the best fit. B) Average daily soil CH₄ flux during the experimental rainfall period for each precipitation regime and land use (right; mean ± s.e.). Letters denote statistical differences across all groups.

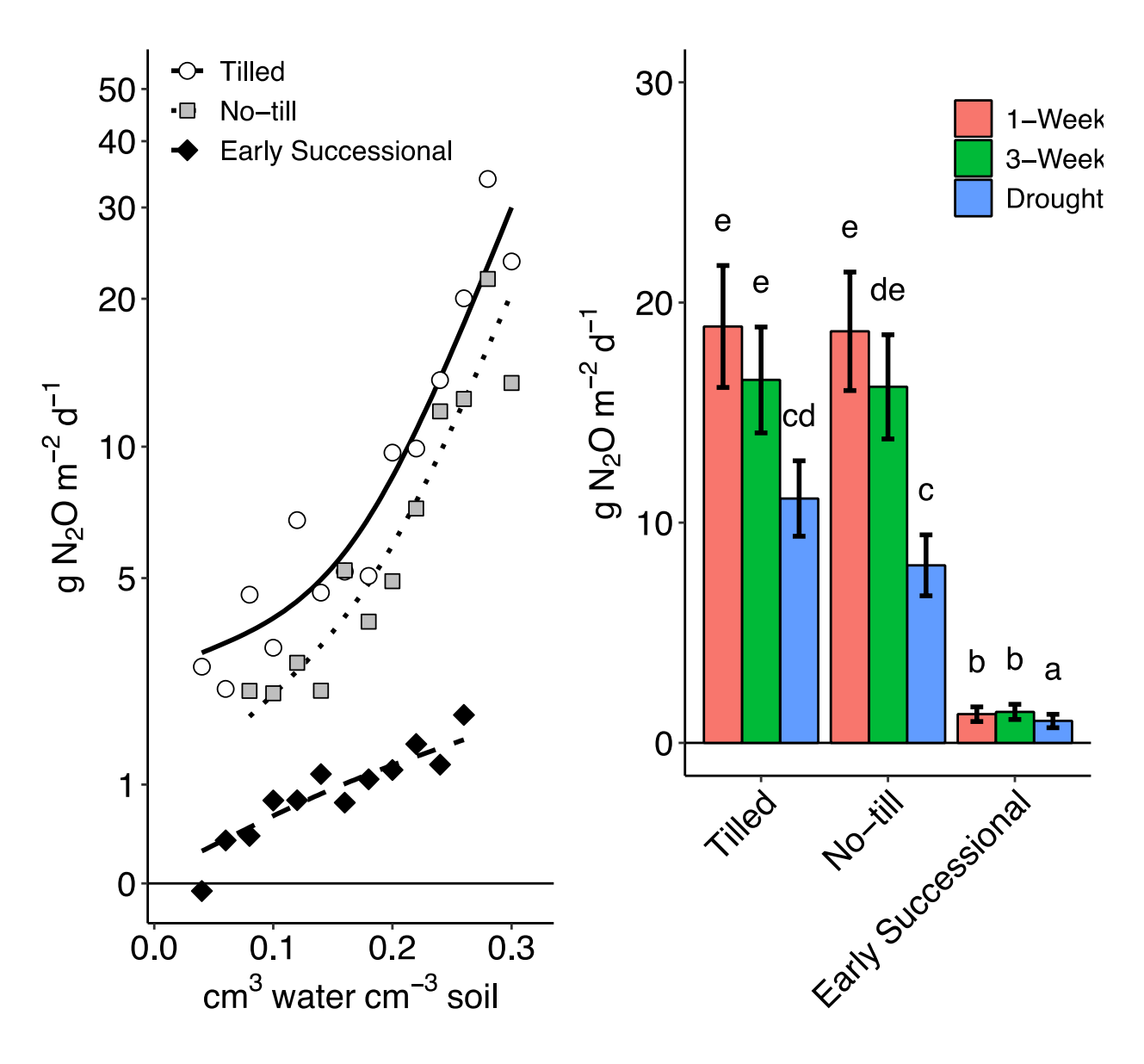


Figure 3.3. A) Daily soil N_2O flux and soil volumetric water content for each land use (left); note the log scale y axis. Points represent the mean nitrous oxide flux for the binned soil volumetric water content, for each land use while the lines represent the best fit. B) Average daily soil N_2O flux (mean \pm s.e.) during experimental rainfall period for each precipitation regime and land use (right). Letters denote statistical differences across all groups.

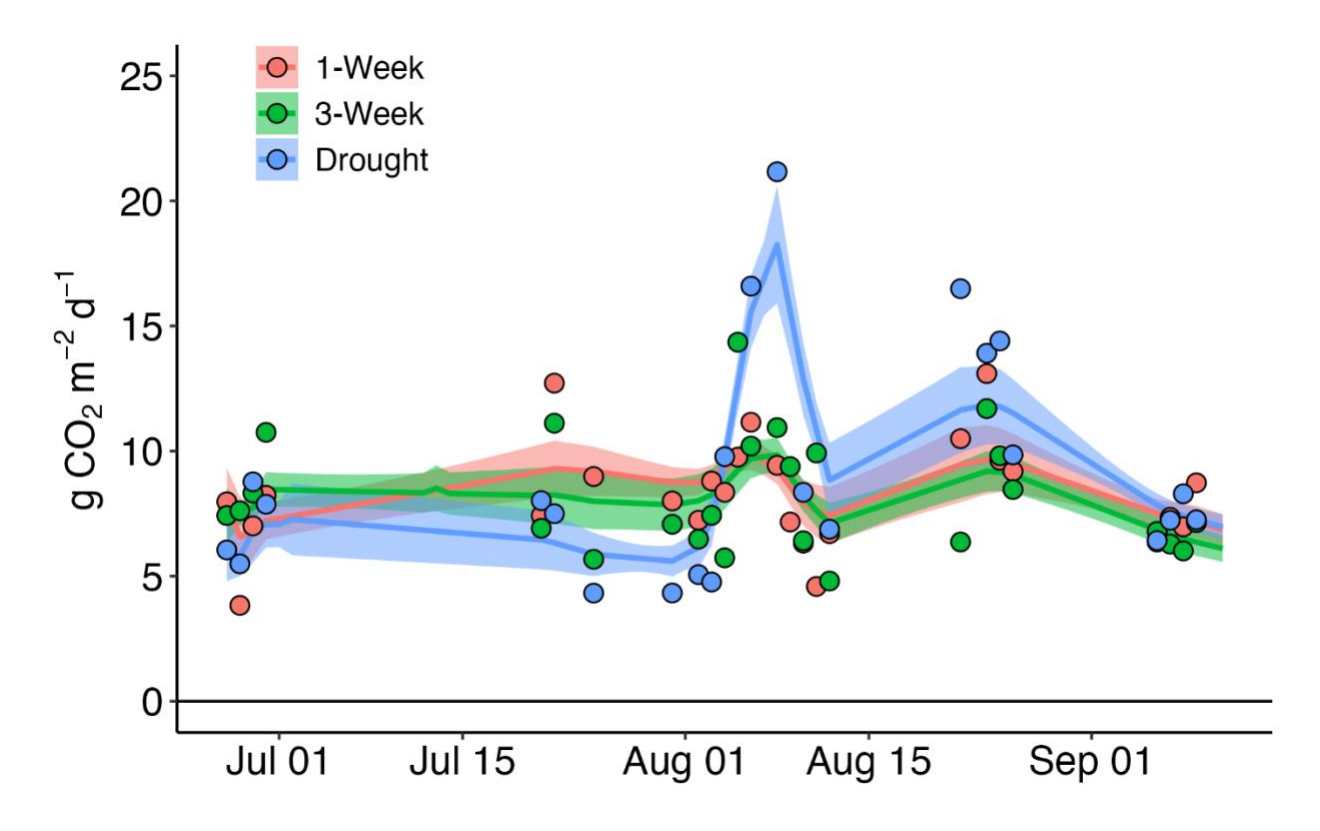


Figure 3.4. Daily soil heterotrophic CO₂ flux for each precipitation regime. Points represent the mean carbon dioxide flux for each day, for each precipitation regime, as measured in situ following wheat harvest with no plants present. Lines and shading represent the linearly interpolated CO₂ fluxes for each experimental unit (mean \pm s.e.). Data are from the CON and NT land uses combined, in 2022 following winter wheat harvest when no plants were present.

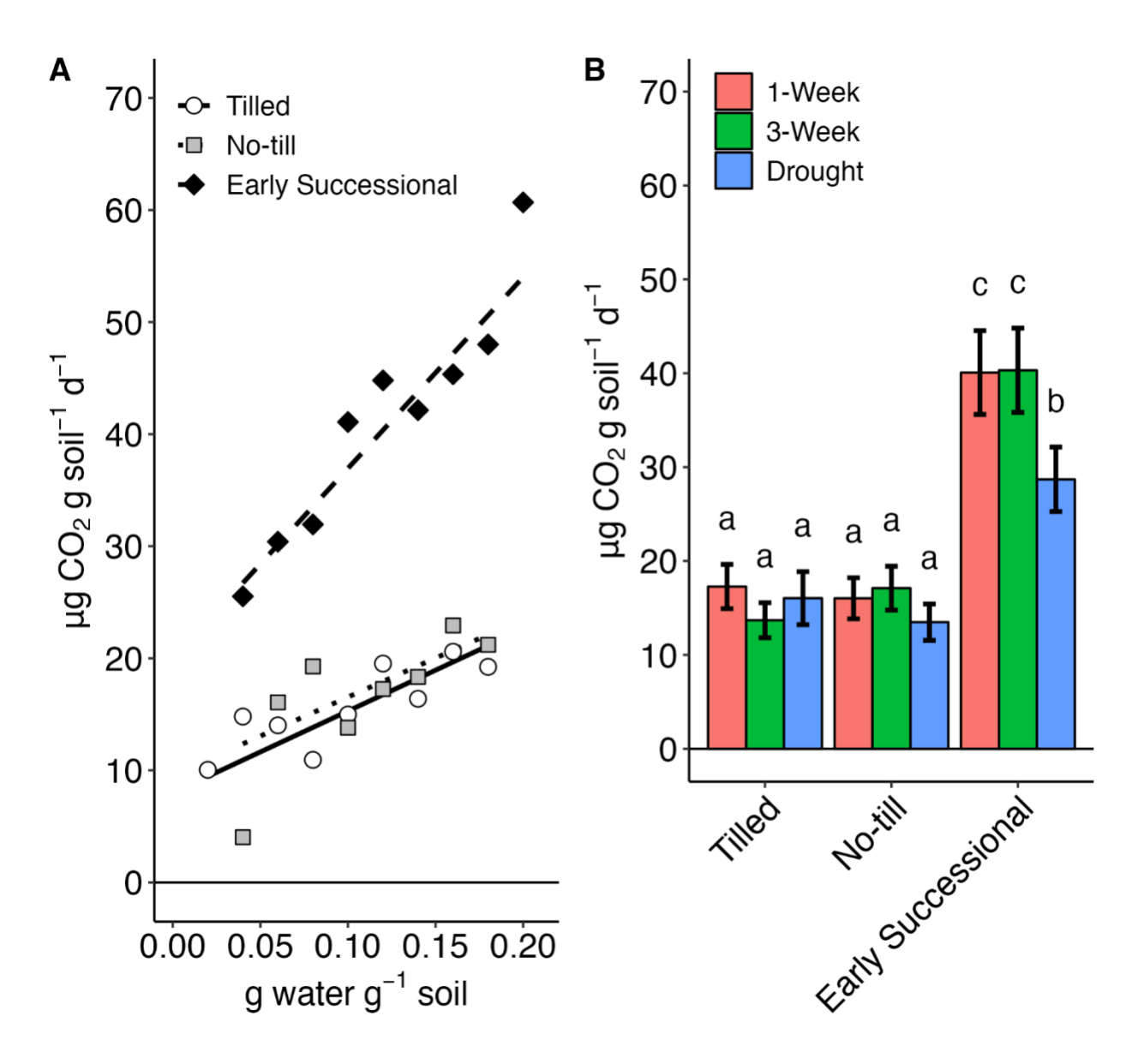


Figure 3.5. A) Relationship between laboratory-measured potential respiration and gravimetric soil water content for each land use (left). Points represent the carbon dioxide flux for each bin of gravimetric soil water content for each land use while lines represent the best fit. B) Soil CO_2 flux (mean \pm s.e.) measured just before the end of the drought for each precipitation regime and land use (right). Letters denote statistical differences across all groups. Data are from 2021-2023 sieved soil samples.

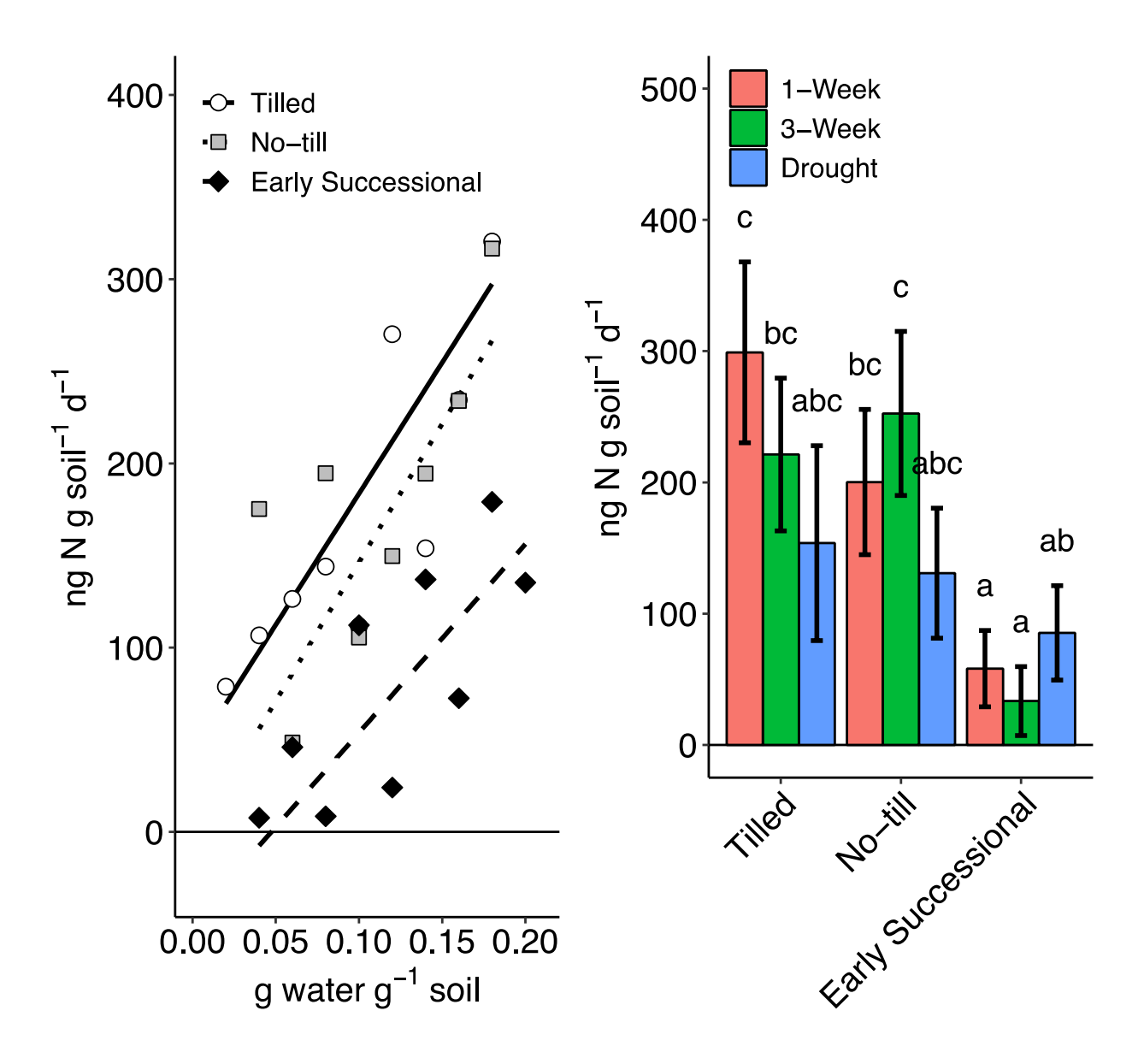


Figure 3.6. A) Relationship between **s**oil N mineralization rates and soil gravimetric water content for each land use (left). Points represent the mean soil nitrogen mineralization rates for each bin of gravimetric soil water content by land use. B) Soil nitrogen mineralization rates (mean \pm s.e.) measured just before the end of the drought for each precipitation regime and land use (right). Letters denote statistical differences across all groups. Data are from 2021-2022 sieved soil samples, measured in the lab.

CHAPTER 4: Symbiotic nitrogen fixation is resistant to increased precipitation variability but not to drought

Abstract

Symbiotic nitrogen fixation (SNF) is the predominant natural pathway for reactive nitrogen to enter terrestrial ecosystems. To a large extent, the terrestrial nitrogen supplies depend on the biogeochemical sensitives of legumes and their microbial symbionts. With projected shifts in precipitation patterns from a changing climate, SNF and the supply of reactive nitrogen to terrestrial ecosystems may also change. Furthermore, different land uses and vegetation types may mediate this response. At a site in SW Michigan USA, we experimentally manipulated precipitation quantity and distribution at the field scale with rain exclusion shelters in conventionally tilled (CON) and no-till (NT) row crops as well as an early successional (ES) plant community. We imposed a weekly small precipitation event treatment (1-Week) to represent historic rainfall, a three-week large precipitation event treatment (3-Week) to represent punctuated rainfall, and a six-week drought (Drought) during the middle of the growing season, and measured SNF rates as well as other plant and soil responses. We found that drought reduced SNF most in the CON land use (66 ± 7 % reduction), followed by the NT (35 ± 7 % reduction), and ES land uses (32 ± 20 % reduction) relative to their 1-Week precipitation treatment counterparts. Increasing precipitation variability did not significantly alter SNF rates (i.e., 1-Week vs 3-Week) in any of the land uses. Our results suggest that SNF rates for this critical terrestrial nitrogen supply pathway may be resistant to increases in precipitation variability, but not to prolonged precipitation deficits, and that agricultural management such as no-till can attenuate responses.

Introduction

Nitrogen is an essential resource for life and nitrogen availability is the starting point for terrestrial N pollution pathways such as NO₃* leaching and N₂O emissions. Symbiotic nitrogen fixation (SNF) in legumes is a major natural pathway for reactive nitrogen (N_r) to enter terrestrial ecosystems, responsible for 72% of all natural terrestrial N_r inputs globally, and 44% of combined natural and anthropogenic terrestrial N_r inputs (Robertson & Groffman, 2024; Vitousek et al., 2013). The terrestrial N_r supply is thus beholden to the physical, chemical and biological sensitivities of legumes and their microbial symbionts. Alterations of the biogeochemical factors controlling SNF are of global importance as their cascading impacts on terrestrial primary productivity, biodiversity, and N pollution have wide reaching effects (Robertson & Vitousek, 2009; Vitousek et al., 1997). One of the ecological factors controlling SNF is soil water status, a key determinant of SNF rates (Kirda et al., 1989). That soil water regimes of both natural and human-influenced ecosystems are changing in response to global climate change suggests that SNF rates and downstream N cycling may also be impacted (Robertson et al., 2013).

In the Midwestern region of the United States, projections from the World Climate Research Program's Coupled Model Intercomparison Project phase 6 suggest an increasing gap between growing season precipitation and potential evapotranspiration (PET), prompting questions about how SNF in agricultural and native legumes will respond (IPCC 2021). Gaps between water supply and demand will directly impact soil water storage. For example, Cook et al. (2020) evaluated surface soil moisture dynamics for Shared Socioeconomic Pathway 3-7.0 and their results suggest that by the end of the 21st century a one-in-ten year summer drought in

the Midwestern United States may become as frequent as one-in-three years (see also, Berg et al., 2017; Marvel et al., 2021).

There are also reports of contemporary changes in the timing and size of precipitation events and PET rates (Li et al., 2021; Rastogi et al., 2024; Zhao et al., 2023). Even with periods of equivalent total precipitation, the size and distribution of precipitation events can directly change soil water storage and its distribution through the vertical profile. For example, distributing precipitation over fewer but larger events can increase the partitioning of water to overland flow, decreasing overall infiltration, especially in ecosystems with significant slope, low vegetation cover, or fine textured surface soils. On the other hand, a shift towards fewer and larger precipitation events can distribute water deeper in the soil profile than an equivalent amount of precipitation spread over a greater number of smaller-sized events (Hess et al., 2018). For PET, the duration and intensity of hot, windy, and dry atmospheric conditions can cause non-linear changes in soil water dynamics and plant water stress when thresholds such as the permanent wilting point are crossed.

Legumes with their microbial symbionts may be able to resist short duration drought through mechanisms such as stomatal closure, leaf orientation adjustments, and reliance on stored C and water (Freitas et al., 2022; Valentine et al., 2010). However, longer duration droughts may draw down C and water stores beyond critical levels and impact overall growth and SNF rates (Serraj et al., 1999; Vitousek et al., 2013). Investigations of SNF responses to changes in soil water status are often performed in growth chambers or greenhouses and have provided important mechanistic detail about stress responses of both legumes and their symbionts (Dollete et al., 2023; Marino et al., 2007; Serraj, 2003). There have, however, been far fewer field scale investigations, with many focused on SNF response to supplemental irrigation

(e.g., Purcell & King, 1996) rather than to precipitation reductions and alterations of event size and timing. This is important because field scale processes not represented in growth chamber and greenhouse studies can interact with experimental treatments to alter conclusions about the relation of SNF to different precipitation regimes. For example, in situ differences in soil texture, organic matter content, and slope provide a set of pre-existing factors that can mediate the response of SNF to changing precipitation. These factors partition precipitation into overland flow, interception, and infiltration and are likely to be more variable at the field scale than in growth chambers and greenhouses, making field experiments crucial for estimating the real-world impact of changing precipitation regimes on SNF. Furthermore, field scale precipitation experiments allow for testing additional hypotheses about how different land uses alter soil characteristics and thus further affect the response of SNF to different precipitation regimes.

In agricultural ecosystems, soil management practices such as tillage and residue management are known to impact several aspects of the hydrologic cycle including precipitation partitioning and PET rates. Soil tillage can immediately expose buried soil to the surface environment, promoting evaporation and increasing the potential for soil erosion and overland flow. The removal of crop residue through harvest, tillage, or fire can increase direct absorption of solar radiation by soil, increasing soil temperatures and PET rates (Schwartz et al., 2010). Residue removal can also expose more soil surface area to direct raindrop impacts and cause surface sealing when suspended silt and clay particles redistribute to surface soil pores, which can shift the partitioning of precipitation from infiltration towards overland flow. On the other hand, the retention of surface residue can also increase the proportion of precipitation that is intercepted and decrease the amount that enters the soil (Zhai et al., 1990). Thus, in situ investigations of how land management practices can mediate the resistance and resilience of

SNF to changing precipitation regimes can provide insights on land uses that could serve as climate change adaptation strategies (Robertson & Vitousek, 2009).

Here we investigate the in situ response of SNF to changing precipitation regimes in a field experiment with contrasting land managements. We use the natural abundance ¹⁵N isotope technique (e.g., Gelfand & Robertson, 2015) to examine SNF under three different precipitation regimes in order to test hypotheses about precipitation amount as well as event size and timing. We use two agricultural fields planted to soybeans (*Glycine max* L.) managed with or without tillage, as well as an early successional land use that has red clover (*Trifolium pratense*) and is maintained by annual prescribed fire. These fields allow us to test hypotheses about how alternative management practices might mediate the resistance and resilience of SNF to changing precipitation regimes.

We test three hypotheses: (H1) soil water limitations that cause stomatal closure will limit the supply of photosynthate to nodules and thus SNF; (H2) land management practices that increase soil water infiltration and retention will promote the resistance of SNF to soil water limitations; and (H3) land management practices that increase the mineralization of organic N will promote the substitution of soil derived N for atmospheric N during periods of water limitation. To test these hypotheses, we measured N fixation rates, soil water content, soil C and N mineralization rates, and plant productivity and water stress metrics under different experimental rainfall regimes.

Methods

Study Site

We conducted this study at the W.K. Kellogg Biological Station's Long Term Ecological Research (LTER) site in Southwest Michigan USA (42.4 N, 85.4 W). Established in 1989, this

experiment has followed the impacts of several different land management treatments for 33 years (Robertson & Hamilton, 2015). Prior to the initiation of the experiment the site was managed with a rotation of annual row crops from circa 1850 to 1988. Before 1850 the site existed in a matrix of mid- to late succession temperate deciduous broadleaf forest. The mean annual surface air temperature is 9.3 °C and the mean annual precipitation is 1067 mm (Thornton et al., 2022). During the growing season, from April to October, the mean weekly precipitation is 24.1 mm. Soils are well-drained fine-loamy, mixed, active, mesic Typic Hapludalfs and consists of loamy glacial outwash overlying sand (Luehmann et al., 2016).

In this study we utilized the LTER Main Cropping System Experiment's Conventional (CON) and No-till (NT) agriculture treatments (Robertson & Hamilton, 2015) which are managed as three-year corn, soybean, and winter wheat rotations. We also utilized the Early Successional (ES) treatment, which is managed by annual prescribed fire each spring. All treatments are replicated as 1 ha plots in each of six blocks in a randomized complete block design. In 2021 the agricultural land use treatments were in the soybean phase of their rotation. For both the CON and NT land use treatments we used four experimental replicates. For the ES land use treatment, which has considerably more variation in plant community composition, we used six experimental replicates.

Three rain exclusion shelters 4 by 5 m (Kahmark et al. 2024) were deployed during the growing season in each experimental replicate. Each shelter was fitted with plastic roofing to block precipitation but not light. The shelters were equipped with irrigation sprinklers managed to meet three different scenarios: 1) a 1-Week irrigation schedule to represent historical rainfall patterns (one 30.8 mm event per week), 2) a 3-Week irrigation schedule to represent punctuated rainfall (one 92.4 mm event every 3rd week), and 3) a 6-week drought. Over the 9-week period

when the shelters were in place, the 6-week drought received a rainfall deficit of 66% relative to the other treatments (82 mm in the drought vs 240 mm in the 1-Week precipitation treatment). *Nitrogen fixation*

We used the ¹⁵N natural abundance isotope technique for measuring nitrogen fixation (e.g., Gelfand & Robertson, 2015). This method takes advantage of the different ¹⁵N:¹⁴N isotope ratios of N derived from the soil and from the atmosphere. We planted a non-nodulating genetic variant of soybean (USDA Soybean Germplasm Collection accession number PI547695) in each of the agricultural experimental units, with up to six individuals per rainout shelter at spacings that mimic standard agronomic practice at the site. All of the N assimilated by non-nodulating soybeans comes from the soil, allowing them to serve as one end member in the ¹⁵N mixing model (Eq. 1). The other end member was taken from commercial variety soybeans grown in N-free potting media at the study site, which forces them to assimilate only atmospheric N. Because the majority (84%) of fixed N in soybeans ends up in the seeds by the end of the growing season (Gelfand & Robertson, 2015), we used seed ¹⁵N to assay plant SNF response. In the ES land use, red clover is the dominant legume that we used to assay SNF responses. The soybean derived end members were also used for the red clover.

The proportion of N coming from the atmosphere was calculated according to Eq. 1.

$$SNF = \frac{\delta^{15}N_{non} - \delta^{15}N_{com}}{\delta^{15}N_{non} - \delta^{15}N_{atm}}$$
 Eq. 1)

where $\delta^{15}N_{non}$, $\delta^{15}N_{com}$, and $\delta^{15}N_{atm}$ are the $\delta^{15}N$ signatures of the non-nodualting, commercial, and N-free potting media plants, respectively. For the soybeans and clover, a 1 and 0.2 m² quadrat, respectively, were used to sample aboveground biomass after plant senescence. Seeds were separated from the aboveground biomass and were dried at 60 °C, weighed, and pulverized using an Shatterbox 8530 (SPEX SamplePrep NJ, USA) for isotope analysis. For each

sample the C and N concentration as well as the δ^{13} C and δ^{15} N isotope values were measured at the Michigan State University Isotope Analysis Lab using an IsoPrime Vision isotope ratio mass spectrometer (Elementar, NY, USA).

Soil measurements

Soil volumetric water content was measured hourly over a 0-25 cm depth interval with soil moisture probes (Campbell Scientific CS650) installed in each plot. For potential soil heterotrophic respiration and N mineralization rates, in each plot one soil sample 0-25 cm deep was collected with a 1.25 cm diameter probe 1 week before and 1 week after the drought ended. Soil samples were immediately sieved to 2 mm, and 40 g subsamples were placed into glass jars with loosely fitted lids to allow for minimal water loss but sufficient gas exchange. The jars were placed in an incubator at 25 °C and 80 % relative humidity. The sample's C mineralization rate was measured the following day as described below. A 10 g subsample was taken from each jar for gravimetric water content measurements, which were determined by drying in a 60 °C oven. For soil inorganic N analysis two 10 g subsamples were immediately extracted in 100 mL of 1 M KCl. The soil and KCl mixture were shaken for 60 s, allowed to sit overnight, shaken again for 60 s, allowed to sit for 1 h, and then filtered through a 1 um paper filter to remove soil particles.

To measure net N mineralization rates samples in glass jars were incubated for 14 days and two 10 g samples were similarly extracted and analyzed for their inorganic N content.

Extracts were frozen until analysis on a Lachat QuickChem 8500 Series 2 Flow Injection

Analysis System (Hach, CO, USA) for NH₄⁺ and NO₃⁻ concentrations. The difference in NH₄⁺-N plus NO₃⁻-N concentrations between samples before and after the 14-day incubation period were used as a measure of net N mineralization.

For soil C mineralization rates the jars with soil samples were sealed with airtight caps fitted with rubber septa the day after they were taken from the field. The headspace of each jar was sampled with a 1 mL syringe 4 times over the course of 2 h and immediately injected into a LICOR 820 infrared gas absorption analyzer (LICOR NE, USA) that was fed by a stream of N2 carrier gas. The change in jar headspace CO2 concentration was calculated by linear regression and taken as a measurement of soil C mineralization. The gravimetric water contents of these samples were used to express both the C and N mineralization rates on a per g dry soil basis. *Plant measurements*

The δ^{13} C values of the seeds was measured in the same samples used for 15 N. The δ^{13} C in plant biomass has been used to infer growing season-integrated plant water stress because the restriction of stomatal conductance during drought results in greater CO₂ limitation within the plant cells, which in turn results in a higher proportion of assimilation of 13 CO₂ relative to 12 CO₂ in comparison to non-water stressed conditions.

An overhead canopy image was taken during the peak of the drought by temporarily removing the rain exclusion shelters. A DJI Matrice 100 model drone (DJI, Shenzhen, China) equipped with an Altum-PT multispectral and thermal camera (Micasense WA, USA) was flown at 150 m height over the study site on 2021-08-20. The enhanced vegetation index (EVI) was calculated for each pixel using Eq. (2) following (Huete et al., 2002).

$$EVI = 2.5 * \frac{NIR - Red}{NIR + 6*Red - 7.5*Blue + 1}$$
 Eq. 2)

where NIR, Red and Blue represent the surface reflectance values of the near-infrared, red and blue bands, respectively. We used EVI to represent absorbed photosynthetically active radiation in a light use efficiency model to calculate gross primary production following Bao et al. (2022).

$$GPP = LUE * APAR * F_T$$
 Eq. 3)

where GPP is gross primary production in g C m⁻² d⁻¹, LUE is the light use efficiency of each plant type in g C MJ⁻¹ photosynthetically active radiation, APAR is the absorbed photosynthetically active radiation in MJ m⁻² d⁻¹, and F_{vpd} , F_T and F_{Cl} represent scaling factors of vapor pressure deficit, air temperature, and cloudiness respectively. Equations for APAR and F_T are:

$$APAR = FPAR * Rs$$
 Eq. 4)

$$F_T = if \ T_a < T_{min} \ or \ T_a > T_{max}, 0, \ else \ \frac{(T_a - T_{min}) * (T_a - T_{max})}{(T_a - T_{min}) * (T_a - T_{opt})^2}$$
 Eq. 5)

where FPAR is the fraction of photosynthetically active radiation that is absorbed by green leaves, which in this study is approximated by EVI, and Rs is the incoming solar radiation. T_a is the mean daily air temperature at 2 m, T_{min} is 0 °C, T_{max} is 40 °C, and T_{opt} is 25 °C. Meteorological data was provided by a weather station maintained on site (https://lter.kbs.msu.edu/datatables/12).

Surface evapotranspiration (ET) was estimated with the surface temperature derived from the thermal infrared image. We utilized the Operational Simplified Surface Energy Balance (SSEBop) model using the Forcing and Normalizing Operation following Senay et al. (2023)/

$$ETa = ETr * (1 - \gamma^{s} * (Ts - Tc))$$
 Eq. 8)

where ETa is the actual evapotranspiration rate in mm d⁻¹, ETr is the potential evapotranspiration derived from the Penman-Montieth equation (mm d⁻¹), γ^s is the surface psychrometric constant (°C⁻¹), Ts is the surface temperature °C, and Tc is the wet-bulb reference surface temperature limit °C. Both the light use efficiency model and ET model were validated with two eddy covariance towers located nearby.

During the peak of the drought leaf level gas exchange measurements were made with a LICOR 6800 Portable Photosynthesis System (LICOR NE, USA) in the soybean systems. Due to

the need to maintain the integrity of other plants in the ES plots it was not possible to measure leaf level gas exchange of clover with the LICOR 6800 unit. Two soybean plants were selected at random within each plot and the uppermost fully mature sunlit leaf was clamped with the instrument. After a three-minute equilibration period, gas exchange measurements of CO₂ and H₂O were made for five minutes. Chamber light conditions were set at 1400 µmol m⁻² s⁻¹. Chamber temperature and vapor pressure deficit were set at 33 °C and 70% relative humidity. *Statistical Analysis*

The experiment follows a split plot design where land use treatment is the whole plot factor and precipitation treatment is the split plot factor. For statistical methods we used linear mixed effect models. For each of the response variables analyzed (e.g., SNF rates) we used land use, precipitation regime and their interaction as fixed effects. For random effects the whole plot. Residuals were examined for normality and homogeneous variances across treatment groups. Normality corrections were performed by transformations of the response variable with a square root or logarithmic transformation. Heterogeneous variance was identified where clover and soybeans had substantial scale differences and were addressed by fitting an unequal variance linear mixed effect regression model where variance was specific for each plant type, i.e., clover and soybean. Statistical differences were evaluated at an alpha of 0.05.

Results

Soil water content

The imposed drought significantly reduced soil water content while the 3-Week precipitation treatment significantly increased the range of soil water content variability relative to the 1-Week precipitation treatment (Figure 4.1). Land management practices mediated the impact of the three precipitation treatments on soil water content. During the four weeks leading

up to the final precipitation event, the imposed Drought caused a 42%, 30% and 43% reduction of soil water content in the CON, NT, and ES land use treatments compared to their 1-Week precipitation treatment counterparts, respectively. For the imposed Drought precipitation treatment during this period the CON, NT and ES land use treatments had soil volumetric water contents of 0.12, 0.20, and 0.13 cm³ cm⁻³, respectively (s.e. for all < 0.03; Table 4.1). During the same 4 week period, within each land use, soil water contents were similar between the 1-Week and 3-Week precipitation treatments. For the CON, NT and ES land use treatments soil water contents ranged from 0.17 - 0.20, 0.25 - 0.28, and 0.23 - 0.24 cm³ cm⁻³, respectively.

Nitrogen fixation

SNF declined with imposed drought in soybean, but not in clover (Figure 4.2). SNF rates in the Drought precipitation treatment were 66%, 35%, and 32% lower in the CON, NT and ES land use treatments when compared with their 1-Week precipitation counterparts, respectively. For the Drought treatment, the CON, NT and ES land use treatments had SNF rates of 5.73, 10.50, and 0.10 g N m⁻² y⁻¹, respectively (soybean s.e. all < 1.27; clover s.e. = 0.03; Table 4.3). Within each land use, SNF rates were similar between the 1-Week and 3-Week precipitation treatments: $15.60 - 17.02 \text{ g N m}^{-2} \text{ y}^{-1}$ for soybeans and $0.06 - 0.15 \text{ g N m}^{-2} \text{ y}^{-1}$ for clover. The percentage of N derived from the atmosphere was not statistically different across land use and precipitation treatments and the concentration of N in the seeds only differed by plant species (i.e. higher in soybeans than clover; Table 4.1).

Stomatal conductance

SNF results were mirrored by the ¹³C isotope ratios, with less negative ¹³C values, which correspond to lower stomatal conductance, in plots with lower rates of SNF (Figure 4.3). The correlation coefficient between SNF rates and seed ¹³C was 0.69 (p < 0.01) for soybeans, but

uncorrelated for clover (r = 0.69, p = 0.62; data shown in Figures 4.2 and 4.3). For the Drought treatment, the CON, NT and ES land use treatments had 13 C values of -25.8 ‰, -27.0 ‰, and -28.8 ‰, respectively (s.e. all < 0.2 ‰; Figure 4.3). The 13 C isotope values in the ES land use treatment were not significantly affected by the three precipitation treatments. Similarly, in the CON and NT land use treatments, the 1-Week and 3-Week precipitation treatments had equivalent 13 C isotope values (-28.3 ‰ to -28.6 ‰, s.e. all < 0.21 ‰; Figure 4.3).

Evapotranspiration and gross primary production

Canopy ET rates were reduced by the imposed drought across each land use treatment, but not by increased precipitation variability (Figure 4.4). Drought reduced ET rates more in the CON land use treatment (42 % reduction) than in the NT (27 % reduction) or ES land use treatments (17 % reduction; Figure 4.4). For the Drought precipitation treatment, the CON, NT and ES land use treatments had ET rates of 1.6, 2.0, and 2.3 mm d⁻¹, respectively (s.e. all < 0.15 mm d⁻¹; Figure 4.4). ET rates were statistically similar across all land uses for the 1-Week and 3-Week precipitation treatments.

Drone images also showed that GPP rates were reduced by drought across each land use treatment, but not by increased precipitation variability. Drought reduced GPP rates more in the CON land use treatment (19 % reduction) than in the NT (7 % reduction) or ES (10 % reduction) land use treatments (Figure 4.5). For the Drought precipitation treatment, the CON, NT and ES land use treatments had GPP rates of 14.2, 16.7, and 14.0 g C m⁻² d⁻¹, respectively (s.e. all < 0.5 g C m⁻² d⁻¹; Figure 4.5). Within each land use treatment, GPP rates were statistically similar for the 1-Week and 3-Week precipitation treatments. ES GPP rates were lower (15.4 – 15.7 g C m⁻² d⁻¹) than the CON and NT GPP rates (16.7 – 17.4 g C m⁻² d⁻¹; Figure 4.5).

Leaf level gas exchange

Leaf level gas exchange for the soybeans mirrored canopy scale GPP and ET derived from the drone images as well as the 13 C isotope data (Table 4.4). Net CO₂ assimilation (A_{net}) rates were reduced by the imposed drought across each land use treatment, but not by increased precipitation variability. Drought reduced A_{net} rates equally in the CON land use treatment (69 % reduction) and the No-till (63 % reduction) land use treatments. For the imposed Drought precipitation treatment, the CON and NT land use treatments had A_{net} rates of 8.4, and 10.2 μ mol CO₂ m⁻² s⁻¹, respectively (s.e. all < 4.3 μ mol CO₂ m⁻² s⁻¹). A_{net} rates were statistically similar across each land use for the 1-Week and 3-Week precipitation treatments (27.4 – 34.6 μ mol CO₂ m⁻² s⁻¹, s.e. all < 4.3 μ mol CO₂ m⁻² s⁻¹).

Leaf level transpiration (E) rates were reduced by the imposed drought across each land use treatment, but not by increased precipitation variability. Drought reduced leaf level transpiration rates equally in the CON (89% reduction) and the NT (81% reduction) land use treatments. For the Drought precipitation treatment, the CON and NT land use treatments had transpiration rates of 0.79 and 1.47 mmol $\rm H_2O~m^{-2}~s^{-1}$, respectively (s.e. for all < 0.37 mmol $\rm H_2O~m^{-2}~s^{-1}$). Transpiration rates were statistically similar across each land use for the 1-Week and 3-Week precipitation treatments (7.10 – 8.85 mmol $\rm H_2O~m^{-2}~s^{-1}$, s.e. for all < 1.95 mmol $\rm H_2O~m^{-2}~s^{-1}$).

Intercellular CO₂ concentrations (Ci) as estimated by the LICOR 6800 gas exchange measurements were reduced by the imposed drought across each land use treatment, but not by increased precipitation variability. Drought reduced Ci more in the CON land use treatment (59% reduction) than in the NT land use treatment. (32% reduction). For the Drought precipitation treatment, the CON and NT land use treatments had Ci's of 132 and 221 ppm CO₂, respectively

(s.e. for all < 17.5 ppm CO_2). Ci estimates were statistically similar across each land use for the 1-Week and 3-Week precipitation treatments (316 – 326 ppm CO_2 , s.e. for all < 9.3 ppm CO_2) Plant N uptake

Soil derived N and total N uptake had similar patterns when compared to atmospheric derived N (Table 4.3). Soil N uptake declined with the imposed drought in soybean, but not in clover (Figure 4.2). Soil N uptake in the Drought precipitation treatment was 45 %, 39 % and 10 % lower in the CON, NT and ES land use treatments when compared with their 1-Week precipitation counterparts, respectively. For the Drought precipitation treatment, the CON, NT and ES land use treatments had soil N uptake rates of 5.72, 4.70, and 0.09 g N m⁻² y⁻¹, respectively (soybean s.e. for all < 1.15; clover s.e. = 0.03; Table 4.3). Within each land use, soil N uptake rates were similar between the 1-Week and 3-Week precipitation treatments: 6.26 - 10.43 g N m⁻² y⁻¹ for soybeans and 0.04 - 0.10 g N m⁻² y⁻¹ for clover.

Total plant N uptake declined with the imposed drought in soybean, but not in clover (Figure 4.2). Total plant N uptake in the Drought precipitation treatment was 53 %, 47 %, and 41 % lower in the CON, NT and ES land use treatments when compared with their 1-Week precipitation counterparts, respectively. For the imposed Drought precipitation treatment, the CON, NT and ES land use treatments had total plant N uptake rates of 13.03, 15.26, and 0.17 g N m⁻² y⁻¹, respectively (soybean s.e. for all < 1.06; clover s.e. = 0.05; Table 4.3). Within each land use, total plant N uptake rates were similar between the 1-Week and 3-Week precipitation treatments: 22.7 - 27.8 g N m⁻² y⁻¹ for soybeans and 0.13 - 0.29 g N m⁻² y⁻¹ for clover. *Soil C and N mineralization*

Soil C mineralization rates were significantly reduced by drought in the CON (44 % reduction) and ES (31 % reduction) land uses, but not in the NT land use treatment relative to

their 1-Week precipitation treatments (Table 4.2). For the Drought precipitation treatment, the CON, NT and ES land use treatments had soil C mineralization rates of 3.64, 4.80 and 9.22 $\mu g CO_2 - C g^{-1}$ soil d⁻¹, respectively (soybean s.e. for all < 0.91; clover s.e. = 1.49; Table 4.2). Within each land use, the 1-Week and 3-Week precipitation treatments mineralized C at similar rates: 3.64 - 6.79 $\mu g CO_2 - C g^{-1}$ soil d⁻¹ for soybeans and 12.79 - 13.28 $\mu g CO_2 - C g^{-1}$ soil d⁻¹ for clover. The CON 1-Week treatment mineralized C at a rate 79 % higher that the NT 1-Week treatment while the ES 1-Week treatment mineralized C at a rate 349 % higher than the NT 1-Week treatment.

Soil N mineralization rates were significantly reduced by drought, but only in the CON land use treatment (Table 4.2). Relative to its 1-Week precipitation treatment, the CON land use mineralized 46 % less N during the drought. However, within the 1-Week precipitation treatments, the CON land use treatment had an 81 % higher rate of N mineralization than the NT land use during the same period. For the Drought precipitation treatment, the CON, NT and ES land use treatments had soil N mineralization rates of 2.02, 1.50 and 0.23 μ g N g⁻¹ soil d⁻¹, respectively (soybean s.e. all < 0.52; clover s.e. = 0.35; Table 4.2). Within each land use, the 1-Week and 3-Week precipitation treatments mineralized soil N at similar rates: 2.06 – 3.72 μ g N g⁻¹ soil d⁻¹ for soybeans and 0.36 - 1.00 μ g N g⁻¹ soil d⁻¹ for clover. The ES land use tended to have lower rates of N mineralization than the other two land use treatments with a range of 0.23 - 1.00 μ g N g⁻¹ soil d⁻¹, respectively.

Discussion

Our results show clear effects of precipitation regime on soil water availability and SNF rates as well as on other plant and soil responses. Our first hypothesis (H1) is that soil water limitations cause stomatal closure, limiting the supply of photosynthate to nodules and thus

limiting SNF. We found support for each component of H1. First, soil water availability was limited by our experimental rainfall treatments as shown in Figure 4.1. Second, stomatal closure and the resulting slowdown in transpiration and gross primary production was shown by the ¹³C isotope values of the seeds, the drone-based ET and GPP data, and as well by the leaf level gas exchange data Ci, E and A_{net} (Figures 4.3 & 4.4; Table 4.4). While this water stress response was able to reduce the loss of water, the closure of the stomata also limited CO₂ uptake. This caused a reduced supply of photosynthate to the nodules, limiting SNF rates as shown by the ¹⁵N isotope data (Figure 4.2). Other studies investigating these mechanisms have found that stomatal responses to soil water limitations are key to resisting drought stress but the resulting slowdown in CO₂ assimilation is also consequence that impacts SNF (Huber et al., 2019; Martin-StPaul et al., 2017; Pirasteh-Anosheh et al., 2016; Reynolds-Henne et al., 2010).

Our second hypothesis (H2) is that land management practices that increase soil water infiltration and retention will promote the resistance of SNF to precipitation limitations. We found higher soil water content levels in the NT land use when compared to the CON land use across all three precipitation treatments when the rain exclusion shelters were present. The NT land use also had higher soil water content than the ES land use treatment in the 1-Week and Drought precipitation treatments. We thus infer that the soil water content differences between the CON and NT land uses are caused by differences in the water and energy partitioning of these treatments. NT management has been shown to reduce overland flow and thus increase water infiltration when compared to conventional tillage (Schwartz et al., 2010). Furthermore, preserving plant residue on the soil surface buffers the transfer of incoming solar radiation to the soil column and thus mitigates soil evaporation rates (Aiken et al., 1997; Kozak et al., 2007). We interpret the differences in soil water content between the ES and NT land uses as being

influenced by the differences in the vegetation community present. Plants in the ES land use has an earlier phenological start than the soybeans in the CON and NT land uses (i.e., early April vs late May, respectively) and the ES plant community has a more extensive root system earlier in the season. Both of these factors would support higher ET rates and higher interception rates early in the growing season. Other studies of how vegetation type influences the partitioning of water and energy have found that both vegetation phenology and plant residue are important drivers of how water enters the soil and how much energy is available to support evaporation (Gong et al., 2017; Gonzalez-Sosa et al., 1999; Marchesini et al., 2015; Wilson et al., 2000).

We found support for H2 by documenting a lower reduction in SNF rates in the NT drought treatment when compared to the CON drought treatment (Figure 4.2). However, we observed no statistical differences in SNF rates between the three precipitation treatments of the ES land use. The lack of support for H2 in the ES land use treatment may be related to flowering period differences. While in this experiment the soybean flowering period largely overlapped with the precipitation manipulations, clover has a much longer flowering period that precedes and follows the precipitation manipulation (i.e. April through October). When making our measurements of SNF we did not distinguish between clover seeds that were produced before, during, or after the precipitation manipulation period, which may have muted the precipitation effects on SNF rates that we were able to capture. Other studies of SNF and precipitation variability have shown that precipitation timing is a key determinant of SNF rates and that land management practices can mediate this response (Barbieri et al., 2023; Dollete et al., 2023; Lumactud et al., 2023; Van Kessel & Hartley, 2000).

Our third hypothesis (H3) is that land management practices that increase the mineralization of organic N will promote the substitution of soil derived N for atmospheric N

during periods of water limitation. Within the 1-Week precipitation treatment we found that the CON land use had higher rates of soil N mineralization, soil C mineralization, and total plant N uptake in seeds when compared with the NT land use (Tables 4.2 & 4.3). We infer that the higher total seed N uptake in the CON plots was caused by the higher soil organic matter mineralization rates supplying organic N to the plants. When comparing the Drought precipitation treatments, we found that total N uptake in seeds was not different between the CON and NT land uses, while the SNF rates were relatively higher in the NT land use. Furthermore, we found that the soil C and N mineralization rates in these Drought precipitation treatments were equivalent. This suggests that the ability of the CON land use to maintain C and N mineralization rates similar to the NT land use despite having lower soil water contents during the drought may be the reason why the two land uses had equal resistance of total plant N uptake to drought (Table 4.3) but no resistance to SNF. Other studies of soil C and N mineralization and precipitation regimes have found that rates can decline as soils dry but that the accumulation of mineralizable substrates and the rapid response of microorganism following rewetting can cause overall rates to be similar when compared to non-water stressed conditions (Borken & Matzner, 2009; Cregger et al., 2014; Deng et al., 2021; Homyak et al., 2017; Schaeffer et al., 2017).

The ES land use had higher C mineralization rates than the other land uses but lower N mineralization rates. This suggests that a larger amount of soil organic matter was being decomposed but that a smaller amount of N was being released into the soil solution. While gross N mineralization rates could have been high, the retention of that N in microbial biomass limited the release of it to the soil solution and to plants. This suggests that the ES land use would not be able to confer resistance of total plant N uptake to a drought. However, we were not able to detect statistical differences between total plant N uptake between the 1-Week and

Drought precipitation treatments in the ES land use. Therefore, while the CON and NT land uses offered support for H3, the ES land use did not.

Overall, the differences in the soil water contents of the 3-Week precipitation treatments did not translate into differences in SNF rates. This suggests that future climate change scenarios with increased precipitation variability may not necessarily lead to changes in the rates of N fixation. Our results suggest instead that the type of change in future precipitation regimes (quantity vs distribution) may determine the response of SNF. Legumes and their microbial symbionts may be more well buffered against increases in precipitation variability than against prolonged precipitation deficits. However, the other aspects of a changing climate, especially surface air temperature and CO₂ fertilization effects, may change the sign and/or magnitude of the soil and plant responses measured here (Ainsworth, 2003; Butterly et al., 2016; Parvin et al., 2019; Rogers et al., 2009; Vadez et al., 2012; Whittington et al., 2013). Future studies that examine the interaction of precipitation, temperature and CO₂ concentration changes on SNF will be useful for disentangling the separate and combined effects of these climate change drivers.

REFERENCES

- Aiken, R. M., Flerchinger, G. N., Farahani, H. J., & Johnsen, K. E. (1997). Energy balance simulation for surface soil and residue temperatures with incomplete cover. *Agronomy Journal*, 89(3), 404–415. https://doi.org/10.2134/agronj1997.00021962008900030007x
- Ainsworth, E. A. (2003). Variation in acclimation of photosynthesis in *Trifolium repens* after eight years of exposure to Free Air CO₂ Enrichment (FACE). *Journal of Experimental Botany*, *54*(393), 2769–2774. https://doi.org/10.1093/jxb/erg309
- Bao, S., Wutzler, T., Koirala, S., Cuntz, M., Ibrom, A., Besnard, S., Walther, S., Šigut, L., Moreno, A., Weber, U., Wohlfahrt, G., Cleverly, J., Migliavacca, M., Woodgate, W., Merbold, L., Veenendaal, E., & Carvalhais, N. (2022). Environment-sensitivity functions for gross primary productivity in light use efficiency models. *Agricultural and Forest Meteorology*, 312, 108708. https://doi.org/10.1016/j.agrformet.2021.108708
- Barbieri, P., Starck, T., Voisin, A.-S., & Nesme, T. (2023). Biological nitrogen fixation of legumes crops under organic farming as driven by cropping management: A review. *Agricultural Systems*, 205, 103579. https://doi.org/10.1016/j.agsy.2022.103579
- Berg, A., Sheffield, J., & Milly, P. C. D. (2017). Divergent surface and total soil moisture projections under global warming. *Geophysical Research Letters*, 44(1), 236–244. https://doi.org/10.1002/2016GL071921
- Borken, W., & Matzner, E. (2009). Reappraisal of drying and wetting effects on C and N mineralization and fluxes in soils. *Global Change Biology*, *15*(4), 808–824. https://doi.org/10.1111/j.1365-2486.2008.01681.x
- Butterly, C. R., Armstrong, R., Chen, D., & Tang, C. (2016). Free-air CO₂ enrichment (FACE) reduces the inhibitory effect of soil nitrate on N₂ fixation of *Pisum sativum*. *Annals of Botany*, *117*(1), 177–185. https://doi.org/10.1093/aob/mcv140
- Cook, B. I., Mankin, J. S., Marvel, K., Williams, A. P., Smerdon, J. E., & Anchukaitis, K. J. (2020). Twenty-first century drought projections in the CMIP6 forcing scenarios. *Earth's Future*, 8(6), e2019EF001461. https://doi.org/10.1029/2019EF001461
- Cregger, M. A., McDowell, N. G., Pangle, R. E., Pockman, W. T., & Classen, A. T. (2014). The impact of precipitation change on nitrogen cycling in a semi-arid ecosystem. *Functional Ecology*, 28(6), 1534–1544. https://doi.org/10.1111/1365-2435.12282
- Deng, L., Peng, C., Kim, D.-G., Li, J., Liu, Y., Hai, X., Liu, Q., Huang, C., Shangguan, Z., & Kuzyakov, Y. (2021). Drought effects on soil carbon and nitrogen dynamics in global natural ecosystems. *Earth-Science Reviews*, 214, 103501. https://doi.org/10.1016/j.earscirev.2020.103501
- Dollete, D., Lumactud, R. A., Carlyle, C. N., Szczyglowski, K., Hill, B., & Thilakarathna, M. S. (2023). Effect of drought stress on symbiotic nitrogen fixation, soil nitrogen availability

- and soil microbial diversity in forage legumes. *Plant and Soil*. https://doi.org/10.1007/s11104-023-06348-1
- Freitas, V. F. D., Cerezini, P., Hungria, M., & Nogueira, M. A. (2022). Strategies to deal with drought-stress in biological nitrogen fixation in soybean. *Applied Soil Ecology*, *172*, 104352. https://doi.org/10.1016/j.apsoil.2021.104352
- Gelfand, I., & Robertson, G. P. (2015). A reassessment of the contribution of soybean biological nitrogen fixation to reactive N in the environment. *Biogeochemistry*, 123(1–2), 175–184. https://doi.org/10.1007/s10533-014-0061-4
- Gong, T., Lei, H., Yang, D., Jiao, Y., & Yang, H. (2017). Monitoring the variations of evapotranspiration due to land use/cover change in a semiarid shrubland. *Hydrology and Earth System Sciences*, 21(2), 863–877. https://doi.org/10.5194/hess-21-863-2017
- Gonzalez-Sosa, E., Braud, I., Jean-Louis, T., Michel, V., Pierre, B., & Jean-Christophe, C. (1999). Modelling heat and water exchanges of fallow land covered with plant-residue mulch. *Agricultural and Forest Meteorology*, *97*(3), 151–169. https://doi.org/10.1016/S0168-1923(99)00081-7
- Hess, L. J. T., Hinckley, E.-L. S., Robertson, G. P., Hamilton, S. K., & Matson, P. A. (2018). Rainfall intensification enhances deep percolation and soil water content in tilled and notill cropping systems of the US Midwest. *Vadose Zone Journal*, *17*(1), 1–12. https://doi.org/10.2136/vzj2018.07.0128
- Homyak, P. M., Allison, S. D., Huxman, T. E., Goulden, M. L., & Treseder, K. K. (2017). Effects of drought manipulation on soil nitrogen cycling: A meta-analysis. *Journal of Geophysical Research: Biogeosciences*, *122*(12), 3260–3272. https://doi.org/10.1002/2017JG004146
- Huber, A. E., Melcher, P. J., Piñeros, M. A., Setter, T. L., & Bauerle, T. L. (2019). Signal coordination before, during and after stomatal closure in response to drought stress. *New Phytologist*, 224(2), 675–688. https://doi.org/10.1111/nph.16082
- Huete, A., Didan, K., Miura, T., Rodriguez, E. P., Gao, X., & Ferreira, L. G. (2002). Overview of the radiometric and biophysical performance of the MODIS vegetation indices. *Remote Sensing of Environment*, 83(1–2), 195–213. https://doi.org/10.1016/S0034-4257(02)00096-2
- Kahmark, K., Jones, M., Bohm, S., Baker, N., & Robertson, G. P. (2024). Rainfall manipulation shelters for agricultural research. https://doi.org/10.5281/zenodo.10607631
- Kirda, C., Danso, S. K. A., & Zapata, F. (1989). Temporal water stress effects on nodulation, nitrogen accumulation and growth of soybean. *Plant and Soil*, *120*(1), 49–55. https://doi.org/10.1007/BF02370289
- Kozak, J. A., Aiken, R. M., Flerchinger, G. N., Nielsen, D. C., Ma, L., & Ahuja, L. (2007). Comparison of modeling approaches to quantify residue architecture effects on soil

- temperature and water. *Soil and Tillage Research*, 95(1–2), 84–96. https://doi.org/10.1016/j.still.2006.11.006
- Li, C., Zwiers, F., Zhang, X., Li, G., Sun, Y., & Wehner, M. (2021). Changes in annual extremes of daily temperature and precipitation in CMIP6 models. *Journal of Climate*, *34*(9), 3441–3460. https://doi.org/10.1175/JCLI-D-19-1013.1
- Luehmann, M. D., Peter, B. G., Connallon, C. B., Schaetzl, R. J., Smidt, S. J., Liu, W., Kincare, K. A., Walkowiak, T. A., Thorlund, E., & Holler, M. S. (2016). Loamy, two-storied soils on the outwash plains of southwestern lower Michigan: Pedoturbation of loess with the underlying sand. *Annals of the American Association of Geographers*, 106(3), 551–572. https://doi.org/10.1080/00045608.2015.1115388
- Lumactud, R. A., Dollete, D., Liyanage, D. K., Szczyglowski, K., Hill, B., & Thilakarathna, M. S. (2023). The effect of drought stress on nodulation, plant growth, and nitrogen fixation in soybean during early plant growth. *Journal of Agronomy and Crop Science*, 209(3), 345–354. https://doi.org/10.1111/jac.12627
- Marchesini, V. A., Fernández, R. J., Reynolds, J. F., Sobrino, J. A., & Di Bella, C. M. (2015). Changes in evapotranspiration and phenology as consequences of shrub removal in dry forests of central Argentina. *Ecohydrology*, 8(7), 1304–1311. https://doi.org/10.1002/eco.1583
- Marino, D., Frendo, P., Ladrera, R., Zabalza, A., Puppo, A., Arrese-Igor, C., & González, E. M. (2007). Nitrogen fixation control under drought stress: Localized or systemic? *Plant Physiology*, *143*(4), 1968–1974. https://doi.org/10.1104/pp.107.097139
- Martin-StPaul, N., Delzon, S., & Cochard, H. (2017). Plant resistance to drought depends on timely stomatal closure. *Ecology Letters*, 20(11), 1437–1447. https://doi.org/10.1111/ele.12851
- Marvel, K., Cook, B. I., Bonfils, C., Smerdon, J. E., Williams, A. P., & Liu, H. (2021). Projected changes to hydroclimate seasonality in the continental United States. *Earth's Future*, *9*(9), e2021EF002019. https://doi.org/10.1029/2021EF002019
- Parvin, S., Uddin, S., Fitzgerald, G. J., Tausz-Posch, S., Armstrong, R., & Tausz, M. (2019). Free air CO₂ enrichment (FACE) improves water use efficiency and moderates drought effect on N₂ fixation of *Pisum sativum L. Plant and Soil*, 436(1–2), 587–606. https://doi.org/10.1007/s11104-019-03949-7
- Pirasteh-Anosheh, H., Saed-Moucheshi, A., Pakniyat, H., & Pessarakli, M. (2016). Stomatal responses to drought stress. *Water Stress and Crop Plants*, 24–40. https://doi.org/10.1002/9781119054450.ch3
- Purcell, L. C., & King, C. A. (1996). Drought and nitrogen source effects on nitrogen nutrition, seed growth, and yield in soybean. *Journal of Plant Nutrition*, *19*(6), 969–993. https://doi.org/10.1080/01904169609365173

- Rastogi, D., Trok, J., Depsky, N., Monier, E., & Jones, A. (2024). Historical evaluation and future projections of compound heatwave and drought extremes over the conterminous United States in CMIP6. *Environmental Research Letters*, 19(1), 014039. https://doi.org/10.1088/1748-9326/ad0efe
- Reynolds-Henne, C. E., Langenegger, A., Mani, J., Schenk, N., Zumsteg, A., & Feller, U. (2010). Interactions between temperature, drought and stomatal opening in legumes. *Environmental and Experimental Botany*, 68(1), 37–43. https://doi.org/10.1016/j.envexpbot.2009.11.002
- Robertson, G. P., Bruulsema, T. W., Gehl, R. J., Kanter, D., Mauzerall, D. L., Rotz, C. A., & Williams, C. O. (2013). Nitrogen–climate interactions in US agriculture. *Biogeochemistry*, 114(1–3), 41–70. https://doi.org/10.1007/s10533-012-9802-4
- Robertson, G. P., & Groffman, P. M. (2024). Nitrogen transformations. In *Soil Microbiology, Ecology and Biochemistry* (pp. 407–438). Elsevier. https://doi.org/10.1016/B978-0-12-822941-5.00014-4
- Robertson, G. P., & Hamilton, S. K. (2015). Long-term ecological research in agricultural landscapes at the Kellogg Biological Station LTER site: Conceptual and experimental framework. In *The Ecology of Agricultural Landscapes: Long-Term Research on the Path to Sustainability* (pp. 1–32). Oxford University Press.
- Robertson, G. P., & Vitousek, P. M. (2009). Nitrogen in agriculture: Balancing the cost of an essential resource. *Annual Review of Environment and Resources*, *34*(1), 97–125. https://doi.org/10.1146/annurev.environ.032108.105046
- Rogers, A., Ainsworth, E. A., & Leakey, A. D. B. (2009). Will elevated carbon dioxide concentration amplify the benefits of nitrogen fixation in legumes? *Plant Physiology*, 151(3), 1009–1016. https://doi.org/10.1104/pp.109.144113
- Schaeffer, S. M., Homyak, P. M., Boot, C. M., Roux-Michollet, D., & Schimel, J. P. (2017). Soil carbon and nitrogen dynamics throughout the summer drought in a California annual grassland. *Soil Biology and Biochemistry*, *115*, 54–62. https://doi.org/10.1016/j.soilbio.2017.08.009
- Schwartz, R. C., Baumhardt, R. L., & Evett, S. R. (2010). Tillage effects on soil water redistribution and bare soil evaporation throughout a season. *Soil and Tillage Research*, 110(2), 221–229. https://doi.org/10.1016/j.still.2010.07.015
- Senay, G. B., Parrish, G. E. L., Schauer, M., Friedrichs, M., Khand, K., Boiko, O., Kagone, S., Dittmeier, R., Arab, S., & Ji, L. (2023). Improving the operational simplified surface energy balance evapotranspiration model using the forcing and normalizing operation. *Remote Sensing*, 15(1), 260. https://doi.org/10.3390/rs15010260
- Serraj, R. (2003). Effects of drought stress on legume symbiotic nitrogen fixation: Physiological mechanisms. *Indian Journal of Experimental Biology*, 41(10), 1136–1141.

- Serraj, R., Sinclair, T. R., & Purcell, L. C. (1999). Symbiotic N₂ fixation response to drought. *Journal of Experimental Botany*, 50(331), 143–155. https://doi.org/10.1093/jxb/50.331.143
- Thornton, M. M., Shrestha, R., Wei, Y., Thornton, P. E., Kao, S.-C., & Wilson, B. E. (2022). Daymet: Daily surface weather data on a 1-km grid for North America, Version 4 R1. ORNL DAAC, Oak Ridge, Tennessee, USA. https://doi.org/10.3334/ORNLDAAC/2129
- Vadez, V., Berger, J. D., Warkentin, T., Asseng, S., Ratnakumar, P., Rao, K. P. C., Gaur, P. M., Munier-Jolain, N., Larmure, A., Voisin, A.-S., Sharma, H. C., Pande, S., Sharma, M., Krishnamurthy, L., & Zaman, M. A. (2012). Adaptation of grain legumes to climate change: A review. *Agronomy for Sustainable Development*, 32(1), 31–44. https://doi.org/10.1007/s13593-011-0020-6
- Valentine, A. J., Benedito, V. A., & Kang, Y. (2010). Legume nitrogen fixation and soil abiotic stress: From physiology to genomics and beyond. In C. H. Foyer & H. Zhang (Eds.), *Annual Plant Reviews Volume 42* (1st ed., pp. 207–248). Wiley. https://doi.org/10.1002/9781444328608.ch9
- Van Kessel, C., & Hartley, C. (2000). Agricultural management of grain legumes: Has it led to an increase in nitrogen fixation? *Field Crops Research*, 65(2–3), 165–181. https://doi.org/10.1016/S0378-4290(99)00085-4
- Vitousek, P. M., Aber, J. D., Howarth, R. W., Likens, G. E., Matson, P. A., Schindler, D. W., Schlesinger, W. H., & Tilman, D. G. (1997). Human alteration of the global nitrogen cycle: Sources and consequences. *Ecological Applications*, 7(3), 737–750. https://doi.org/10.1890/1051-0761(1997)007[0737:HAOTGN]2.0.CO;2
- Vitousek, P. M., Menge, D. N. L., Reed, S. C., & Cleveland, C. C. (2013). Biological nitrogen fixation: Rates, patterns and ecological controls in terrestrial ecosystems. *Philosophical Transactions of the Royal Society B: Biological Sciences*, 368(1621), 20130119. https://doi.org/10.1098/rstb.2013.0119
- Whittington, H. R., Tilman, D., & Powers, J. S. (2013). Consequences of elevated temperatures on legume biomass and nitrogen cycling in a field warming and biodiversity experiment in a North American prairie. *Functional Plant Biology*, 40(11), 1147. https://doi.org/10.1071/FP12345
- Wilson, K. B., Hanson, P. J., & Baldocchi, D. D. (2000). Factors controlling evaporation and energy partitioning beneath a deciduous forest over an annual cycle. *Agricultural and Forest Meteorology*, 102(2–3), 83–103. https://doi.org/10.1016/S0168-1923(00)00124-6
- Zhai, R., Kachanoski, R. G., & Voroney, R. P. (1990). Tillage effects on the spatial and temporal variations of soil water. *Soil Science Society of America Journal*, *54*(1), 186–192. https://doi.org/10.2136/sssaj1990.03615995005400010029x

Zhao, J., Gan, T. Y., Zhang, G., & Zhang, S. (2023). Projected changes of precipitation extremes in North America using CMIP6 multi-climate model ensembles. *Journal of Hydrology*, 621, 129598. https://doi.org/10.1016/j.jhydrol.2023.129598

APPENDIX C: CHAPTER 4 TABLES AND FIGURES

Table 4.1. Soil volumetric water contents during the 4-week period leading up to the final precipitation event, the percentage of N derived from the atmosphere, and the N concentration of the seeds. Values represent means from the linear mixed effect model and letters denote statistical differences among all groups, with a column.

Land Use	Precipitation treatment	Soil volumetric water content	N source	N concentration
		cm³ cm-³	% atm.	%
Tilled	1-Week	$0.21\pm0.02~bcd$	$64\pm7~abc$	$6.19\pm0.12~\mathrm{c}$
	3-Week	$0.17\pm0.02~\text{ab}$	$66\pm6~abc$	$6.47\pm0.11~\text{c}$
	Drought	$0.12\pm0.02~\text{a}$	54 \pm 8 ab	$6.32\pm0.15~\text{c}$
No-till	1-Week	$0.28\pm0.02~\text{e}$	74 ± 6 bc	$6.29\pm0.11~\text{c}$
	3-Week	$0.25\pm0.02\;\text{de}$	78 ± 6 c	$6.15\pm0.11~\text{c}$
	Drought	$0.20\pm0.02\;bc$	75 ± 7 bc	$6.32\pm0.12~\text{c}$
Early Successional	1-Week	$0.23\pm0.01~\text{cd}$	61 ± 4 ab	$3.56\pm0.12~\text{b}$
	3-Week	$0.24\pm0.01~\text{de}$	55 ± 4 a	$3.08 \pm 0.12 \ a$
	Drought	$0.13\pm0.01~\text{a}$	$54\pm4~\text{a}$	$3.52\pm0.12~\textrm{b}$

Table 4.2. Soil carbon nitrogen mineralization rates directly before and after the final precipitation event. Values represent the means from the linear mixed effect model averaged over the two timepoints and letters denote statistical differences among all groups.

Land Use	Precipitation treatment	Soil C	Soil N
		Mineralization	Mineralization
		μg CO2-C g ⁻¹ soil d ⁻¹	μg N g ⁻¹ soil d ⁻¹
Tilled	1-Week	6.79 ± 1.13 bc	$3.72 \pm 0.58 \text{ f}$
	3-Week	5.50 ± 0.91 ab	3.34 ± 0.56 ef
	Drought	3.64 ± 0.81 a	2.02 ± 0.51 cde
No-till	1-Week	3.80 ± 0.63 a	2.06 ± 0.51 cde
	3-Week	$6.41 \pm 1.07 \text{ bc}$	$2.71 \pm 0.54 \text{ def}$
	Drought	$4.80 \pm 0.90 \text{ ab}$	$1.50 \pm 0.48 \ bcd$
Early Successional	1-Week	13.28 ± 1.81 e	$1.00 \pm 0.38 \text{ abc}$
	3-Week	$12.79 \pm 1.74 de$	$0.36 \pm 0.36 \text{ ab}$
	Drought	$9.22 \pm 1.49 \text{ cd}$	$0.23 \pm 0.35 \text{ a}$

Table 4.3. Plant seed N uptake from the atmosphere and soil after plant senescence across each land use and precipitation treatment. Values represent the means from the linear mixed effect model and letters denote statistical differences among all groups, within a column.

Land use	Precipitation	Atm. N uptake	Soil N uptake	Total N uptake
		$gNm^{-2}y^{-1}$	$g N m^{-2} y^{-1}$	$gNm^{-2}y^{-1}$
Tilled	1-Week	$17.02 \pm 1.39 d$	$10.43 \pm 1.65 \text{ f}$	$27.75 \pm 1.09 d$
	3-Week	$15.60 \pm 1.33 d$	8.91 ± 1.41 ef	25.14 ± 1.04 cd
	Drought	$5.73 \pm 1.14 \text{ b}$	$5.72 \pm 1.14 \text{ cd}$	$13.03 \pm 1.05 \text{ b}$
No-till	1-Week	$16.24 \pm 1.36 d$	$7.73 \pm 1.22 \text{ def}$	24.14 ± 1.02 c
	3-Week	$16.40 \pm 1.36 d$	$6.26 \pm 0.99 \text{ cde}$	22.67 ± 0.98 c
	Drought	10.50 ± 1.26 c	4.70 ± 0.81 c	$15.26 \pm 0.93 \text{ b}$
Early Successional	1-Week	0.15 ± 0.04 a	$0.10 \pm 0.04 \text{ b}$	0.29 ± 0.07 a
	3-Week	0.06 ± 0.02 a	0.04 ± 0.01 a	0.13 ± 0.05 a
	Drought	0.10 ± 0.03 a	$0.09 \pm 0.03 \text{ ab}$	0.17 ± 0.05 a

Table 4.4. Leaf level gas exchange measurements across each land use and precipitation treatment. Values represent the means and standard errors from the linear mixed effect model and letters denote statistical differences among all groups, within a column.

Land use	Precipitation treatment	Anet	E	Ci
		$\mu mol\ CO_2\ m^{-2}\ s^{-1}$	$mmol H_2O m^{-2} s^{-1}$	CO2 ppm
Tilled	1-Week	$27.38 \pm 4.06 \text{ b}$	$7.38 \pm 1.62 \text{ b}$	320.18 ± 9.27 c
	3-Week	$28.80 \pm 4.16 \text{ b}$	$7.10 \pm 1.55 \text{ b}$	316.06 ± 9.27 c
	Drought	8.36 ± 4.32 a	0.79 ± 0.32 a	132.46 ± 17.49 a
No-till	1-Week	$27.52 \pm 4.07 \text{ b}$	$7.93 \pm 1.74 \text{ b}$	326.48 ± 9.27 c
	3-Week	$34.58 \pm 4.56 \text{ b}$	$8.85 \pm 1.94 \text{ b}$	325.70 ± 9.27 c
	Drought	10.23 ± 2.83 a	1.47 ± 0.36 a	220.52 ± 10.51 b

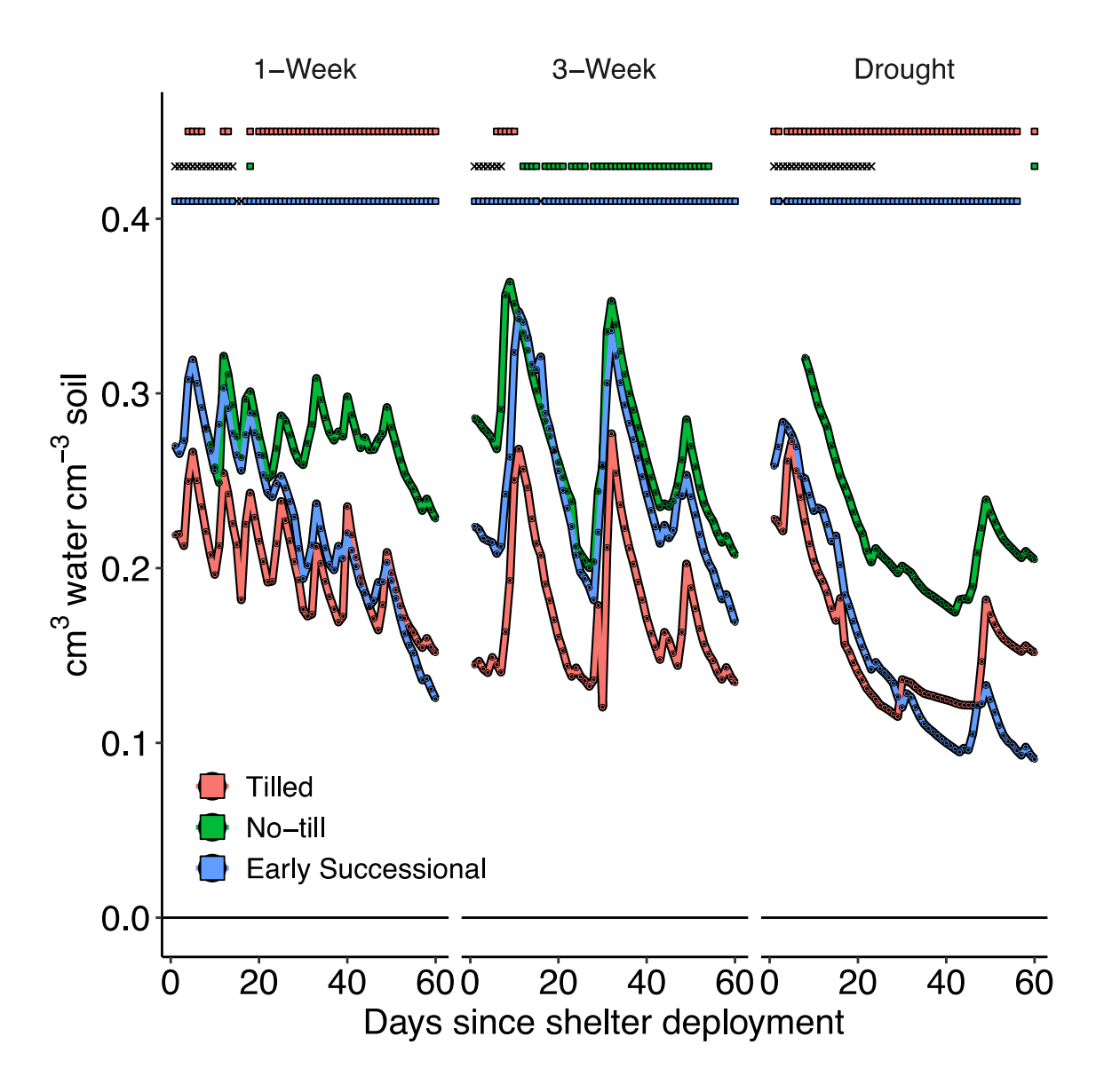


Figure 4.1. Soil volumetric water content for the - 25 cm depth across each land use and precipitation treatment. Points denote the mean of all replicates within a land use and precipitation treatment, with the color corresponding to the in-figure legend. The squares above each observation denote land use treatments with statistically similar values, while blank spaces denote land use treatments that are statistically different from each other. 'X's denote treatments with insufficient observations to determine statistical differences (e.g., n < 2). Observations following exogenous overland flow events (see Methods) were removed.

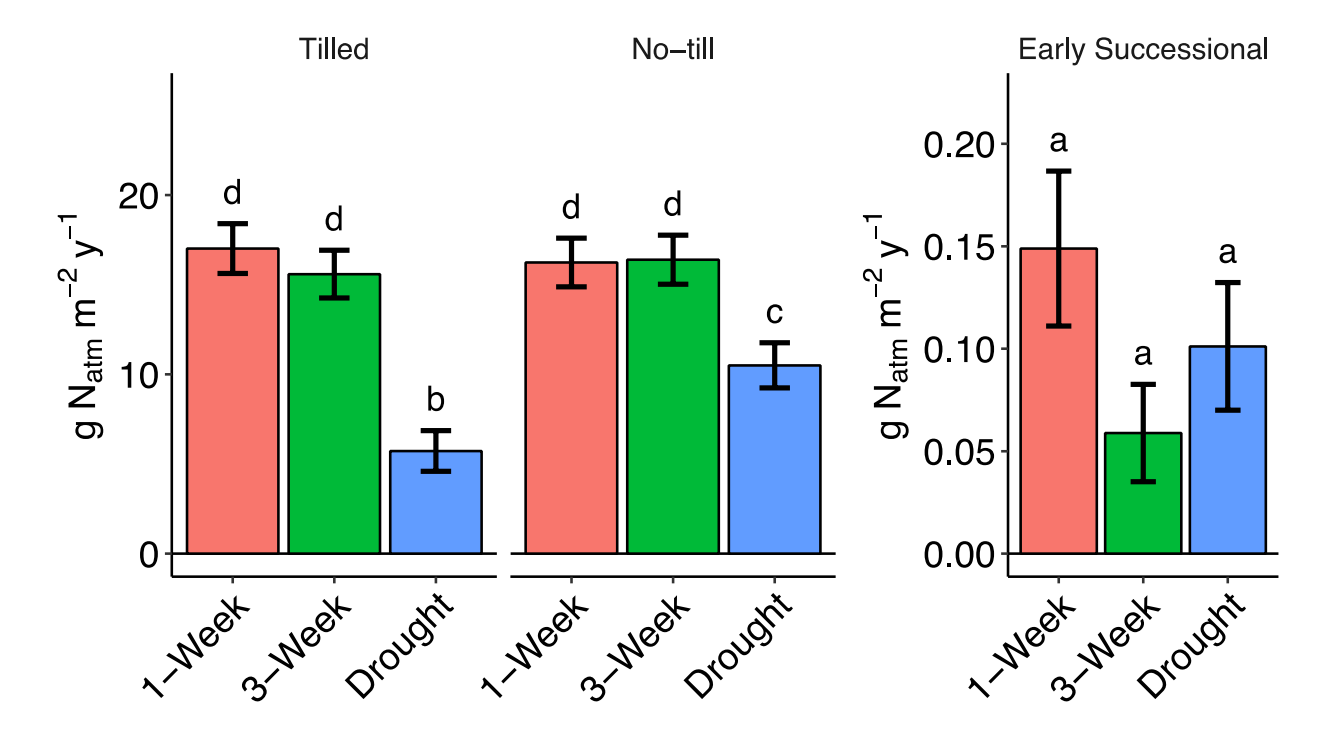


Figure 4.2. Atmospheric nitrogen fixed in seeds across each land use treatment and precipitation treatment. Units are g of N derived from the atmosphere measured in seeds per square meter per year; note the scale difference for Early Successional. Shown are means and standard errors estimated from the linear mixed effect model. Letters denote statistical differences among all groups.

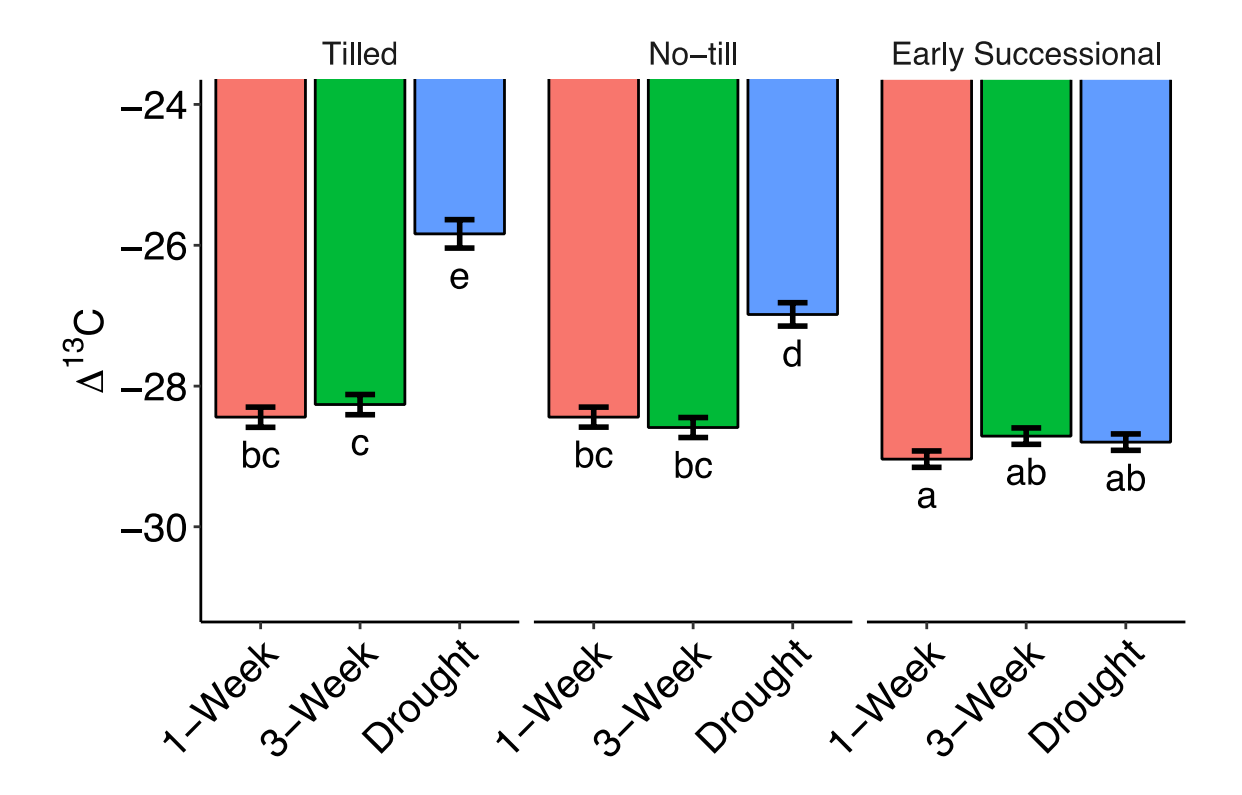


Figure 4.3. Seed ¹³C isotope values in ‰ units across each land use and precipitation treatment. Shown are means and standard errors estimated from the linear mixed effect model. Letters denote statistical differences among all groups.

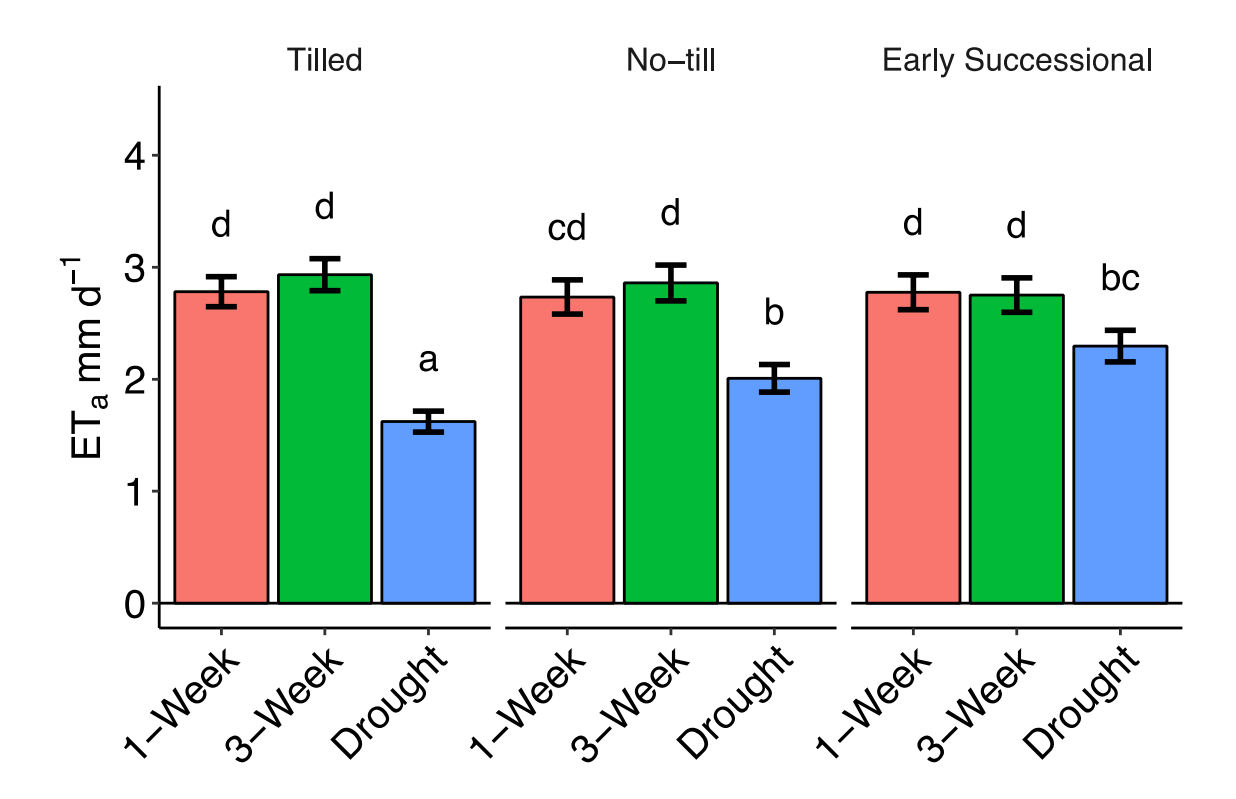


Figure 4.4. Evapotranspiration rates across each land use and precipitation treatment during the peak of the drought. Shown are means and standard errors estimated from the linear mixed effect model. Letters denote statistical differences among all groups.

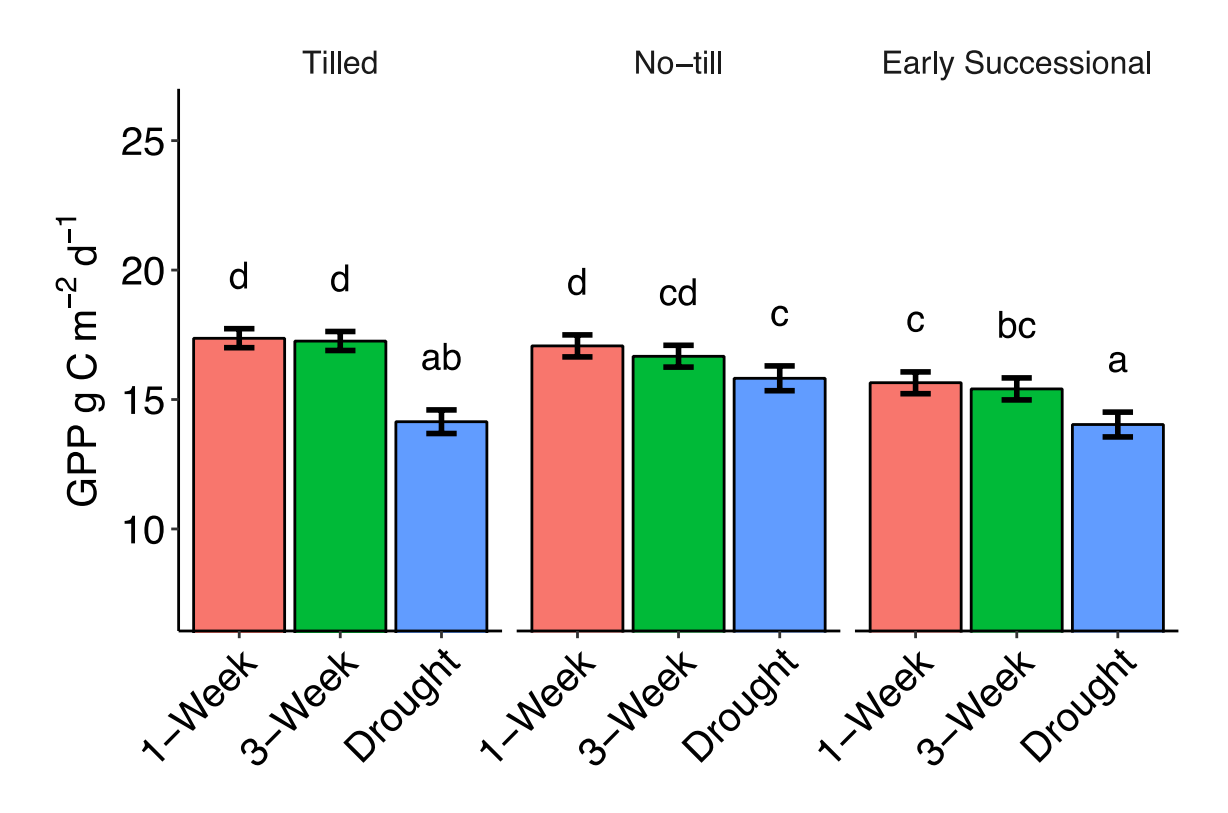


Figure 4.5. Gross primary production across each land use and precipitation treatment during the peak of the drought (note that y-axis scale does not start at origin). Shown are means and standard errors estimated from the linear mixed effect model. Letters denote statistical differences among all groups.

CHAPTER 5: Combining field measurements, eddy covariance towers and an ecosystem model improves confidence in the climate impacts of bioenergy with carbon capture and storage

Abstract

Bioenergy with carbon capture and storage (BECCS) is a negative emissions technology that features prominently in scenarios that limit the rise in global near surface temperature to below 2 °C. The environmental impacts of extensive land use for BECCS could potentially undermine its climate mitigation impact. The combination of the previous land use and the proposed biomass production system can create positive or negative radiative forcing impacts upstream of the BECCS facility through changes to greenhouse gas fluxes and/or land surface albedo. Furthermore, even at a single site, different approaches to quantifying radiative forcing impacts can affect their sign and magnitude. Here we show how three common methods for estimating the net ecosystem carbon balance of bioenergy crops established on former grassland or former cropland can differ in their central estimates and uncertainty. We place these carbon stock changes in the context of the associated radiative forcing impacts of changes to soil N2O and CH₄ fluxes, land surface albedo, and geologically stored carbon. Results from a field soil and plant carbon inventory, eddy covariance flux measurements, and a novel process-based ecosystem model all agree that establishing perennials such as Switchgrass or Prairie on former cropland results in net negative radiative forcing of -13.5 to -20.2 W m⁻² over 100 years. Establishing these perennials on former grassland sites had similar climate mitigation impacts of -9.9 to -21.7 W m⁻². However, the largest climate mitigation came from establishing corn for BECCS on former cropland or grassland, with radiative forcings from -19.7 to -25.7 W m⁻², due

to its higher productivity. Our results highlight the strengths and limitations of each method for

quantifying the field scale climate impacts of BECCS and show that utilizing multiple methods can increase confidence in the final outcome.

Introduction

Bioenergy with carbon capture and storage (BECCS) is predicted to be necessary, in combination with reductions in fossil fuel use and other greenhouse-gas mitigation measures for keeping the anthropogenic rise in global atmospheric temperature to below 2 °C by 2100 (Hanssen et al., 2020). In particular, carbon dioxide removal will be necessary to avoid the effects of climate change that extend well beyond 2100 such as sea level rise and ocean acidification, and BECCS could be a key method for doing so at scale (Clark et al., 2016). BECCS extracts energy from biomass through combustion, with the resulting CO₂ captured and stored in subsurface geologic formations. Proposals that use BECCS as a climate mitigation strategy have extensive land use requirements to produce enough plant biomass for meaningful carbon sequestration (Azar et al., 2013). Some scenarios project land use requirements of up to 10 x 10⁶ km² by the year 2100 (Roe et al. 2019), which would make plant biomass production for BECCS the largest transformation of land since the advent of agriculture and forestry. These land use requirements motivate the study of associated impacts on terrestrial ecosystems. While the primary mechanism that BECCS uses to reduce global radiative forcing is the storage of new plant biomass carbon in geologic formations, there are further contributions to radiative forcing that derive from biomass production. These include changes to 1) standing plant and soil carbon stocks, 2) soil N₂O emissions, 3) soil CH₄ oxidation and 4) land surface albedo. However, the direction and magnitude of these radiative forcing contributions are uncertain due to the lack of long-term land use change experiments measuring these phenomena in a bioenergy context. Closing this knowledge gap is critical for constraining uncertainty in projections of how to achieve reduced radiative forcing with BECCS.

A common method for estimating the net ecosystem carbon balance (NECB) of BECCS production is using a process-based ecosystem model that simulates a particular land use change scenario, relative to a baseline scenario (Lark et al., 2022). There are several structural uncertainties stemming from this method that impact the final NECB of BECCS. These include the parameterization of bioenergy crops like switchgrass or miscanthus in the plant sub-modules, which have relatively greater uncertainty in their parameter values due to their novelty in the modeling community. Furthermore, estimating the initial plant and soil carbon stocks as affected by the previous land use at the site and correctly modeling the fate of that carbon further challenges model veracity. Finally, as is true with all model simulations, validation at a representative site with in situ measurements is rare, adding further to the uncertainty of modeled results (Augusiak et al., 2014).

Eddy covariance flux measurements are another commonly used technology for estimating the NECB of BECCS production (Harris et al., 2017). By continuously measuring the net ecosystem exchange of CO₂, and adjusting for other carbon pools that leave a site (e.g., biomass via harvest and dissolved organic carbon via leaching), eddy covariance measurements can provide a spatially and temporally integrated in situ estimate of a site's NECB. However, several structural uncertainties cloud the interpretation of eddy covariance measurements. For instance, it is common for 30-50% of flux measurements to be missing data due to low turbulence conditions or sensor malfunctions (Moffat et al., 2007). Gap-filling methods required to calculate the NECB introduce uncertainties in the flux estimates (Mahabbati et al., 2021). Furthermore, arriving at the NECB requires the cumulative addition of all net ecosystem exchange measurements, meaning that any deviation in the systematic bias from zero, even if small, can add up over time to bias final (cumulative) NECB estimates.

Plant and soil carbon inventories can also estimate a site's NECB by measuring standing carbon stocks before and after a BECCS land use change event. Structural uncertainties of this approach mainly stem from sampling effort. The size of each plot or soil sample is usually small compared to the size of the field and the natural heterogeneity of the field's carbon stocks necessitates taking numerous labor-intensive samples. While the carbon content of any individual sample can be derived with high accuracy and low uncertainty, the heterogeneity among samples and the lack of sufficient numbers of samples often results in relatively high uncertainty in the final NECB.

Most site-based studies of the NECB of BECCS production use only one of these three methods. We are not aware of any study that compares all three approaches in the same experimental setting. Usually the circumstances of the site, experimental design, study duration, available measurements and investigator expertise dictate the viable methods. We suspect that the conclusions of these studies may change if a different method was used. Long term BECCS land use change experiments are essential for robustly estimating the NECB as plant and especially soil carbon changes can take many years to reach a new steady state and become detectable by the three methods mentioned.

Here we use a long term BECCS land use change experiment to compare three methods for quantifying each site's NECB over 13 years, namely 1) a novel process-based ecosystem model, 2) eddy covariance flux measurements and 3) in-situ inventories of plant and soil C stock changes. Our objectives are to 1) estimate the NECB of three proposed bioenergy production systems with contrasting land use history, 2) quantify the uncertainty of each of the three estimation methods and 3) place these NECB estimates in context of other sources of radiative forcing measured at the site, in particular, soil-atmosphere fluxes of N₂O and CH₄ as well as land

surface albedo. We hypothesize that the NECB will be highest at sites with low initial ecosystem C stocks that transition to high belowground productivity plant types. Furthermore, we postulate that the eddy covariance method will have the lowest uncertainty in detecting these changes. Finally, apart from the geologically stored carbon, we expect the NECB to largely determine the overall radiative forcing budget of each site.

Methods

Site description

The study site is in southwestern Michigan, USA and was established by Michigan State University as part of the Great Lakes Bioenergy Research Center (42.4 N, 85.4 W, elevation 281 m). The mean annual temperature of the site is 9.3 °C and the mean annual precipitation is 1067 mm (Thornton et al., 2022). Soils at the site are well drained fine-loamy, mixed, active, mesic Typic Hapludalfs and consist of loamy glacial outwash overlying sand (Luehmann et al., 2016). Prior to industrial settlement of the area circa 1850, the site existed in a matrix of mid to late succession temperate deciduous broadleaf forests. Following more than a century of row crop agriculture, in 1987 one set of sites was converted to a perennial grassland (*Bromus inermis*) through enrollment in the USDA's Conservation Reserve Program (CRP), while the other set of sites continued to be used for row crop agriculture.

In 2009 the BECCS experiment was established by terminating all vegetation with herbicides at each site, except for one of the grassland sites that was maintained as a reference. In the initial year, herbicide resistant soybeans (*Glycine max*) were planted to allow further termination of preexisting vegetation. In 2010, either corn (*Zea mays*), switchgrass (*Panicum virgatum*) or restored prairie (hereafter "prairie," a mixture of 19 species; see Abraha et al., 2016) was established on both the former grassland and former cropland sites. The field sizes range

from 9 – 14 ha and were managed throughout the study period without tillage. The corn was fertilized with N at a rate of 180 kg N ha⁻¹ y⁻¹, the Switchgrass at 56 kg N ha⁻¹ y⁻¹, and the Prairie at 0 kg N ha⁻¹ y⁻¹. From 2010-2014, only grain was harvested from the corn sites. From 2015-2021 both grain and residue were harvested in the Fall. For the Switchgrass and Prairie sites, biomass was harvested annually in the Fall from 2011-2021.

Eddy covariance measurements

Each of the seven sites has had an eddy covariance tower in continuous operation since 2009. Each tower had an LI-7500 open-path infrared gas analyzer (LI-COR Biosciences, Lincoln, NE) that measures CO₂ and H₂O concentrations. A CSAT3 sonic anemometer (Campbell Scientific Inc., Logan, UT) is used for wind speed and direction measurements. The infrared gas analyzers were calibrated every four to six months and were mounted along with the sonic anemometer 1.5 – 2 m above the canopy. A Campbell CR5000 datalogger recorded data from these sensors at 10 Hz. Incoming and outgoing long and shortwave radiation were measured with CNR1 sensors (Delft, The Netherlands) as was air temperature and relative humidity (HMP45C, Campbell Scientific Inc., Logan, UT). Soil heat flux at 2 cm depth was measured (HFT3, Campbell Scientific Inc., Logan, UT) as was soil temperature (CS107, Campbell Scientific Inc., Logan, UT) at 2, 5 and 10 cm. Precipitation was measured at a nearby weather station (http://lter.kbs.msu.edu/datatables/12).

The 10 Hz eddy covariance data were processed with the EdiRe software (University of Edinburgh, v 1.5.0.32, 2012). Despiking and time lag corrections between scalars and vertical velocity were conducted following McMillen (1988). The planar fit coordinate rotation was used to rotate the three velocity components into the mean streamline coordinate system following Wilczak et al. (2001). Pressure and humidity corrections to the sonic temperature were

performed according to Schitanus et al. (1983). Frequency response, air density flux and surface heating corrections of the CO₂ and H₂O data were conducted according to Moore (1986), Webb et al. (1980), and Burba et al. (2008), respectively. Periods of low turbulence were removed using the stationarity, flux-variance similarity, and friction velocity thresholds from Foken & Wichura (1996). Further details regarding the 10 Hz data quality and processing is provided in Abraha et al. (2015).

Friction velocity thresholding, gap-filling, and uncertainty estimation were conducted with the Reddyproc package in R (Wutzler et al., 2018). Friction velocity thresholds are a significant source of uncertainty in final NECB estimates as they dictate how much low turbulence data is removed. For each year and each 3 month period, 100 bootstrapped samples of data were used to estimate the distribution of probable friction velocity thresholds. The median, 2.5 %, and 97.5 % friction velocity thresholds were used for estimating the central, lower, and upper net ecosystem exchange estimates, respectively.

For each of the three friction velocity thresholds, the marginal distribution sampling algorithm following Reichstein et al. (2005) was used for gap filling the net ecosystem exchange and latent heat flux data. Artificial gaps at each measurement were created to facilitate uncertainty estimation. The standard deviation of the look up table values for real gaps were used as the uncertainty estimate for the gap filling procedure. The standard deviation of the look up table values for artificial gaps were used as the uncertainty estimate for the measurement procedure. The final uncertainty in the cumulative net ecosystem exchange was calculated by numerical simulation. For 100 simulations, a new net ecosystem exchange value was sampled at each half-hour interval from a normal distribution with the mean and standard deviation derived from the real and artificial gap filling procedure described above. The median, 2.5 % and 97.5 %

quantiles of the cumulative net ecosystem exchange from the 100 simulations were used as the central, lower and upper estimates for the eddy covariance method, respectively. The NECB was then calculated following Eq. (1).

$$NECB = NEE - C_{Harvest} - DOC$$
 Eq. (1)

Where NEE is the net ecosystem exchange of CO₂, C_{Harvest} is the carbon removed from the site, and DOC is the dissolved organic carbon leached below 100 cm. DOC losses are not measured by eddy covariance towers. We utilized the DOC output from the process-based ecosystem model as described below.

Plant biomass measurements

All plant biomass that was removed from the site for bioenergy production was measured directly by weighing harvested biomass on trucks and adjusting by measured moisture contents. Plant biomass weights were converted to plant C and N weights by measuring their C and N concentrations through dry combustion with an elemental analyzer (Costech ECS 4010 CHNSO Analyzer, CA, USA).

To evaluate annual net primary productivity, plant biomass measurements were made annually from 2009-2016 at ten geolocated sampling stations within each field by clipping, drying, and weighing 1 m⁻² of live aboveground biomass. Surface litter was also collected from these stations simultaneously and weighed separately. Peak biomass sampling was timed to occur after most aboveground net primary production had occurred but before most senesce and biomass decomposition had taken place, usually in late August. Plant biomass weights were converted to plant C and N weights by measuring their C and N concentrations as above.

Belowground net primary production measurements were made annually from 2009-2017 through the use of the in-growth core technique (Lei et al., 2021). Briefly, a 25 cm deep soil core

measuring 6 cm in diameter was excavated and roots were removed in the field. A cylinder of 2 mm mesh was placed in the excavated hole and the soil, mixed with 25% additional sand to prevent compaction, was replaced. Core installation occurred annually before the growing season began and the cores were removed for measurement after the growing season ended. Roots that had grown into the mesh cylinder were considered to represent the belowground net primary productivity.

Standing belowground biomass carbon stocks were measured directly in Winter 2022 by taking a 7 cm diameter soil core to a depth of 25 cm to capture >75 % of root biomass. Cores were taken at each of the ten georeferenced sampling stations in each of the seven fields. Roots were carefully washed with water from the soil on top of a 0.25 mm sieve, dried at 60 °C and weighed. Root biomass weights were converted to root C and N weights by measuring their C and N concentrations as above.

Soil measurements

Soil sampling at each field's georeferenced sampling stations occurred in 2009 before land use conversion and in 2014 and 2021 after the growing season ended. Intact cores were taken from the 0-100 cm depth with a 6 or 7.6 cm diameter hydraulic probe and split into four sections by depth: 0-10 cm, 10-25 cm, 25-50 cm and 50-100 cm. Surface litter was removed prior to inserting the probe. Soils were sieved to 4 mm by hand and roots were discarded. The coarse fragment > 4 mm was weighed as was the < 4 mm soil fraction after drying in a 60 °C oven to constant weight. These weights were used to calculate the total and gravel-free bulk densities using the volume of the section. Subsamples of the soil were pulverized to a fine powder for dry combustion analysis of their C and N concentrations. Each sample's C and N concentrations were measured with three technical replicates in an elemental analyzer.

Subsamples of the pulverized soil were also measured for mid-infrared ($1.3-25~\mu m$) spectroscopy. Samples were measured with four technical replicates with a Digilab FTS 7000 spectrometer (Varian, Inc., CA, USA). Absorbance was obtained using a KBr background and deuterated triglycine sulfate detector. Each spectrum was made of 64 co-added scans at 5000 μm resolution.

Soil physical fraction measurements

A 10 g subsample of bulk soil was used to measure the mineral-associated and particulate organic matter C and N concentrations, referred to as MAOM and POM, respectively. Mixtures of soil and 0.5 % sodium hexametaphosphate were shaken for 18 h and then separated over a 53 µm sieve and dried in a 60 °C oven to constant weight. Each fraction was weighed and pulverized for C and N concentration analyses as above. Because this is a labor-intensive procedure, only a subset of 403 soil samples were processed directly. The rest of the MAOM and POM C and N were predicted from the MIR spectra. A Partial Least Squares Regression statistical model was constructed the MIR spectra as predictors and the MAOM and POM C and N as response variables. A minimized number of principal components and cross validation was used to limit out of sample errors associated with over fitting these types of models. *Soil gas flux measurements*

Soil N₂O and CH₄ exchange was measured bi-weekly to monthly during the growing season from 2009-2016 with the static chamber technique (Abraha et al., 2018). Briefly, 28 cm diameter metal cylinders were inserted 5 cm into the soil and covered with a lid for 1.5 h, over which four headspace gas samples were extracted and analyzed for N₂O and CH₄ concentrations in the lab with a gas chromatograph (Hewlett-Packard 5890 series, CA, USA, until 2008 and 7890A Agilent Technologies Inc., CA, USA, thereafter) equipped with a ⁶³Ni electron capture

detector (350 °C), a Poropak Q column (1.8 m, 80/100 mesh) at 80 °C, and a carrier gas of argon/methane (90/10). Changes in headspace gas concentrations were scaled to areal fluxes with the ideal gas law and assumed to represent the daily flux.

Separately, 10 cm diameter metal cylinders were installed 5 cm deep in the soil from 2011-2014 and kept free from live plant biomass through trenching and herbicide applications, allowing the quantification of heterotrophic respiration. A recirculating pump passed headspace air through an LICOR LI-7815 infrared gas analyzer (LICOR, NE, USA) and the change in CO₂ concentrations were similarly scaled to areal fluxes with the ideal gas law and assumed to represent the daily flux.

Land surface albedo and vegetation index measurements

Land surface albedo was measured for each experimental unit from 2009 to 2023 with the Landsat 5, 7, 8, and 9 satellites as well as the Sentinel 2A and 2B satellites following Wang et al. (2017). Data were acquired from Google Earth Engine. For Sentinel 2, Level 1C top of atmosphere reflectances were processed to surface reflectance with the Sensor Invariant Atmospheric Correction method (Yin et al., 2022). Sentinel 2 clouds were detected with the s2cloudless method (Skakun et al., 2022). For Landsat, Level 2 surface reflectances were taken from Collection 2 Tier 1 which the United States Geologic Survey (USGS) certifies to meet inter-sensor calibration standards and < 12 m georegistration accuracy. These are the highest quality data available and lower quality data were not used. The mean georegistation accuracy at our site was 5.1 m. Accordingly, plot boundaries were shrunk in order for the USGS to certify that all pixels used in this analysis were wholly within the plot boundaries. For each overpass, the shrunk boundaries of each experimental unit were used to extract the mean surface reflectance of each band, as well as the associated quality control and metadata information.

Observations with clouds, shadows, excessive aerosols and radiometric saturation were filtered out and the bands were combined into total shortwave reflectance using narrow to broadband coefficients (Bonafoni & Sekertekin, 2020; Liang, 2001).

Shortwave broadband albedo was calculated using the albedo:reflectance ratio technique (Shuai et al., 2011, 2014; Wang et al., 2017). Landsat and Sentinel surface reflectance data are provided without surface anisotropy corrections, which are necessary to estimate land surface albedo. The bidirectional reflectance distribution function (BRDF) was used for this correction. To obtain the parameters for the BRDF, adjacent representative pixels were taken from the MODIS albedo product during overpasses concurrent with the Landsat and Sentinel overpasses. The MCD43A1 V6.1 Bidirectional Reflectance Distribution Function and Albedo Model Parameters data product was acquired from the National Aeronautics and Space Administration's Application for Extracting and Exploring Analysis Ready Samples application programing interface. Pre-MODIS era Landsat observations used the climatologically averaged BRDF parameters from the study site. The Landsat and/or Sentinel sun-sensor geometry, MODISderived BRDF parameters, and the diffuse radiation fraction are used to calculate the shortwave surface albedo and shortwave reflectance. The diffuse radiation fraction at the land surface level for the study site was obtained for the hour of each satellite over pass from the ERA5 data product produced by the European Centre for Medium-Range Weather Forecasts as distributed by the Copernicus Climate Change Service Climate Data Store (Hersbach et al., 2023). The resulting albedo:reflectance ratio is applied to the Landsat and Sentinel surface reflectance to calculate the land surface albedo at 30 and 20 m resolution, respectively. Between 554 and 721 albedo observations that passed all quality screening criteria were available for each land use, resulting in a total of 4,520 albedo observations measured from 2009 to 2023.

Vegetation phenology metrics were also extracted from the satellite surface reflectance data to facilitate calibration of the plant module of the process-based ecosystem model described below. The enhanced vegetation index was calculated and used as a proxy for the fraction of photosynthetically active radiation absorbed by green leaves (Huete et al., 2002).

Field management and weather data

Management activities were recorded as they were executed, including planting date and density, fertilizer date and rate, herbicide date and rate, and harvest dates. A weather station located 10 km from the study site provided soil temperature, air temperature, precipitation, windspeed, vapor pressure, air pressure, and incoming shortwave radiation (https://lter.kbs.msu.edu/datatables/12).

Process-based ecosystem modeling

The Microbial Efficiency and Matrix Stabilization model version 2.0 was used to solve daily C, N, water and temperature fluxes at the field scale (Zhang et al., 2021). This 1-dimensional model requires initial condition and forcing data: soil C and N stocks in the POM and MAOM fractions, soil texture, soil bulk density, field management events, plant specific attributes (e.g. specific leaf area), air temperature, incoming shortwave radiation, precipitation, windspeed and relative humidity.

Initial conditions were taken from the above-described soil and plant data. A model spin-up period of 100 years was used before the start of the study period, which was January 1st, 2009 – December 31st, 2021. Custom software was written in the R programing language to facilitate automated calibration and uncertainty estimation. The R package 'BayesianTools' was used to perform Markov-Chain Monte Carlo (MCMC) simulations of different parameter combinations. Parameters in the plant sub-module were identified as the major sources of uncertainty in the

final NECB. The chosen parameters are listed in supplemental Table 5.1. Uniform prior distributions for selected parameters were constructed from plausible parameter value ranges.

A likelihood-based cost function was used to calculate the difference between each observation and their associated model prediction (function *dnorm* in R). The following observations were used in the calibration scheme: eddy covariance net ecosystem exchange and latent heat flux, soil heterotrophic respiration, harvested plant biomass, peak plant biomass, root productivity, satellite vegetation index, soil total, and POM and MAOM carbon and nitrogen stocks. Likelihoods for each observation variable were summed to represent a global likelihood for each parameter set (Cameron et al., 2022). 10,000 MCMC simulations were conducted in parallel for each site as diagnostic plots showed acceptable convergence at this point. Following this calibration procedure, uncertainty in the final NECB was estimated by drawing a random set of parameters from the latter half of the MCMC simulations. After drawing 100 such sets, the median, 2.5% and 97.5% quantiles of the final NECB were utilized as the central, lower and upper estimates, respectfully.

Radiative forcing calculations

Radiative forcing of CO₂, N₂O, CH₄ and land surface albedo were calculated over a 100-year timeline assuming that the changes during the 13-year study period represent the new steady state fluxes. The radiative forcing of each gas was modeled with their net exchange rates, atmospheric lifetimes, and radiative efficiencies following Neubauer & Megonigal (2015) and their associated correction (Neubauer & Megonigal, 2019). This facilitated use of common units of W m⁻² and thus the direct use of top of atmosphere shortwave radiation fluxes. The atmospheric lifetime of N₂O and CH₄ was modeled according to Eq. (2)

$$C_{i+1} = F_i + C_i * e^{(-\frac{1}{L})}$$
 Eq. (2)

Where C_i is the atmospheric concentration in the i^{th} year, F_i is the annual flux in the i^{th} year, and L is the atmospheric lifetime of the gas. The atmospheric lifetime of CO_2 was modeled according to Eq. (3).

$$C_{i+1} = \sum_{p=1}^{4} (f_p * F_i) + C_{i,p} * e^{(-\frac{1}{L_p})}$$
 Eq. (3)

Where C_i is the atmospheric concentration in the ith year, f_p is the fraction of emissions associated with each pool, F_i is the annual flux in the ith year, C_{i,p} is the atmospheric concentration of the pth pool in the ith year and L_p is the atmospheric lifetime of CO₂ in the pth pool. Radiative forcings for each gas were calculated as the product of the atmospheric concentration and the radiative efficiency. Constants for atmospheric lifetimes and pool fractions for Eqs. 2 and 3 can be found in Neubauer & Megonigal, 2015, 2019), as can the constants for the radiative efficiencies of each gas.

Dissolved organic carbon (DOC) is a significant component of the NECB but it is not measured by eddy covariance towers. Furthermore, for the purpose of radiative forcing calculations, the fate of this DOC can alter the climate impacts of terrestrial land use changes. While DOC leaching was not measured directly in this study, the MEMS model provides an estimate. We assumed in the radiative forcing calculations that 74% of DOC is eventually decomposed to CO₂ with a half-life of 2.5 years (Catalán et al., 2016; Ward et al., 2017).

Geologic storage of CO₂ captured during bioenergy production was modeled here according to Eq. (4).

$$CO_2^{BECCS} = C_{harvest} * E_{BECCS}$$
 Eq. (4).

Where CO_2^{BECCS} is the carbon stored in geologic formations, $C_{harvest}$ is the carbon harvested for bioenergy from each site, which was measured directly as described above, and E_{BECCS} is the total efficiency of the BECCS process in terms of CO_2 emitted during the processing stages. We

utilize a value of 80% for E_{BECCS} following the integrated assessment model used in Klein et al., (2014).

The CO₂ emissions originating from fossil fuels used in synthetic N fertilizer production and field management operations were included here following Brentrup et al. (2018) and Gelfand et al. (2020), respectively. Synthetic N fertilizer application rates and field management activity information (expressed in terms of liters of fuel used) were used to calculate the amount of CO₂ emitted each year.

Top of atmosphere shortwave radiation fluxes were calculated with the measured land surface albedo and downwelling shortwave radiation measurements described above using Eq. (5).

$$SW_{out}^{toa} = SW_{in} * a * T_{SW}$$
 Eq. (5).

where SW_{out}^{toa} is the outgoing shortwave radiation at the top of the atmosphere, a is the land surface albedo, and T_{SW} is the all-sky transmittance of shortwave radiation through the atmosphere, calculated here as the ratio of top of atmosphere to bottom of atmosphere incoming shortwave radiation. Top of atmosphere incoming radiation was provided by the ERA5 reanalysis product described above. The radiative forcing from changes in albedo was estimated as the difference in annual average SW_{TOA} relative to a reference field. For the former grassland sites the reference field is the grassland site maintained as a reference. For the former cropland sites, the reference field is the former cropland site converted to corn.

Statistical analysis

Each eddy covariance tower measures each field as a whole. Therefore, as is common with eddy covariance studies, this experiment does not have replicated fields. Statistical differences within a treatment over time were assumed to be present when the 95% confidence

intervals did not overlap with zero. Similarly, statistical differences between methods and sites were assumed to be present when their 95% confidence intervals did not overlap.

For the carbon inventory methods NECB calculation, the longitudinal changes in plant and soil carbon stocks were used. The changes in soil carbon stocks were estimated by fitting a linear mixed effect model following Eq. (6).

$$SOC = site * depth * year + r(site: station)$$
 Eq. (6)

where SOC is the bulk soil C stock in Mg C ha⁻¹, site is a categorical variable representing each study site, depth is a categorical variable representing the four depth intervals, year is a continuous variable representing the year of each soil sample, and r(site:station) is the random intercept for each station at each site. The changes in the other three components of the C inventory method's NECB, namely roots and surface litter, were estimated directly using the winter 2022 sampling data. We assumed that all former grassland sites had the same root and surface litter biomass in 2009 as measured in the reference grassland site in 2022. Similarly, we assumed that all former cropland sites had the same root and surface litter biomass in 2009 as measured in the cropland site converted to corn in 2022. The 95 % confidence interval of the final NECB for the C inventory method was calculated by arithmetic error propagation according to Eq. (7).

$$NECB_{ci} = \sqrt{\sum ci_i^2}$$
 Eq. (7)

where, $NECB_{ci}$ is the 95 % confidence interval of the NECB, ci_i^2 is the squared 95 % confidence interval of each i component, (i.e. soil, root and surface litter).

Results

Net ecosystem carbon balance estimates

Here we report the range of the central estimates of the three methods, followed by the range of their 95 % confidence intervals. Fully disaggregated results for each method and site are reported in Figure 5.1 and Table 5.1. Over 13 years, switchgrass planted on former cropland sequestered between 9.0 and 13.7 Mg C ha⁻¹ (95 % C.I. 2.3 – 25.1). Similarly, prairie established on former cropland sequestered between 4.1 and 15.8 Mg C ha⁻¹ (95 % C.I. 1.7 – 28.4) during the study period. The conversion of grassland to these same perennials had more carbon neutral results. Switchgrass planted on former grassland had a NECB between 4.6 and 10.5 Mg C ha⁻¹ (95 % C.I. -0.7 – 21.7). Similarly, for prairie established on former grassland, the NECB was between -0.9 – 5.0 Mg C ha⁻¹ (95 % C.I. -6.8 – 16.8). The results for corn were more variable with the former cropland site having a NECB of -13.0 – 0.6 Mg C ha⁻¹ (95 % C.I. -24.2 – 2.6) and the corn at the former grassland site having a NECB of -34.3 – 3.3 Mg C ha⁻¹ (95 % C.I. - 38.8 – 13.9). The reference grassland site that was unmanaged and not harvested had a NECB of -3.6 – 4.1 Mg C ha⁻¹ (95 % C.I. -14.4 – 7.2).

Plant and soil carbon dynamics

While the eddy covariance towers do not allow for the disaggregation of the NECB into its plant and soil components, our carbon inventory and process-based ecosystem model results show that surface litter, roots, POM, and MAOM carbon stock changes contributed to NECB changes of up to 3.4, 5.2, 14.7 and 12.7 Mg C ha⁻¹, respectively (Figure 5.2 and Table 5.2). For surface litter, we found that changes in standing carbon stocks from the beginning to the end of the study period estimated using the C Inventory method ranged from -1.6 Mg C ha⁻¹ in the Prairie established on former grassland to 0.0 Mg C ha⁻¹ in the prairie on former cropland (Table

5.2). For surface litter in the MEMS Model, we found greater carbon loss, with a range of -3.4 Mg C ha⁻¹ in the Corn on former grassland to -0.2 Mg C ha⁻¹ in the Grassland reference site (Table 5.2).

For roots, we found that changes in standing carbon stocks from the beginning to the end of the study period estimated using the C Inventory method ranged from -2.0 Mg C ha⁻¹ in the Corn established on former grassland to 5.2 Mg C ha⁻¹ in the Prairie on former cropland (Table 5.2). For roots in the MEMS Model, we found lower carbon gains with a range of -0.5 Mg C ha⁻¹ in the Corn on former grassland to 2.3 Mg C ha⁻¹ in Switchgrass on former cropland (Table 5.2).

For POM, we found that changes in standing carbon stocks from the beginning to the end of the study period estimated using the C Inventory method ranged from -3.6 Mg C ha⁻¹ in the Corn established on former cropland to 14.7 Mg C ha⁻¹ in the Switchgrass on former grassland (Table 5.2). For POM in the MEMS Model, we found lower carbon gains with a range of -1.3 Mg C ha⁻¹ in the Corn on former grassland to 5.7 Mg C ha⁻¹ in Switchgrass on former grassland (Table 5.2).

For MAOM, we found that changes in standing carbon stocks from the beginning to the end of the study period estimated using the C Inventory method ranged from -12.7 Mg C ha⁻¹ in the Grassland reference site to 4.4 Mg C ha⁻¹ in the Switchgrass on former cropland (Table 5.2). For MAOM in the MEMS Model, we found greater carbon gains with a range of 1.2 Mg C ha⁻¹ in the Prairie on former grassland to 3.5 Mg C ha⁻¹ in Corn on former grassland (Table 5.2). *Soil N₂O and CH₄*

Soil gas fluxes were significantly affected by both the current and previous land use. Soil nitrous oxide emissions were highest in the sites fertilized with synthetic N. The Corn site on former grassland had the highest emissions (0.67 g N₂O m⁻² y⁻¹, s.e. 0.06, Figure 5.4), while the

Corn site on former cropland had lower emissions (0.44 g N₂O m⁻² y⁻¹, s.e. 0.05). For the Switchgrass grown on former grassland, N₂O emissions were lower at (0.17 g N₂O m⁻² y⁻¹, s.e. 0.04), while the Switchgrass grown on former cropland emitted N₂O at a similar rate (0.28 g N₂O m⁻² y⁻¹, s.e. 0.05). Prairie on former grassland shared the lowest N₂O emissions (0.12 g N₂O m⁻² y⁻¹, s.e. 0.04), along with prairie on former cropland (0.14 g N₂O m⁻² y⁻¹, s.e. 0.04) and the grassland reference site (0.12 g N₂O m⁻² y⁻¹, s.e. 0.04). Soil methane oxidation rates were highest at the prairie and switchgrass on former grassland sites (-0.14 & -0.11 g CH₄ m⁻² y⁻¹, respectively, s.e. < 0.03). The other sites all had similarly low methane oxidation rates ranging from -0.03 to -0.08 g CH₄ m⁻² y⁻¹ (s.e. < 0.03).

Albedo

Land use change and land use history significantly altered the albedo of the land surface and caused changes to the outgoing shortwave radiation at the top of the atmosphere (SW_{out}^{toa}). The conversion of grassland to bioenergy crops increased the land surface albedo while the conversion of cropland to bioenergy crops reduced it. SW_{out}^{toa} in the Corn, Switchgrass, and Prairie grown on the former grassland changed by 2.3, 3.0, and 2.2 W m⁻² (s.e. < 0.2), respectively, relative to the grassland reference site (Figure 5.5). On the other hand, SW_{out}^{toa} in the Switchgrass and Prairie grown on the former cropland changed by -1.9 and -1.3 (s.e. < 0.2), respectively, relative to the Corn on former cropland.

Radiative forcing

Each component of the overall radiative forcing budget of each land use had a significant effect on the net outcome, apart from soil methane oxidation, which was relatively minor. The largest component of the radiative forcing budget was the geologically stored carbon harvested from each site for BECCS. This component followed patterns of aboveground plant productivity

with the Corn on former grassland and cropland having the largest forcing of -28.7 and -23.4 W m⁻², respectively (Figure 5.3 & Table 5.3). Switchgrass grown on former grassland and cropland had the next largest forcing with -18.3 and -14.3 W m⁻², respectively. The lowest forcing from geologic storage of harvested carbon came from the Prairie on former grassland and cropland (-8.5 and -9.7 W m⁻², respectively).

The radiative forcing from NECB CO₂, soil CH₄, soil N₂O and albedo each follow the results reported above in their original flux units. However, the magnitude of each component's contribution to the overall radiative forcing budget follows a different scalar (Figure 5.3 and Table 5.3). The Corn on former grassland had the largest net negative radiative forcing with the C Inventory, EC tower and MEMS Model methods yielding -25.7, -19.6, and -23.8 W m⁻², respectively (Figure 5.3 and Table 5.3). The Corn on former cropland had the next largest net negative radiative forcing with each method yielding -23.4 W m⁻². The Switchgrass on former grassland had the next largest net negative radiative forcing with the C Inventory, EC tower and MEMS Model methods yielding -21.6, -19.9, and -19.7 W m⁻², respectively. The Switchgrass on former cropland followed, with the C Inventory, EC tower and MEMS Model methods yielding -20.2, -18.0, and -17.1 W m⁻², respectively. The Prairie on former cropland had the next lowest net negative radiative forcing with the C Inventory, EC tower, and MEMS Model methods yielding -17.5, -15.6 and -13.5 W m⁻², respectively. Finally, the Prairie on former grassland had the lowest net negative radiative forcing with the C Inventory, EC Tower and MEMS Model methods yielding -12.0, -10.9, and -9.9 W m⁻², respectively. The reference grassland site being a baseline reference was assumed to have a neutral radiative forcing.

Discussion

Net ecosystem carbon balance

Deriving biomass for BECCS from Corn, Switchgrass and Prairie grown on former grassland and former cropland resulted in net climate change mitigation. However, the method for estimating NECB significantly impacted the portion of climate mitigation attributed to in situ CO₂. Our NECB results show that the C inventory method had on average the highest uncertainty (22.7 Mg C ha⁻¹ 95 % C.I.), followed by eddy covariance towers (7.9 Mg C ha⁻¹) and then the MEMS model (4.6 Mg C ha⁻¹; Table 5.1). The magnitude in NECB estimates tended to be largest with the C inventory in comparison to the eddy covariance towers and the MEMS model, which had somewhat more carbon neutral (i.e. more conservative) results. However, one exception is the NECB for the Corn grown on the former grassland site, where the eddy covariance tower suggested a change of -31.2 Mg C ha⁻¹ (95 % C.I. -35.5 - -26.9 Mg C ha⁻¹; Table 5.1) over the thirteen-year study period. This figure corresponds to a 52% reduction of the site's total ecosystem carbon stocks (60.5 Mg C ha⁻¹), which is excessive and almost certainly in error. Moreover, the tower-based NECB does not agree with the C inventory or MEMS model at the site, which suggest a small sink to a small source (3.3 and -1.7 Mg C ha⁻¹, respectively). After careful consideration and much scrutiny, we have yet to find a satisfactory explanation for this disparity.

Changes in POM, MAOM, roots, and surface litter each contributed to the overall NECB. While they differed in magnitude, both the C inventory and the MEMS model agree that, on average, NECB changes were attributed most to POM (7.9 and 3.0 Mg C ha⁻¹, respectively), then MAOM (5.2 and 2.3 Mg C ha⁻¹, respectively), followed by roots (2.1 and 1.1 Mg C ha⁻¹, respectively), and finally surface litter (0.4 and 1.9 Mg C ha⁻¹, respectively), though that order

differed by site (Table 5.2). Roots were more of a contributor to carbon sequestration in the perennials as compared to the Corn and reference grassland where soil C differences dominated.

If well designed and calibrated, process-based ecosystem models are an attractive option for estimating the NECB of BECCS landscapes as they are straightforward and inexpensive to set up and run quickly (Cheng et al., 2024). On the other hand, in situ plant and soil sampling are labor intensive, expensive to carry out and can require waiting years for ecological changes to take place (Chatterjee et al., 2009). Eddy covariance towers similarly require waiting and are expensive but can be relatively less labor intensive than plant and soil sampling (Baldocchi, 2014). The ideal measurement technique will vary given the set of research sites, questions and resources (Smith et al., 2020).

Soil N₂O

Changes in soil N₂O emissions tracked differences in the synthetic N fertilization management regime. Converting highly fertilized cropland to lower or zero N fertilization rates in Switchgrass and Prairie, respectively, resulted in negative radiative forcing impacts of -1.8 and -2.0 W m⁻², respectively. On the other hand, converting unfertilized grasslands to corn, Switchgrass, and Prairie (high, low and zero N fertilization rates) corresponded to N₂O related radiative forcings of 3.7, 1.1, and 0.0 W m⁻², respectively. Other studies of N₂O emissions following changes in land use have shown that N fertilization is a key determinant of emission strength and timing (McDaniel et al., 2019).

Albedo

Changes to land surface albedo followed changes in both inherent canopy reflectance properties as well as the height of standing biomass during periods of snow cover. During periods without snow cover, Switchgrass and Prairie were relatively brighter than the reference

grassland site but were relatively darker than the continuous corn on the former cropland. Planting corn on former grassland also yielded a more reflective land surface during periods without snow cover. When snow was present, the lower stature vegetation of harvested fields allowed for more unobstructed reflectance of shortwave radiation from the snow surface. These phenomena lead us to conclude that establishing perennial bioenergy crops on former cropland resulted in positive radiative forcing due to albedo change (i.e. warming; 1.2 - 1.9 W m⁻²; Table 5.3) while establishing bioenergy crops on former grassland resulted in negative radiative forcing due to albedo change (i.e. cooling; -2.1 - -3.0 W m⁻²; Table 5.3). Other studies of land use change and land surface albedo have found that both the inherent reflectivity of the vegetation as well as the covering of snow is the high latitudes are important drivers of land surface albedo changes (Abraha et al., 2021; Cai et al., 2016; Lei et al., 2023).

Bioenergy with carbon capture and storage

More productive lands support greater storage of carbon in geologic formations (García-Freites et al., 2021; Rosa et al., 2021). Continuous corn consistently provided more biomass for BECCS than Switchgrass or Prairie, resulting in substantial negative radiative forcing (i.e. cooling). Furthermore, the former grassland sites had higher productivity than the former cropland sites, except when planted to the mixed Prairie, where both sites were equally productive. From the perspective of climate mitigation, the reference grassland is penalized because it is not harvested for BECCS. The potential onsite carbon sequestration of establishing an unmanaged grassland can be inferred here from the differences in initial ecosystem carbon stocks with the grassland and cropland sites. While this difference is substantial, the carbon storage potential will saturate over time, and the opportunity cost of not cultivating crops indefinitely for storing carbon in geologic formations with BECCS is greater. This suggests that,

from a climate perspective, enrolling former cropland in conservation grassland programs could provide mitigation, but utilizing the land for BECCS can provide more climate mitigation (Robertson et al., 2017; Stoy et al., 2018).

Radiative forcing

BECCS commands its popularity as an idea from the substantial carbon removal potential it can deliver and our study is no exception in showing these potentials (Fajardy & Mac Dowell, 2017; Fridahl & Lehtveer, 2018). Each of the bioenergy crops we examined provided substantial climate mitigation whether they were grown on former cropland or former grassland.

Switchgrass and Prairie established on former cropland resulted in net negative radiative forcing -13.5 - -20.2 W m⁻², while establishing the same perennials on former grassland resulted in a similar -9.9 - -21.7 W m⁻². The two Corn sites had the greatest climate mitigation potential of -19.6 to -25.7 W m⁻².

Geologic storage of harvested biomass carbon was, on average, the largest component of the radiative forcing budget (14.7 W m⁻²), followed by on site NECB (0.5 – 1.9 W m⁻²), albedo (1.5 W m⁻²), N₂O (1.2 W m⁻²), farming-related fossil fuels (1.1 W m⁻²) and CH₄ (0.03 W m⁻²; Table 5.3). For former cropland, newly sequestered carbon by the perennials and reductions in soil N₂O emissions contributed significantly to climate mitigation potentials. However, a less reflective land surface offset some of this mitigation (Figure 5.3). Due to the difference in previous land use, the albedo changes on the former grassland had the opposite effect (i.e. net negative radiative forcing). This finding suggests that the location of new BECCS sites and its current albedo are important considerations for climate mitigation (Baik et al., 2018).

Broader impacts

The gap between the amount of land needed to achieve meaningful climate mitigation with BECCS and the amount of land currently dedicated to it is nearly as large as it was when the idea was first proposed (Guo et al., 2015; Ma et al., 2022). The current amount of plant biomass carbon being stored in dedicated geologic formations is 0.32 Tg C y⁻¹ or 0.008 % of the proposed 4000 Tg C y⁻¹ needed by some scenarios in 2100 (Daniels, 2023; Roe et al., 2019). Resistance to adoption can be attributed to an array of complex social and ecological factors (Donnison et al., 2020). A key aim of BECCS is to provide climate mitigation while minimizing impacts to nature and society (Quader & Ahmed, 2017). Concerns about BECCS conflicting with food production have led to the focus on so-called 'marginal lands' (Smith et al., 2019). Our study found that intensively managing corn on productive lands provided the greatest climate mitigation potential due to is high productivity. That said, we found that less productive, former cropland planted to less productive perennials also provides substantial climate benefits and requires less intensive management. Furthermore, utilizing less productive former cropland avoids the conversion of already established grasslands and preserves the biodiversity and ecosystem services that those lands provide (Grass et al., 2019). Currently considerable stretches of grassland are deliberately planted to monocultures of introduced species, suggesting that replacing those monocultures with Switchgrass or Prairie and harvesting the biomass for BECCS could provide similar or greater biodiversity and ecosystem services while simultaneously increasing the climate mitigation services of those lands (Bardgett et al., 2021; Dixon et al., 2014; Gerstner et al., 2014). Our study provides information to land managers and other decision makers about how the climate impacts of BECCS can factor into the tradeoffs involved in balancing other social and environmental goals.

REFERENCES

- Abraha, M., Chen, J., Hamilton, S. K., Sciusco, P., Lei, C., Shirkey, G., Yuan, J., & Robertson, G. P. (2021). Albedo-induced global warming impact of Conservation Reserve Program grasslands converted to annual and perennial bioenergy crops. *Environmental Research Letters*, *16*(8), 084059. https://doi.org/10.1088/1748-9326/ac1815
- Abraha, M., Gelfand, I., Hamilton, S. K., Chen, J., & Robertson, G. P. (2018). Legacy effects of land use on soil nitrous oxide emissions in annual crop and perennial grassland ecosystems. *Ecological Applications*, 28(5), 1362–1369. https://doi.org/10.1002/eap.1745
- Augusiak, J., Van Den Brink, P. J., & Grimm, V. (2014). Merging validation and evaluation of ecological models to 'evaluation': A review of terminology and a practical approach. *Ecological Modelling*, 280, 117–128. https://doi.org/10.1016/j.ecolmodel.2013.11.009
- Azar, C., Johansson, D. J. A., & Mattsson, N. (2013). Meeting global temperature targets—The role of bioenergy with carbon capture and storage. *Environmental Research Letters*, 8(3), 034004. https://doi.org/10.1088/1748-9326/8/3/034004
- Baik, E., Sanchez, D. L., Turner, P. A., Mach, K. J., Field, C. B., & Benson, S. M. (2018). Geospatial analysis of near-term potential for carbon-negative bioenergy in the United States. *Proceedings of the National Academy of Sciences*, *115*(13), 3290–3295. https://doi.org/10.1073/pnas.1720338115
- Baldocchi, D. (2014). Measuring fluxes of trace gases and energy between ecosystems and the atmosphere the state and future of the eddy covariance method. *Global Change Biology*, 20(12), 3600–3609. https://doi.org/10.1111/gcb.12649
- Bardgett, R. D., Bullock, J. M., Lavorel, S., Manning, P., Schaffner, U., Ostle, N., Chomel, M., Durigan, G., L. Fry, E., Johnson, D., Lavallee, J. M., Le Provost, G., Luo, S., Png, K., Sankaran, M., Hou, X., Zhou, H., Ma, L., Ren, W., ... Shi, H. (2021). Combatting global grassland degradation. *Nature Reviews Earth & Environment*, 2(10), 720–735. https://doi.org/10.1038/s43017-021-00207-2
- Bonafoni, S., & Sekertekin, A. (2020). Albedo retrieval from Sentinel-2 by new narrow-to-broadband conversion coefficients. *IEEE Geoscience and Remote Sensing Letters*, 17(9), 1618–1622. https://doi.org/10.1109/LGRS.2020.2967085
- Brentrup, F., Lammel, J., Stephani, T., & Christensen, B. (2018, October 17). *Updated carbon footprint values for mineral fertilizer from different world regions*. International Conference on Green and Sustainable Innovation.
- Cai, H., Wang, J., Feng, Y., Wang, M., Qin, Z., & Dunn, J. B. (2016). Consideration of land use change-induced surface albedo effects in life-cycle analysis of biofuels. *Energy & Environmental Science*, *9*(9), 2855–2867. https://doi.org/10.1039/C6EE01728B
- Cameron, D., Hartig, F., Minnuno, F., Oberpriller, J., Reineking, B., Van Oijen, M., & Dietze, M. (2022). Issues in calibrating models with multiple unbalanced constraints: The

- significance of systematic model and data errors. *Methods in Ecology and Evolution*, 13(12), 2757–2770. https://doi.org/10.1111/2041-210X.14002
- Catalán, N., Marcé, R., Kothawala, D. N., & Tranvik, Lars. J. (2016). Organic carbon decomposition rates controlled by water retention time across inland waters. *Nature Geoscience*, 9(7), 501–504. https://doi.org/10.1038/ngeo2720
- Chatterjee, A., Lal, R., Wielopolski, L., Martin, M. Z., & Ebinger, M. H. (2009). Evaluation of different soil carbon determination methods. *Critical Reviews in Plant Sciences*, 28(3), 164–178. https://doi.org/10.1080/07352680902776556
- Cheng, Y., Lawrence, D. M., Pan, M., Zhang, B., Graham, N. T., Lawrence, P. J., Liu, Z., & He, X. (2024). A bioenergy-focused versus a reforestation-focused mitigation pathway yields disparate carbon storage and climate responses. *Proceedings of the National Academy of Sciences*, 121(7), e2306775121. https://doi.org/10.1073/pnas.2306775121
- Clark, P. U., Shakun, J. D., Marcott, S. A., Mix, A. C., Eby, M., Kulp, S., Levermann, A., Milne, G. A., Pfister, P. L., Santer, B. D., Schrag, D. P., Solomon, S., Stocker, T. F., Strauss, B. H., Weaver, A. J., Winkelmann, R., Archer, D., Bard, E., Goldner, A., ... Plattner, G.-K. (2016). Consequences of twenty-first-century policy for multi-millennial climate and sealevel change. *Nature Climate Change*, *6*(4), 360–369. https://doi.org/10.1038/nclimate2923
- Daniels, J. (2023). *The global status of carbon capture and storage 2023: Scaling up through 2030* (p. 98). Global Carbon Capture and Storage Institute. https://res.cloudinary.com/dbtfcnfij/images/v1700717007/Global-Status-of-CCS-Report-Update-23-Nov/global-Status-of-CCS-Report-Update-23-Nov.pdf? i=AA
- Dixon, A. P., Faber-Langendoen, D., Josse, C., Morrison, J., & Loucks, C. J. (2014). Distribution mapping of world grassland types. *Journal of Biogeography*, 41(11), 2003–2019. https://doi.org/10.1111/jbi.12381
- Donnison, C., Holland, R. A., Hastings, A., Armstrong, L., Eigenbrod, F., & Taylor, G. (2020). Bioenergy with Carbon Capture and Storage (BECCS): Finding the win–wins for energy, negative emissions and ecosystem services—size matters. *GCB Bioenergy*, 12(8), 586–604. https://doi.org/10.1111/gcbb.12695
- Fajardy, M., & Mac Dowell, N. (2017). Can BECCS deliver sustainable and resource efficient negative emissions? *Energy & Environmental Science*, *10*(6), 1389–1426. https://doi.org/10.1039/C7EE00465F
- Fridahl, M., & Lehtveer, M. (2018). Bioenergy with carbon capture and storage (BECCS): Global potential, investment preferences, and deployment barriers. *Energy Research & Social Science*, 42, 155–165. https://doi.org/10.1016/j.erss.2018.03.019
- García-Freites, S., Gough, C., & Röder, M. (2021). The greenhouse gas removal potential of bioenergy with carbon capture and storage (BECCS) to support the UK's net-zero

- emission target. *Biomass and Bioenergy*, *151*, 106164. https://doi.org/10.1016/j.biombioe.2021.106164
- Gelfand, I., Hamilton, S. K., Kravchenko, A. N., Jackson, R. D., Thelen, K. D., & Robertson, G. P. (2020). Empirical evidence for the potential climate benefits of decarbonizing light vehicle transport in the U.S. with bioenergy from purpose-grown biomass with and without BECCS. *Environmental Science & Technology*, *54*(5), 2961–2974. https://doi.org/10.1021/acs.est.9b07019
- Gerstner, K., Dormann, C. F., Stein, A., Manceur, A. M., & Seppelt, R. (2014). Effects of land use on plant diversity A global meta-analysis. *Journal of Applied Ecology*, *51*(6), 1690–1700. https://doi.org/10.1111/1365-2664.12329
- Grass, I., Loos, J., Baensch, S., Batáry, P., Librán-Embid, F., Ficiciyan, A., Klaus, F., Riechers, M., Rosa, J., Tiede, J., Udy, K., Westphal, C., Wurz, A., & Tscharntke, T. (2019). Landsharing/-sparing connectivity landscapes for ecosystem services and biodiversity conservation. *People and Nature*, 1(2), 262–272. https://doi.org/10.1002/pan3.21
- Guo, M., Song, W., & Buhain, J. (2015). Bioenergy and biofuels: History, status, and perspective. *Renewable and Sustainable Energy Reviews*, 42, 712–725. https://doi.org/10.1016/j.rser.2014.10.013
- Hanssen, S. V., Daioglou, V., Steinmann, Z. J. N., Doelman, J. C., Van Vuuren, D. P., & Huijbregts, M. A. J. (2020). The climate change mitigation potential of bioenergy with carbon capture and storage. *Nature Climate Change*, *10*(11), 1023–1029. https://doi.org/10.1038/s41558-020-0885-y
- Harris, Z. M., Alberti, G., Viger, M., Jenkins, J. R., Rowe, R., McNamara, N. P., & Taylor, G. (2017). Land-use change to bioenergy: Grassland to short rotation coppice willow has an improved carbon balance. *GCB Bioenergy*, *9*(2), 469–484. https://doi.org/10.1111/gcbb.12347
- Hersbach, H., Bell, B., & Berrisford, P., Biavati, G., Horányi, A., Muñoz Sabater, J., Nicolas, J., Peubey, C., Radu, R., Rozum, I., Schepers, D., Simmons, A., Soci, C., Dee, D., Thépaut, J-N. (2023). *ERA5 hourly data on single levels from 1940 to present*. Copernicus Climate Change Service Climate Data Store. https://doi.org/10.24381/CDS.ADBB2D47
- Huete, A., Didan, K., Miura, T., Rodriguez, E. P., Gao, X., & Ferreira, L. G. (2002). Overview of the radiometric and biophysical performance of the MODIS vegetation indices. *Remote Sensing of Environment*, 83(1–2), 195–213. https://doi.org/10.1016/S0034-4257(02)00096-2
- Klein, D., Luderer, G., Kriegler, E., Strefler, J., Bauer, N., Leimbach, M., Popp, A., Dietrich, J. P., Humpenöder, F., Lotze-Campen, H., & Edenhofer, O. (2014). The value of bioenergy in low stabilization scenarios: An assessment using REMIND-MAgPIE. *Climatic Change*, 123(3–4), 705–718. https://doi.org/10.1007/s10584-013-0940-z

- Lark, T. J., Hendricks, N. P., Smith, A., Pates, N., Spawn-Lee, S. A., Bougie, M., Booth, E. G., Kucharik, C. J., & Gibbs, H. K. (2022). Environmental outcomes of the US Renewable Fuel Standard. *Proceedings of the National Academy of Sciences*, *119*(9), e2101084119. https://doi.org/10.1073/pnas.2101084119
- Lei, C., Abraha, M., Chen, J., & Su, Y.-J. (2021). Long-term variability of root production in bioenergy crops from ingrowth core measurements. *Journal of Plant Ecology*, *14*(5), 757–770. https://doi.org/10.1093/jpe/rtab018
- Lei, C., Chen, J., & Robertson, G. P. (2023). Climate cooling benefits of cellulosic bioenergy crops from elevated albedo. *GCB Bioenergy*, *15*(11), 1373–1386. https://doi.org/10.1111/gcbb.13098
- Liang, S. (2001). Narrowband to broadband conversions of land surface albedo I. *Remote Sensing of Environment*, 76(2), 213–238. https://doi.org/10.1016/S0034-4257(00)00205-4
- Luehmann, M. D., Peter, B. G., Connallon, C. B., Schaetzl, R. J., Smidt, S. J., Liu, W., Kincare, K. A., Walkowiak, T. A., Thorlund, E., & Holler, M. S. (2016). Loamy, two-storied soils on the outwash plains of southwestern lower Michigan: Pedoturbation of loess with the underlying sand. *Annals of the American Association of Geographers*, *106*(3), 551–572. https://doi.org/10.1080/00045608.2015.1115388
- Ma, J., Li, L., Wang, H., Du, Y., Ma, J., Zhang, X., & Wang, Z. (2022). Carbon capture and storage: History and the road ahead. *Engineering*, *14*, 33–43. https://doi.org/10.1016/j.eng.2021.11.024
- Mahabbati, A., Beringer, J., Leopold, M., McHugh, I., Cleverly, J., Isaac, P., & Izady, A. (2021). A comparison of gap-filling algorithms for eddy covariance fluxes and their drivers. *Geoscientific Instrumentation, Methods and Data Systems*, 10(1), 123–140. https://doi.org/10.5194/gi-10-123-2021
- McDaniel, M. D., Saha, D., Dumont, M. G., Hernández, M., & Adams, M. A. (2019). The effect of land-use change on soil CH₄ and N₂O fluxes: A global meta-analysis. *Ecosystems*, 22(6), 1424–1443. https://doi.org/10.1007/s10021-019-00347-z
- Moffat, A. M., Papale, D., Reichstein, M., Hollinger, D. Y., Richardson, A. D., Barr, A. G., Beckstein, C., Braswell, B. H., Churkina, G., Desai, A. R., Falge, E., Gove, J. H., Heimann, M., Hui, D., Jarvis, A. J., Kattge, J., Noormets, A., & Stauch, V. J. (2007). Comprehensive comparison of gap-filling techniques for eddy covariance net carbon fluxes. *Agricultural and Forest Meteorology*, *147*(3–4), 209–232. https://doi.org/10.1016/j.agrformet.2007.08.011
- Neubauer, S. C., & Megonigal, J. P. (2015). Moving beyond global warming potentials to quantify the climatic role of ecosystems. *Ecosystems*, 18(6), 1000–1013. https://doi.org/10.1007/s10021-015-9879-4

- Neubauer, S. C., & Megonigal, J. P. (2019). Correction to: Moving beyond global warming potentials to quantify the climatic role of ecosystems. *Ecosystems*, 22(8), 1931–1932. https://doi.org/10.1007/s10021-019-00422-5
- Quader, M. A., & Ahmed, S. (2017). Bioenergy With Carbon Capture and Storage (BECCS): Future prospects of carbon-negative technologies. In *Clean Energy for Sustainable Development* (pp. 91–140). Elsevier. https://doi.org/10.1016/B978-0-12-805423-9.00004-1
- Robertson, G. P., Hamilton, S. K., Barham, B. L., Dale, B. E., Izaurralde, R. C., Jackson, R. D., Landis, D. A., Swinton, S. M., Thelen, K. D., & Tiedje, J. M. (2017). Cellulosic biofuel contributions to a sustainable energy future: Choices and outcomes. *Science*, *356*(6345), eaal2324. https://doi.org/10.1126/science.aal2324
- Roe, S., Streck, C., Obersteiner, M., Frank, S., Griscom, B., Drouet, L., Fricko, O., Gusti, M., Harris, N., Hasegawa, T., Hausfather, Z., Havlík, P., House, J., Nabuurs, G.-J., Popp, A., Sánchez, M. J. S., Sanderman, J., Smith, P., Stehfest, E., & Lawrence, D. (2019). Contribution of the land sector to a 1.5 °C world. *Nature Climate Change*, *9*(11), 817–828. https://doi.org/10.1038/s41558-019-0591-9
- Rosa, L., Sanchez, D. L., & Mazzotti, M. (2021). Assessment of carbon dioxide removal potential *via* BECCS in a carbon-neutral Europe. *Energy & Environmental Science*, 14(5), 3086–3097. https://doi.org/10.1039/D1EE00642H
- Shuai, Y., Masek, J. G., Gao, F., & Schaaf, C. B. (2011). An algorithm for the retrieval of 30-m snow-free albedo from Landsat surface reflectance and MODIS BRDF. *Remote Sensing of Environment*, 115(9), 2204–2216. https://doi.org/10.1016/j.rse.2011.04.019
- Shuai, Y., Masek, J. G., Gao, F., Schaaf, C. B., & He, T. (2014). An approach for the long-term 30-m land surface snow-free albedo retrieval from historic Landsat surface reflectance and MODIS-based a priori anisotropy knowledge. *Remote Sensing of Environment*, *152*, 467–479. https://doi.org/10.1016/j.rse.2014.07.009
- Skakun, S., Wevers, J., Brockmann, C., Doxani, G., Aleksandrov, M., Batič, M., Frantz, D., Gascon, F., Gómez-Chova, L., Hagolle, O., López-Puigdollers, D., Louis, J., Lubej, M., Mateo-García, G., Osman, J., Peressutti, D., Pflug, B., Puc, J., Richter, R., ... Žust, L. (2022). Cloud Mask Intercomparison eXercise (CMIX): An evaluation of cloud masking algorithms for Landsat 8 and Sentinel-2. *Remote Sensing of Environment*, 274, 112990. https://doi.org/10.1016/j.rse.2022.112990
- Smith, P., Adams, J., Beerling, D. J., Beringer, T., Calvin, K. V., Fuss, S., Griscom, B., Hagemann, N., Kammann, C., Kraxner, F., Minx, J. C., Popp, A., Renforth, P., Vicente Vicente, J. L., & Keesstra, S. (2019). Land-management options for greenhouse gas removal and their impacts on ecosystem services and the sustainable development goals. *Annual Review of Environment and Resources*, 44(1), 255–286. https://doi.org/10.1146/annurev-environ-101718-033129

- Smith, P., Soussana, J., Angers, D., Schipper, L., Chenu, C., Rasse, D. P., Batjes, N. H., Van Egmond, F., McNeill, S., Kuhnert, M., Arias-Navarro, C., Olesen, J. E., Chirinda, N., Fornara, D., Wollenberg, E., Álvaro-Fuentes, J., Sanz-Cobena, A., & Klumpp, K. (2020). How to measure, report and verify soil carbon change to realize the potential of soil carbon sequestration for atmospheric greenhouse gas removal. *Global Change Biology*, 26(1), 219–241. https://doi.org/10.1111/gcb.14815
- Stoy, P. C., Ahmed, S., Jarchow, M., Rashford, B., Swanson, D., Albeke, S., Bromley, G., Brookshire, E. N. J., Dixon, M. D., Haggerty, J., Miller, P., Peyton, B., Royem, A., Spangler, L., Straub, C., & Poulter, B. (2018). Opportunities and trade-offs among BECCS and the food, water, energy, biodiversity, and social systems nexus at regional scales. *BioScience*, 68(2), 100–111. https://doi.org/10.1093/biosci/bix145
- Thornton, M. M., Shrestha, R., Wei, Y., Thornton, P. E., Kao, S.-C., & Wilson, B. E. (2022). Daymet: Daily surface weather data on a 1-km grid for North America, Version 4 R1. ORNL DAAC, Oak Ridge, Tennessee, USA. https://doi.org/10.3334/ORNLDAAC/2129
- Wang, Z., Schaaf, C. B., Sun, Q., Kim, J., Erb, A. M., Gao, F., Román, M. O., Yang, Y., Petroy, S., Taylor, J. R., Masek, J. G., Morisette, J. T., Zhang, X., & Papuga, S. A. (2017). Monitoring land surface albedo and vegetation dynamics using high spatial and temporal resolution synthetic time series from Landsat and the MODIS BRDF/NBAR/albedo product. *International Journal of Applied Earth Observation and Geoinformation*, *59*, 104–117. https://doi.org/10.1016/j.jag.2017.03.008
- Ward, N. D., Bianchi, T. S., Medeiros, P. M., Seidel, M., Richey, J. E., Keil, R. G., & Sawakuchi, H. O. (2017). Where carbon goes when water flows: Carbon cycling across the aquatic continuum. *Frontiers in Marine Science*, *4*. https://doi.org/10.3389/fmars.2017.00007
- Wutzler, T., Lucas-Moffat, A., Migliavacca, M., Knauer, J., Sickel, K., Šigut, L., Menzer, O., & Reichstein, M. (2018). Basic and extensible post-processing of eddy covariance flux data with REddyProc. *Biogeosciences*, 15(16), 5015–5030. https://doi.org/10.5194/bg-15-5015-2018
- Yin, F., Lewis, P. E., & Gómez-Dans, J. L. (2022). Bayesian atmospheric correction over land: Sentinel-2/MSI and Landsat 8/OLI. *Geoscientific Model Development*, 15(21), 7933–7976. https://doi.org/10.5194/gmd-15-7933-2022
- Zhang, Y., Lavallee, J. M., Robertson, A. D., Even, R., Ogle, S. M., Paustian, K., & Cotrufo, M. F. (2021). Simulating measurable ecosystem carbon and nitrogen dynamics with the mechanistically defined MEMS 2.0 model. *Biogeosciences*, *18*(10), 3147–3171. https://doi.org/10.5194/bg-18-3147-2021

APPENDIX D: CHAPTER 5 TABLES AND FIGURES

Table 5.1. Net ecosystem carbon balance (NECB) for each previous and current land use. Central, 2.5 %, and 97.5 % NECB estimates are provided for each method. Positive values indicate C sequestration and negative values indicate C loss from the ecosystem.

				NECB	
Previous land use	Current land use	Measurement method	central	2.5 %	97.5 %
			Ì	-1	
Cropland	Corn	C Inventory	-13.02	-24.17	-1.86
		EC Tower	-3.72	-7.87	0.43
		MEMS Model	0.59	-0.12	2.64
	Switchgrass	C Inventory	13.71	2.3	25.13
		EC Tower	9.02	5.14	12.9
		MEMS Model	7.44	5.55	9.91
	Prairie	C Inventory	15.82	3.28	28.36
		EC Tower	13.3	9.42	17.18
		MEMS Model	4.08	1.73	6.7
Grassland	Corn	C Inventory	3.25	-7.37	13.87
		EC Tower	-31.19	-35.53	-26.85
		MEMS Model	-1.67	-3.74	3.18
	Switchgrass	C Inventory	10.47	-0.74	21.69
		EC Tower	4.03	-0.03	8.09
		MEMS Model	5.42	3.78	7.9
	Prairie	C Inventory	5.05	-6.75	16.84
		EC Tower	2.86	-0.66	6.38
		MEMS Model	-0.89	-3.2	1.87
	Grassland	C Inventory	-3.58	-14.38	7.22
		EC Tower	1.15	-2.77	5.07
		MEMS Model	4.06	2.26	5.92

Table 5.2. Net ecosystem carbon balance (NECB) components for the C Inventory and MEMS Model methods. Positive values indicate C sequestration and negative values indicate C loss from the ecosystem.

Previous land use	Current land use	NECB component	NECB			
			C Inventory		MEMS Model	
				95 %		95 %
			Central	C.I.	Central	C.I.
			$Mg\ C\ ha^{-1}$			
Cropland	Corn	Surface	0.00	0.67	-0.43	0.15
		Root	0.00	0.29	0.00	0.00
		POM	-3.55	4.02	-1.20	0.70
		MAOM	-9.47	10.53	2.58	0.78
	Switchgrass	Surface	-0.15	0.55	-1.25	0.15
		Root	4.23	1.45	2.27	1.51
		POM	5.23	4.05	5.50	1.75
		MAOM	4.38	10.73	2.32	0.43
	Prairie	Surface	0.03	0.56	-3.34	0.17
		Root	5.16	3.05	1.13	0.57
		POM	8.56	4.41	2.58	1.73
		MAOM	1.97	11.5	2.37	0.66
Grassland	Corn	Surface	-0.29	0.62	-3.40	0.09
		Root	-1.95	1.28	-0.52	0.00
		POM	8.72	3.77	-1.34	2.64
		MAOM	-3.20	9.96	3.49	0.78
	Switchgrass	Surface	-0.47	0.59	-3.26	0.15
		Root	-0.77	1.28	1.92	2.26
		POM	14.72	4.02	5.67	1.90
		MAOM	-3.04	10.53	2.19	0.38
	Prairie	Surface	-1.63	0.37	-1.38	0.18
		Root	2.50	2.16	1.68	0.69
		POM	5.60	4.11	1.16	1.98
		MAOM	-1.32	11.03	1.16	0.40
	Grassland	Surface	0.00	0.39	-0.18	0.55
		Root	0.00	0.76	-0.06	0.09
		POM	9.13	3.82	3.35	1.60
		MAOM	-12.71	10.22	2.02	0.18

Table 5.3. Average instantaneous radiative forcing for each component and method during the 100-year period following the land use change event. Positive values indicate a warming impact and negative values indicate a cooling impact, relative to their baseline scenario, which is set to zero by definition.

Previous and Current	Method	BECCS CO ₂	Fuel CO ₂	NECB CO ₂	CH ₄	N ₂ O	Albedo	Net
land use					$W m^{-2}$			
Cropland	C Inventory	-23.38	0	0	0	0	0	-23.38
Corn	EC Tower	-23.38	0	0	0	0	0	-23.38
	MEMS Model	-23.38	0	0	0	0	0	-23.38
Cropland	C Inventory	-14.31	-1.77	-4.19	0.03	-1.81	1.85	-20.19
Switchgrass	EC Tower	-14.31	-1.77	-2.00	0.03	-1.81	1.85	-18.00
_	MEMS Model	-14.31	-1.77	-1.07	0.03	-1.81	1.85	-17.08
Cropland	C Inventory	-9.68	-2.51	-4.52	-0.01	-2.02	1.24	-17.49
Prairie	EC Tower	-9.68	-2.51	-2.67	-0.01	-2.02	1.24	-15.64
	MEMS Model	-9.68	-2.51	-0.55	-0.01	-2.02	1.24	-13.52
Grassland	C Inventory	-28.69	2.60	-1.07	-0.02	3.70	-2.26	-25.74
Corn	EC Tower	-28.69	2.60	5.07	-0.02	3.70	-2.26	-19.60
	MEMS Model	-28.69	2.60	0.90	-0.02	3.70	-2.26	-23.77
Grassland	C Inventory	-18.34	0.84	-2.20	-0.05	1.08	-2.98	-21.66
Switchgrass	EC Tower	-18.34	0.84	-0.45	-0.05	1.08	-2.98	-19.91
_	MEMS Model	-18.34	0.84	-0.21	-0.05	1.08	-2.98	-19.67
Grassland	C Inventory	-8.50	0.09	-1.35	-0.09	0.00	-2.14	-11.99
Prairie	EC Tower	-8.50	0.09	-0.27	-0.09	0.00	-2.14	-10.90
	MEMS Model	-8.50	0.09	0.78	-0.09	0.00	-2.14	-9.86
Grassland	C Inventory	0	0	0	0	0	0	0
Grassland	EC Tower	0	0	0	0	0	0	0
	MEMS Model	0	0	0	0	0	0	0

Table 5.4. Parameters included in the MEMS model calibration for each plant type. Values are the lower and upper bound of the uniform distribution used in the calibration.

Variable	Corn	Switchgrass	Prairie	Brome
frac_AbgToStem_DS1	0.2-0.8	0.2-0.8	0.2-0.8	0.2-0.8
frac_CoarseRootDeath	0.01-0.05	0.01-0.05	0.01-0.05	0.01-0.05
frac_FineRootDeath	0.02-0.1	0.02-0.1	0.02-0.1	0.02-0.1
frac_root_senescence		0.1-0.5	0.1-0.5	0.1-0.5
frac_stem_senscence		0.5-0.9	0.5-0.9	0.5-0.9
frac_stem_storage		0.1-0.4	0.1-0.4	0.1-0.4
frac_StemDeath	0.01-0.03	0.01-0.03	0.01-0.03	0.01-0.03
frac_ToBlg_init	0.4-0.6	0.3-0.8	0.2-0.8	0.2-0.8
klight	0.4-0.6	0.4-0.6	0.4-0.6	0.4-0.6
LeafNitrogenConc_max_DS0	0.02-0.04	0.02-0.04	0.02-0.04	0.02-0.04
LeafNitrogenConc_max_DS1	0.015-0.03	0.015-0.03	0.015-0.03	0.015-0.03
NitrogenStressRUEThres	0.5-1.5	0-1.5	0-1.5	0-1.5
PhenoTemperature_Base	0-10	0-10	0-10	0-10
PhenoTemperature_Optimum	15-35	15-35	15-35	15-35
RadiationUseEfficiency	0.6-1.8	0.6-1.8	0.6-1.8	0.6-1.8
RUETemperature_OptLower	15-30	0-15	0-15	0-15
RUETemperature_OptUpper	30-35	15-30	15-30	15-30
SeedNitrogenConc_max	0.01-0.03	0.01-0.03	0.01-0.03	0.01-0.03
SpecificLeafArea	0.01-0.035	0.01-0.035	0.01-0.035	0.01-0.035
Stage_LeafFracDecrease	0.1-0.4	0.1-0.4	0.1-0.4	0.1-0.4
Stage_LeafFracZero	1-1.5	1-1.5	1-1.5	1-1.5
thurmalUnit_Reproductive	30-60	30-60	30-60	30-60
thurmalUnits_Vegetative	30-70	30-70	30-70	30-70
transp_k_max	0.5-1.5	0.5-1.5	0.5-1.5	0.5-1.5

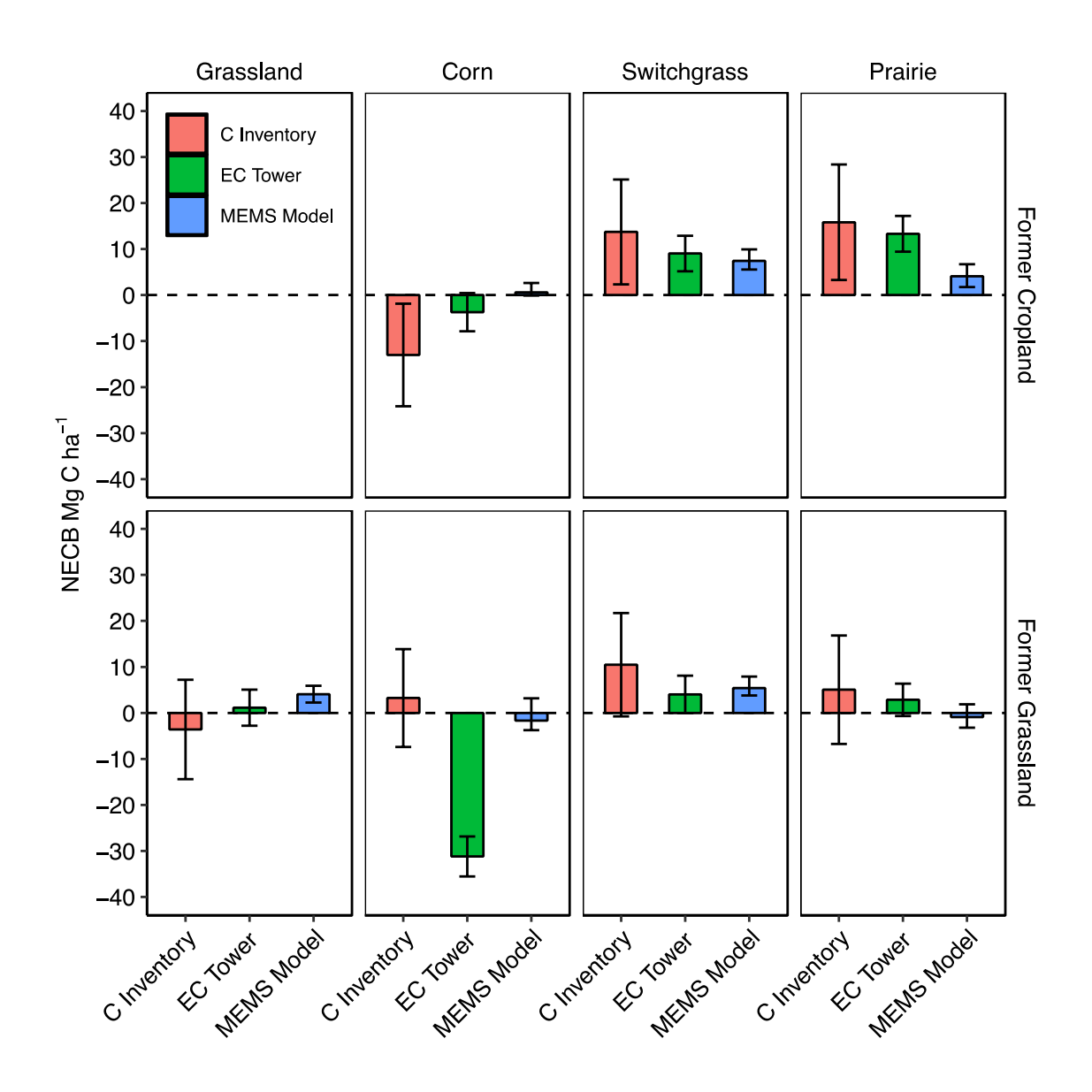


Figure 5.1. The net ecosystem carbon balance (NECB) of each site and each method. Columns and error bars represent the central estimate and 95 % confidence intervals, respectively. Positive values indicate C sequestration and negative values indicate C loss from the ecosystem.

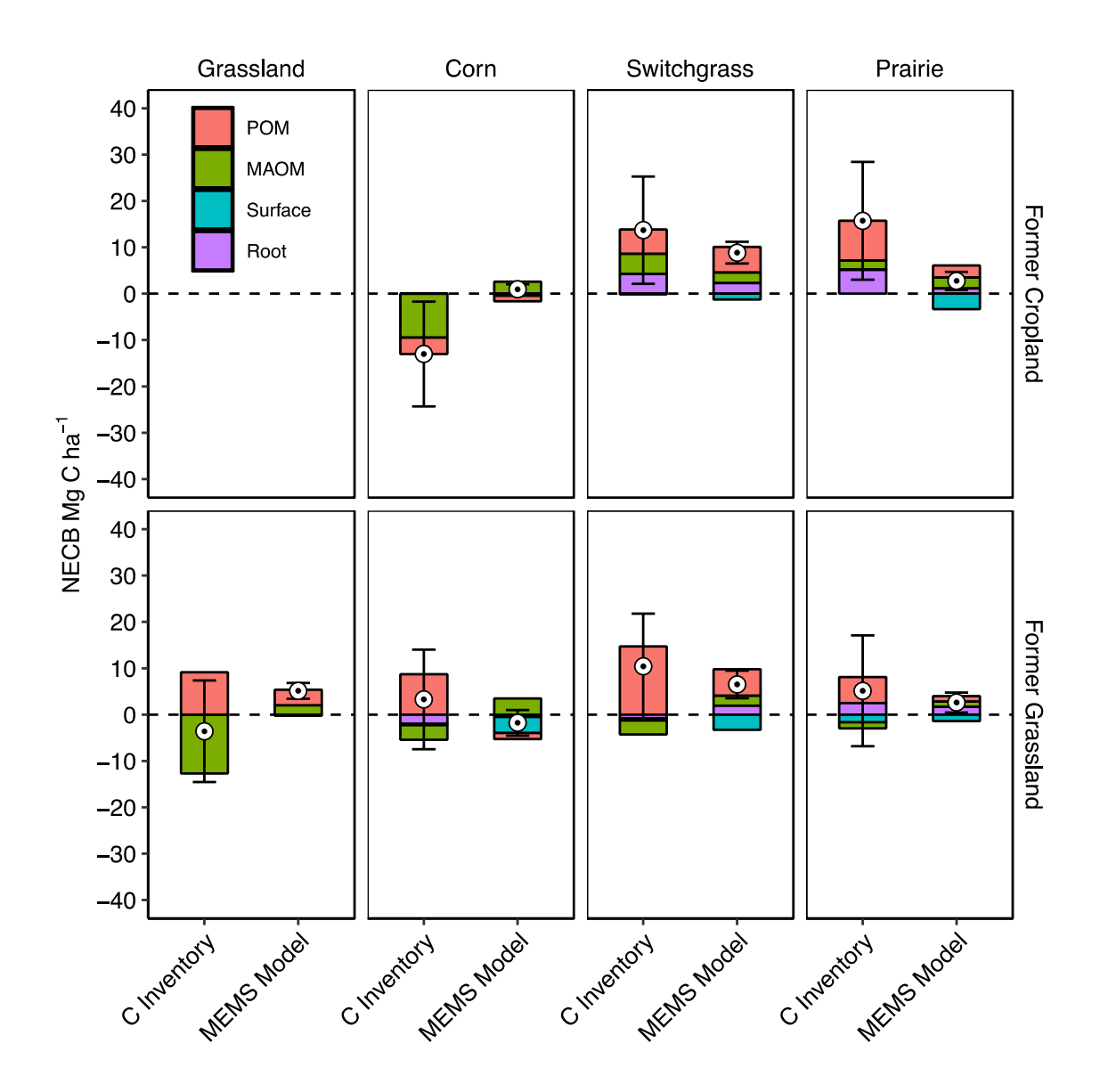


Figure 5.2. The net ecosystem carbon balance (NECB) components of each site and each method. Columns represent each component. The points and error bars represent the net NECB central estimate and 95 % confidence intervals, respectively. Positive values indicate C sequestration and negative values indicate C loss from the ecosystem.

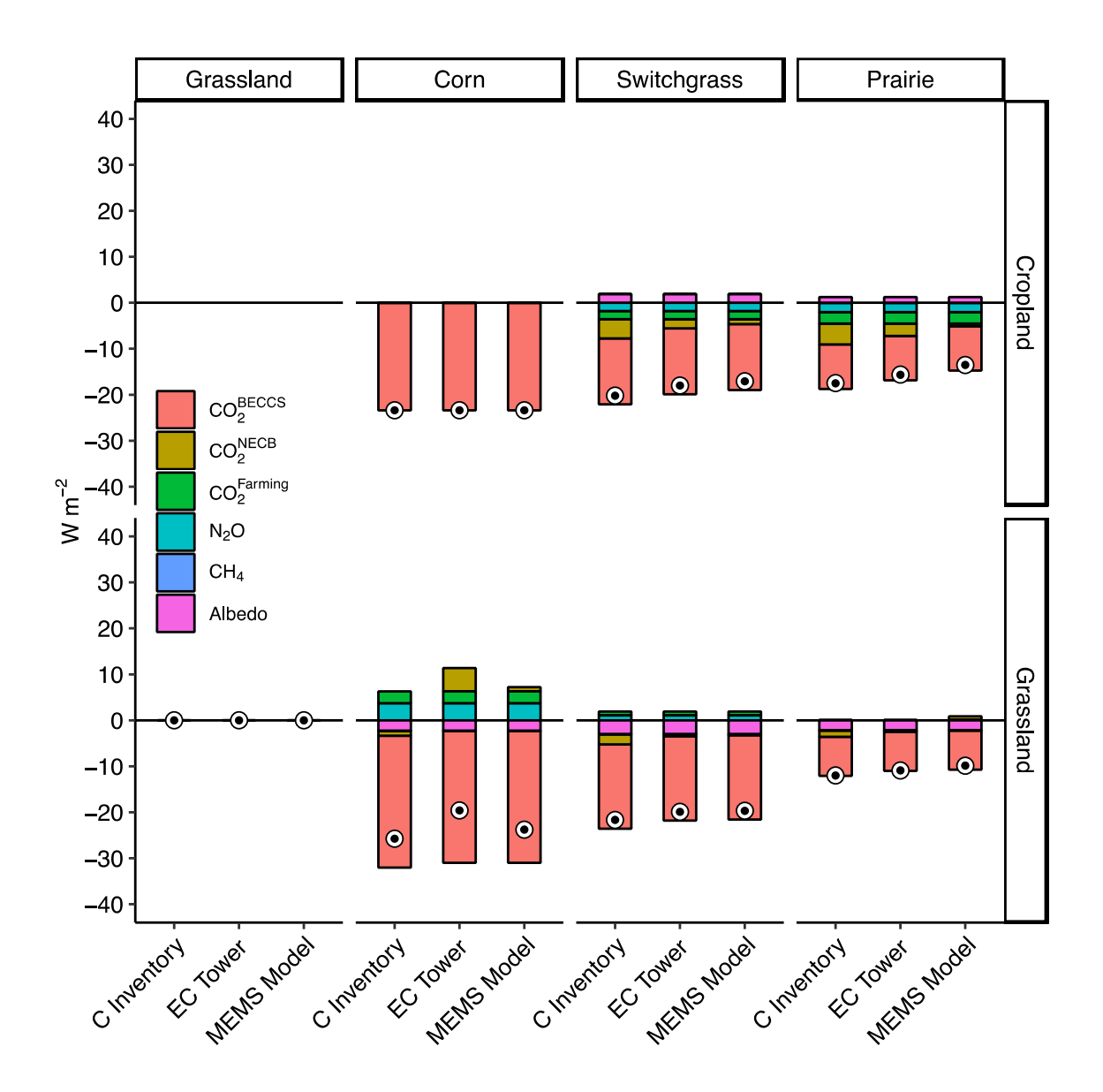


Figure 5.3. Average instantaneous radiative forcing for each component and method during the 100-year period following the land use change event. Positive values indicate a warming impact and negative values indicate a cooling impact, relative to their baseline scenario, which is set to zero by definition.

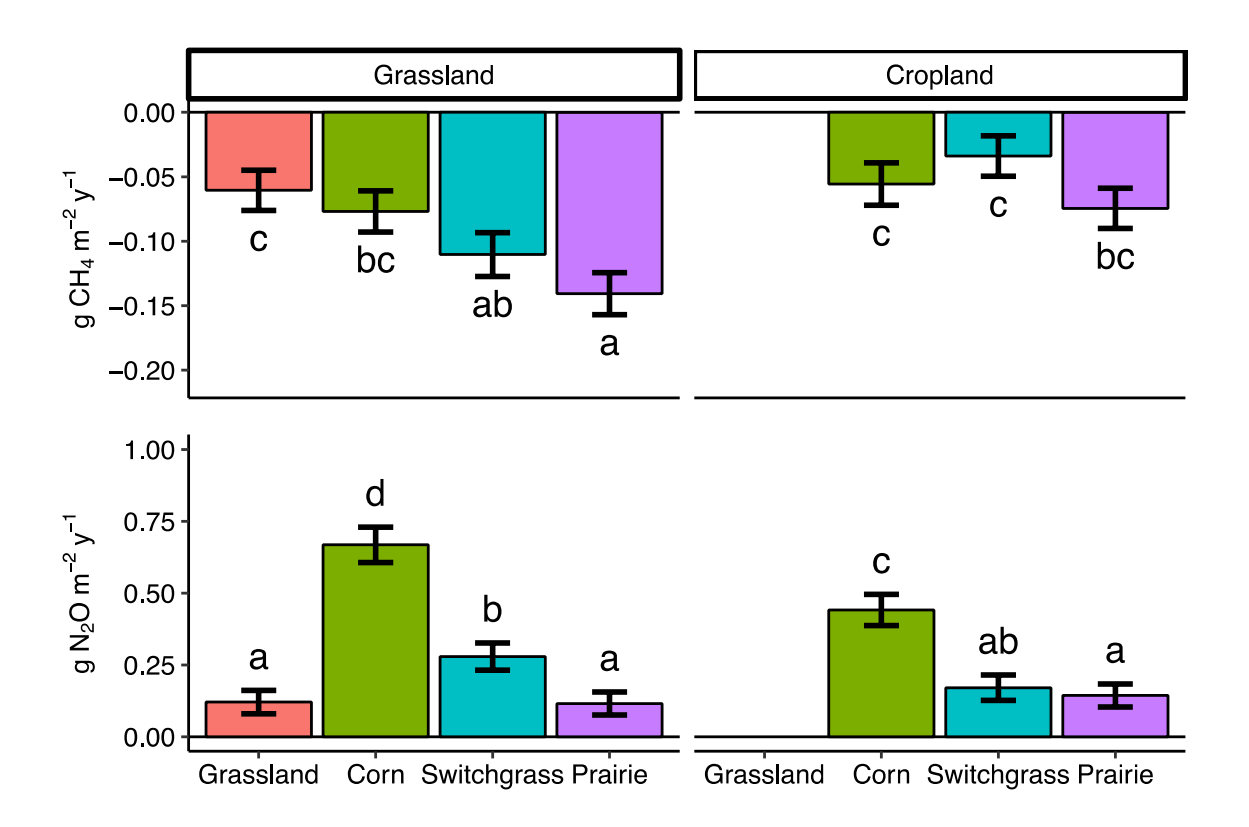


Figure 5.4. Annual soil CH₄ and N₂O fluxes. Columns and error bars represent the mean and standard error. Letters denote statistical differences between sites for each gas.

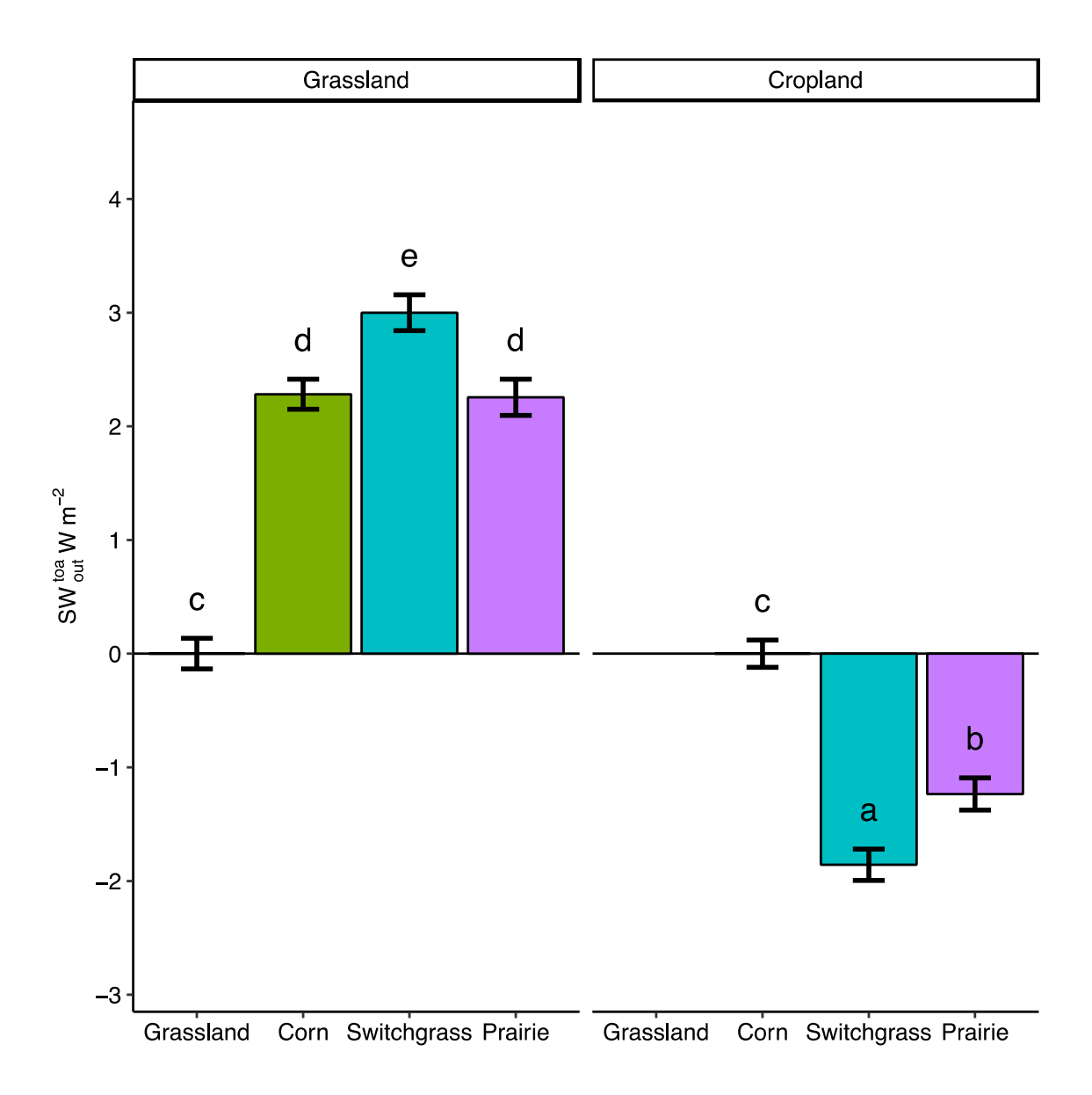


Figure 5.5. Annually averaged changes in outgoing shortwave radiation at the top of the atmosphere. Positive values indicate more radiation leaving the top of the atmosphere, contributing to negative radiative forcing. Reference values for former grassland sites are the Grassland reference site values. Reference values for former cropland sites are the Corn on former cropland site values. Columns and error bars represent the mean and standard error. Letters denote statistical differences between all sites.